U.S. Department of
Transportation

**Federal Railroad
Administration**

Side Impact Test and Analyses of a DOT-111 Tank Car

Office of Research,
Development,
and Technology
Washington, DC 20590

REPORT DOCUMENTATION PAGE

1. AGENCY USE ONLY (Leave blank)	2. REPORT DATE October 2015	3. REPORT TYPE AND DATES COVERED Final Report - September 2014	
4. TITLE AND SUBTITLE Side Impact Test and Analyses of a DOT-111 Tank Car		5. FUNDING NUMBERS DTFR53-12-D-00004 DTFR53-11-D-00008 TTCI-11-033	
6. AUTHOR(S) Steven W. Kirkpatrick, Przemyslaw Rakoczy, Robert A. MacNeill, and Adam Anderson			

7. PERFORMING ORGANIZATION NAME(S) AND ADDRESS(ES) Applied Research Associates, Inc. Transportation Technology Center, Inc. 95 1st Street, Suite 100 55500 DOT Road Los Altos, CA 94022 Pueblo, CO 81001	8. PERFORMING ORGANIZATION REPORT NUMBER
9. SPONSORING/MONITORING AGENCY NAME(S) AND ADDRESS(ES) U.S. Department of Transportation Federal Railroad Administration Office of Research, Development, and Technology Washington, DC 20590	10. SPONSORING/MONITORING AGENCY REPORT NUMBER DOT/FRA/ORD-15/30

11. SUPPLEMENTARY NOTES
COTR: Francisco Gonzalez, III

12a. DISTRIBUTION/AVAILABILITY STATEMENT This document is available to the public through the FRA web site at http://www.fra.dot.gov/eLib/Find or calling 202-493-1300	12b. DISTRIBUTION CODE

13. ABSTRACT (Maximum 200 words)

Transportation Technology Center, Inc. conducted a side impact test on a DOT-111 tank car to evaluate the performance of the tank car under dynamic impact conditions and to provide data for the verification and refinement of a computational model.

The tank car was filled with water to approximately 97 percent of its volume and sealed but not pressurized. The tank car was impacted at 14.0 mph by a 297,125-pound ram car with 12- by 12-inch ram head fitted to the ram car. The ram car impacted the tank center and punctured both the external jacket and tank shell.

The overall purpose of the program is to improve transportation safety for tank cars.

14. SUBJECT TERMS Impact test, DOT-111 tank car, tank car performance, transportation safety	15. NUMBER OF PAGES 96
	16. PRICE CODE

17. SECURITY CLASSIFICATION OF REPORT Unclassified	18. SECURITY CLASSIFICATION OF THIS PAGE Unclassified	19. SECURITY CLASSIFICATION OF ABSTRACT Unclassified	20. LIMITATION OF ABSTRACT

METRIC/ENGLISH CONVERSION FACTORS

ENGLISH TO METRIC

LENGTH (APPROXIMATE)

1 inch (in)	=	2.5 centimeters (cm)
1 foot (ft)	=	30 centimeters (cm)
1 yard (yd)	=	0.9 meter (m)
1 mile (mi)	=	1.6 kilometers (km)

AREA (APPROXIMATE)

1 square inch (sq in, in^2)	=	6.5 square centimeters (cm^2)
1 square foot (sq ft, ft^2)	=	0.09 square meter (m^2)
1 square yard (sq yd, yd^2)	=	0.8 square meter (m^2)
1 square mile (sq mi, mi^2)	=	2.6 square kilometers (km^2)
1 acre = 0.4 hectare (he)	=	4,000 square meters (m^2)

MASS - WEIGHT (APPROXIMATE)

1 ounce (oz)	=	28 grams (gm)
1 pound (lb)	=	0.45 kilogram (kg)
1 short ton = 2,000 pounds (lb)	=	0.9 tonne (t)

VOLUME (APPROXIMATE)

1 teaspoon (tsp)	=	5 milliliters (ml)
1 tablespoon (tbsp)	=	15 milliliters (ml)
1 fluid ounce (fl oz)	=	30 milliliters (ml)
1 cup (c)	=	0.24 liter (l)
1 pint (pt)	=	0.47 liter (l)
1 quart (qt)	=	0.96 liter (l)
1 gallon (gal)	=	3.8 liters (l)
1 cubic foot (cu ft, ft^3)	=	0.03 cubic meter (m^3)
1 cubic yard (cu yd, yd^3)	=	0.76 cubic meter (m^3)

TEMPERATURE (EXACT)

[(x-32)(5/9)] °F = y °C

METRIC TO ENGLISH

LENGTH (APPROXIMATE)

1 millimeter (mm)	=	0.04 inch (in)
1 centimeter (cm)	=	0.4 inch (in)
1 meter (m)	=	3.3 feet (ft)
1 meter (m)	=	1.1 yards (yd)
1 kilometer (km)	=	0.6 mile (mi)

AREA (APPROXIMATE)

1 square centimeter (cm^2)	=	0.16 square inch (sq in, in^2)
1 square meter (m^2)	=	1.2 square yards (sq yd, yd^2)
1 square kilometer (km^2)	=	0.4 square mile (sq mi, mi^2)
10,000 square meters (m^2)	=	1 hectare (ha) = 2.5 acres

MASS - WEIGHT (APPROXIMATE)

1 gram (gm)	=	0.036 ounce (oz)
1 kilogram (kg)	=	2.2 pounds (lb)
1 tonne (t)	=	1,000 kilograms (kg)
	=	1.1 short tons

VOLUME (APPROXIMATE)

1 milliliter (ml)	=	0.03 fluid ounce (fl oz)
1 liter (l)	=	2.1 pints (pt)
1 liter (l)	=	1.06 quarts (qt)
1 liter (l)	=	0.26 gallon (gal)
1 cubic meter (m^3)	=	36 cubic feet (cu ft, ft^3)
1 cubic meter (m^3)	=	1.3 cubic yards (cu yd, yd^3)

TEMPERATURE (EXACT)

[(9/5) y + 32] °C = x °F

QUICK INCH - CENTIMETER LENGTH CONVERSION

Inches	0	1	2	3	4	5
Centimeters	0 1 2 3 4 5	6 7	8 9 10	11	12	13
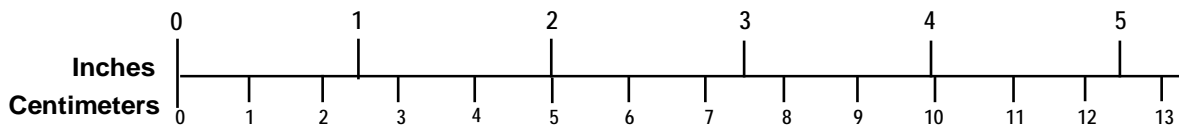
QUICK FAHRENHEIT - CELSIUS TEMPERATURE CONVERSIO

°F	-40°	-22°	-4°	14°	32°	50°	68°	86°	104°	122°	140°	158°	176°	194°	212°
°C	-40°	-30°	-20°	-10°	0°	10°	20°	30°	40°	50°	60°	70°	80°	90°	100°
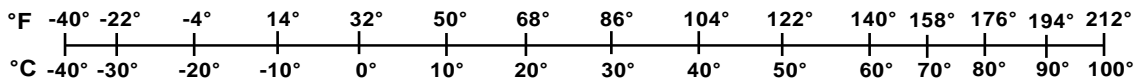
For more exact and or other conversion factors, see NIST Miscellaneous Publication 286, Units of Weights and Measures. Price $2.50 SD Catalog No. C13 10286

Contents

Illustrations

Tables

Acknowledgements

Executive Summary

This report documents the combined efforts of the Transportation Technology Center, Inc. (TTCI) and Applied Research Associates, Inc. (ARA) to perform a side impact puncture test on a DOT-111 tank car and analyze the results. TTCI conducted the side impact test on the tank car to evaluate its performance and provide data for the verification and refinement of a computational model. All test requirements were met. ARA performed both pretest predictions and post-test analyses of the impact response to evaluate, validate, and improve the puncture modeling capabilities.

The tank car was filled with water to approximately 97 percent of its volume. It was then sealed but not pressurized. The tank car was impacted by a 297,125-pound ram car traveling 14.0 mph. A 12- by 12-inch ram head fitted to the ram car impacted the tank center and punctured both the external jacket and tank shell.

Overall, the analyses were consistent with the measured impact response. The lading played a more significant role in the impact response than in previous testing and analyses of pressurized tank cars. This is not surprising, considering the reduced structural stiffness of the DOT-111 tank compared to thicker pressurized tank cars and the reduced effective stiffness from the initially unpressurized tank at impact. The smaller outage volume also contributed to a dramatic increase in the tank pressure as the dent formation reduced the tank volume and compressed the contents of the tank.

The external heater coils on the tank played a significant role in puncture behavior. Although the presence of the heater coil material in the impact zone could aid the tank car in resisting a puncture under ideal conditions, the welds on the tank were found to reduce the ductility and the corresponding stress concentrations were believed to have reduced the effective puncture force and energy for this tank.

The test and analyses described in this report support the overall objective of the Federal Railroad Administration (FRA) research program to improve transportation safety for tank cars.

1. Introduction

In recent years, significant research has been conducted to analyze and improve the impact behavior and puncture resistance of railroad tank cars. Ultimately, the results of this research will be used by the Government regulatory agencies in the United States and Canada to establish performance-based testing requirements and to develop methods to evaluate the crashworthiness and structural integrity of different tank car designs.

FRA's Office of Research, Development, and Technology has a continuing research program that provides the technical basis for rule-making on enhanced and alternative performance standards for tank cars and reviews new and innovative designs. In support of this ongoing research program, full-scale impact tests are necessary to provide the technical information required to validate modeling efforts and to inform regulatory activities.

These tests evaluate the crashworthiness performance of tank cars, examine existing designs that comply with current regulations, and examine new designs that have improved puncture resistance. FRA is currently working very closely with key industry stakeholders to use the information being generated from these programs to revise and refine the construction, design, and use of tank cars.

The objective of this report is to document analyses and test results for a recent side impact test performed on a DOT-111A100W tank car. The objective of the test was to quantify the deformation mode, impact load-time history, and puncture resistance during a side impact. Moreover, the impact conditions were designed to ensure that the test was: (a) safe, (b) repeatable, and (c) analyzable. The objectives of the analyses were both for pre-test planning and for validation of our tank car impact and puncture modeling capabilities.

The DOT-111 tank car selected for the test included a jacket and external heater coils welded to the commodity tank. This allowed the team to investigate if these features have any effect on puncture resistance.

This report documents the impact test and describes the model development and pre-test predictions, comparisons of the test and analyses, and the subsequent post-test analyses performed to address the variations in the pre-test analyses and actual test conditions. The results of these efforts will be used to characterize the puncture performance characteristics of a baseline DOT-111 tank car.

1.1 Objectives

The objective of this test was to evaluate the DOT-111 tank car's performance in a side impact scenario and to perform a validation of the computational models for assessing tank car impact and puncture behaviors.

1.2 Tank Car

The U.S. DOT-111 tank car is a low pressure vessel that is commonly used in North America (1). The test was performed on a DOT-111A100W1 tank car that was equipped with an 11-gauge jacket, insulation materials between the tank and jacket, and external heating coils. Figure 1 shows a diagram of a DOT-111A100W1 tank car. According to the certificate of construction,

the tank car was constructed with ASTM A-515 Gr. 70 steel with shell and head thicknesses of 7/16". Full water capacity is 23,987 gal.
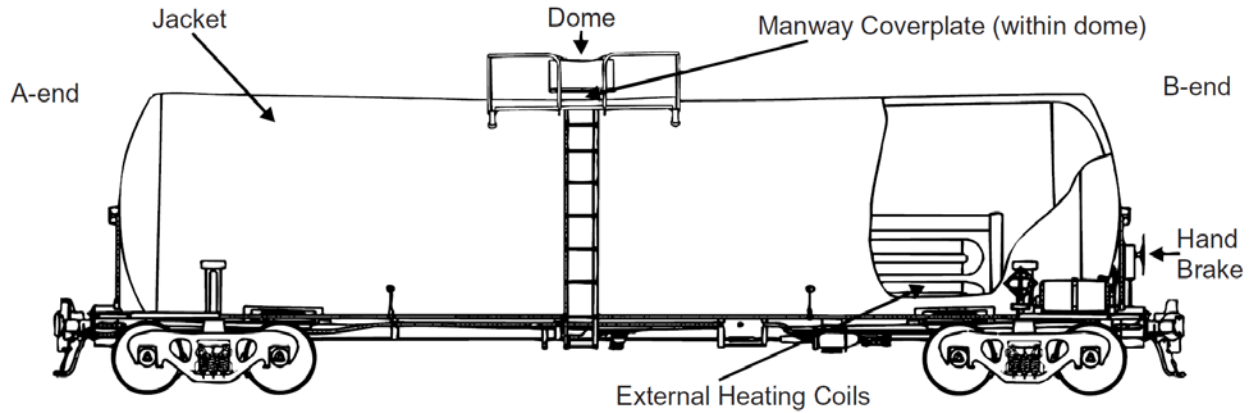
Figure 1. Diagram of a DOT-111A100W1 tank car.

This design has heater coils welded to the outside of the commodity tank (two of which transit across the top and bottom of the impact zone for the test). Some key information about the DOT-111 tank car used in the test:

- Shell and head material: 7/16 inch-thick A515-70 plate
- Heads: 106 in Inner Diameter (ID) 2:1 ellipsoid geometry
- Shell: $110^1/_4$ in ID center ring and sloping bottom design.
- Shell Jacket: 11 gauge ASTM A-569 steel
- Jacket: $114^1/_2$ in ID at head seam and $119^1/_8$ inch at center seam

1.3   Side Impact Test (12x12 impactor)

The side impact test was performed on December 18, 2013, at the TTCI's site in Pueblo, Colorado [1]. In this test, a ram car with a 12 in x 12 in impactor head was impacted into the side of a DOT type 111A100W tank car that was backed by a rigid impact barrier. The tank car configuration prior to the test is shown in Figure 2.

3

Figure 2. Target tank car mounted on support skids.

The tank is supported on skids attached to the tank at the bolsters and center plate, as shown in Figure 3. The skids allow the tank to freely slide on the ground but resist rolling motions and contribute to the controlled impact dynamics of the tank car. The height of the skids allowed the ram height to be aligned as close as possible with the center of gravity (CG) for both the ram car and tank car, which permitted more controlled collision dynamics in the test (dominated primarily by translational motions with minimized off-axis or rotational motions).

(a) Support skids   **(b) Welded I-beam connection**

Figure 3. Photographs of the tank support skid system.

The desired impact speed was 14 mph and the ram car speed was measured optically at 14.04 mph using speed trap reflectors placed within 6 feet of the impact point. The tank was filled

with water to approximately 97 percent of its capacity to simulate standard commodity lading volume.

Additional parameters for the side impact test:

- Wind Speed: 9 mph W-SW
- Temperature: 53.3 °F
- Tank Car Light Weight 75,200 pounds
- Tank Capacity: 24,081 gal
- Fill Material: Water
- Approximate Outage: 3 percent
- Initial Internal Pressure 0 psig (1 atm absolute pressure)
- Ram Car Weight: 297,125 pounds
- Ram Car Speed: 14.04 miles per hour
- Maximum Impact Force (derived): 960,000 lbf
- Ram Car Energy (calculated): 1.96 million foot-pounds

Prior to the test, the tank car structure and all interior welds were visually inspected for any damage or evidence of repair. The tank structure was found to be in good condition without any previous signs of repair.

This test was designed to produce large impact deformations and puncture the tank. The tank's instrumentation measured the impact speed, car motions, and acceleration, as well as the internal tank pressure history in order to quantify the impact and puncture behavior and validate the tank car computer models.

Figure 4 shows the ram car and impactor head prior to the test. When the rigid ram reached the target impact speed, it dented and punctured both the jacket and the shell of the DOT-111 tank car. The ram car remained lodged within the tank car following the test, while the tank car stayed upright throughout the test (with controlled translational motions provided by the skid support).

(a) Complete ram car

(b) Ram head adjacent to the target tank

Figure 4. Ram car and impactor head configuration prior to the test.

2. Test Instrumentation

2.1 Overview

The test's configuration and instrumentation were consistent with the specifications of the test implementation plan [1]. All instrumentation in this test is listed in Table 1 and descriptions of the instrumentation are provided in the sub-sections below.

Table 1. Instrumentation Summary

Type of Instrumentation	Channel Count
Accelerometers	11
Speed Sensors	2
Pressure Transducers	8
String Potentiometers	10
Total Data Channels	**31**
Digital Video	7 Cameras including 3 High Speed Cameras

2.2 Ram Car Accelerometers and Speed Sensors

The local acceleration coordinate system is defined relative to the ram car. Positive x, y, and z directions are forward, left, and up relative to the lead end of the ram.

Three tri-axial accelerometers were mounted along the longitudinal centerline of the ram car at the front, rear, and near the middle of the car. Two uniaxial accelerometers were mounted on the left and right sides of the car to provide supplemental recordings of longitudinal acceleration. The positions of these accelerometers are illustrated in Figure 5. A summary of the ram car accelerometer types and positions are provided in Table 2.
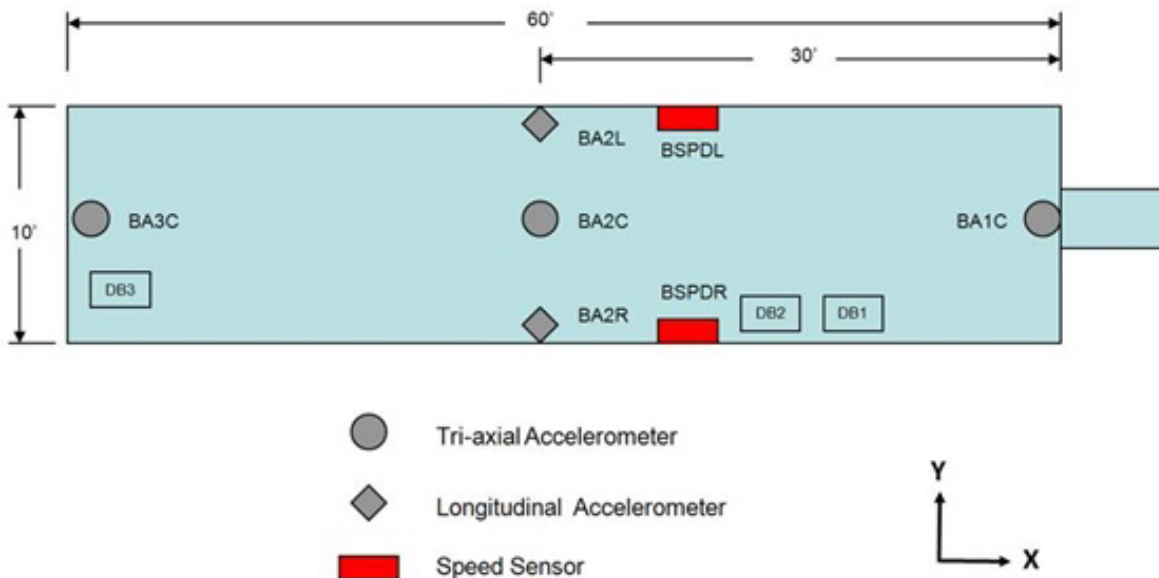
Figure 5. Ram car instrumentation.

Table 2. Ram Car Accelerometers

Channel Name	Sensor Description	Range
BA1CX	Leading End, Centerline, X Accel	200 g
BA1CY	Leading End, Centerline, Y Accel	100 g
BA1CZ	Leading, Centerline, Z Accel	200 g
BA2LX	Middle, Left Side X Accel	100 g
BA2CX	Middle, Centerline, X Accel	50 g
BA2CY	Middle, Centerline, Y Accel	50 g
BA2CZ	Middle, Centerline, Z Accel	50 g
BA2RX	Middle, Right Side X Accel	100 g
BA3CX	Trailing End, Centerline, X Accel	200 g
BA3CY	Trailing End, Centerline, Y Accel	100 g
BA3CZ	Trailing End, Centerline, Z Accel	200 g

Speed sensors were mounted on both sides of the ram car to provide accurate measurements of the car velocity within 2 ft. of the impact point. The speed sensors were reflector based light sensors which used ground reflectors separated by a known distance and car-mounted light sensors that triggered as the ram car passed over the reflector. The last reflector was positioned to align with the sensor when the ram head was within a few inches of the impact point. The time interval between passing the reflectors was recorded and speed was calculated from distance and time. A handheld radar gun was also used to take supplemental speed measurements.

2.3   Tank Car String Potentiometers and Pressure Transducers

The local displacement coordinate system (except for the tank head) is defined relative to the tank car. Positive x, y, and z directions are forward, left (away from the wall), and up relative to the B-end of the tank car. Tank head displacements are positive toward the impact wall.

Six string potentiometers (string pots) were used to measure the tank crush displacements around the immediate impact zone during the test. Five of them measured the dent formation of the tank at the tank center and at locations 24 in and 48 in to either side of the impact point, and they were set to measure up to approximately 24 in of deformation toward the interior and 6 in toward the exterior of the tank car. The sixth string pot measured the vertical deformations of the tank at the center (aligned with the impact point).

Four additional string pots were used to measure the tank's motions. The string pots were attached to each of the tank's skids and to the center of the tank heads at either end of the car. Fixed anchor positions were established so that these measurements are for the longitudinal motions of the tank head and skid movements. Table 3 provides a list of all string pots inside and outside the tank car. Figure 6 and Figure 7 show their placement.

Table 3. Tank Car String Potentiometers

Area	Location	Axis	Channel Name	Range
Impact Area	A-end — 48"offset	Y	TD1Y	30"
Impact Area	A-end — 24" offset	Y	TD2Y	30"
Impact Area	Center	Y	TD3Y	30"
Impact Area	Center	Z	TD3Z	30"
Impact Area	B-end — 24" offset	Y	TD4Y	30"
Impact Area	B-end — 48" offset	Y	TD5Y	30"
Tank Head	A-end	Y	TDAend	50"
Tank Head	B-end	Y	TDBend	50"
Skid	A-end	Y	TDAskid	50"
Skid	B-end	Y	TDBskid	50"
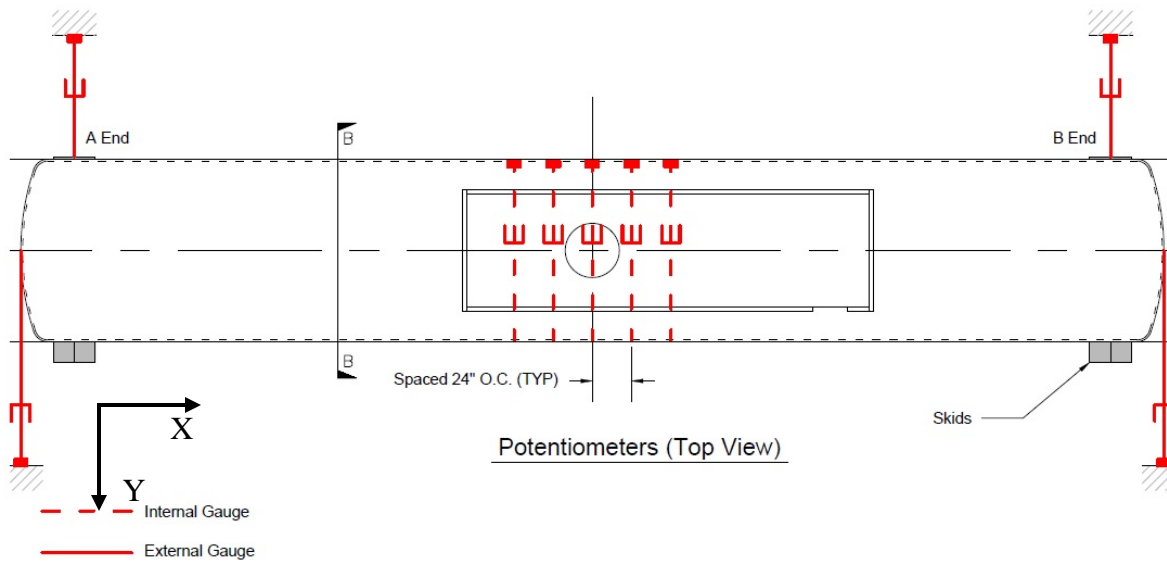
Figure 6. Tank car string potentiometers (top).
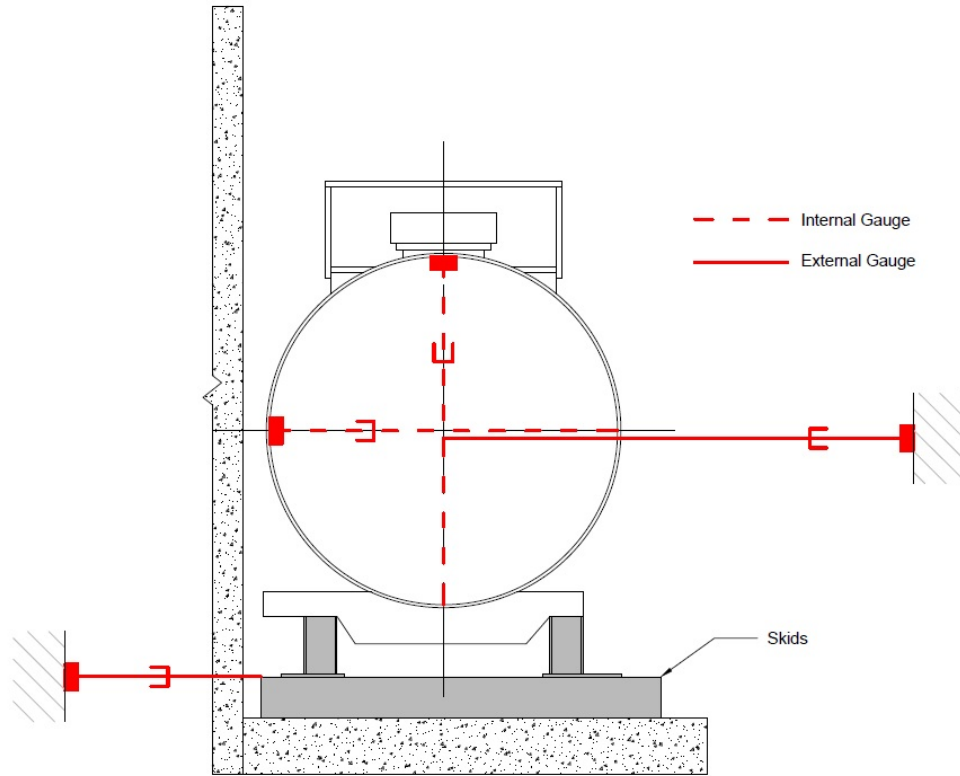
Section B-B (Typical Cross Section At Pressure Gauges)

Figure 7. Tank car string potentiometers (side).

One pressure transducer was attached to the pressure relief valve to measure when the valve was open. Additionally, an array of seven pressure transducers was set up within the tank to record the pressure pulse through the lading. These were mounted in three sections along the sides and bottom of the tank. Table 4 provides a list of all pressure transducers used inside the tank car and their placement is illustrated in Figure 8 and Figure 9.

Table 4. Tank Car Pressure

Location	Channel Name	Sensor Description	Range
PR Valve	PRV	Pressure Relief Valve	300 psi
A Back Wall	P1090	A-end Back Wall Pressure	300 psi
A Front Wall	P1270	A-end Front Wall Pressure	300 psi
B Back Wall	P3090	B-end Back Wall Pressure	300 psi
B Front Wall	P3270	B-end Front Wall Pressure	300 psi
C Back Wall	P2090	Mid-length Back Wall Pressure	300 psi
C Floor	P2180	Mid-length Floor Wall Pressure	300 psi
C Front Wall	P2270	Mid-length Front Wall Pressure	300 psi
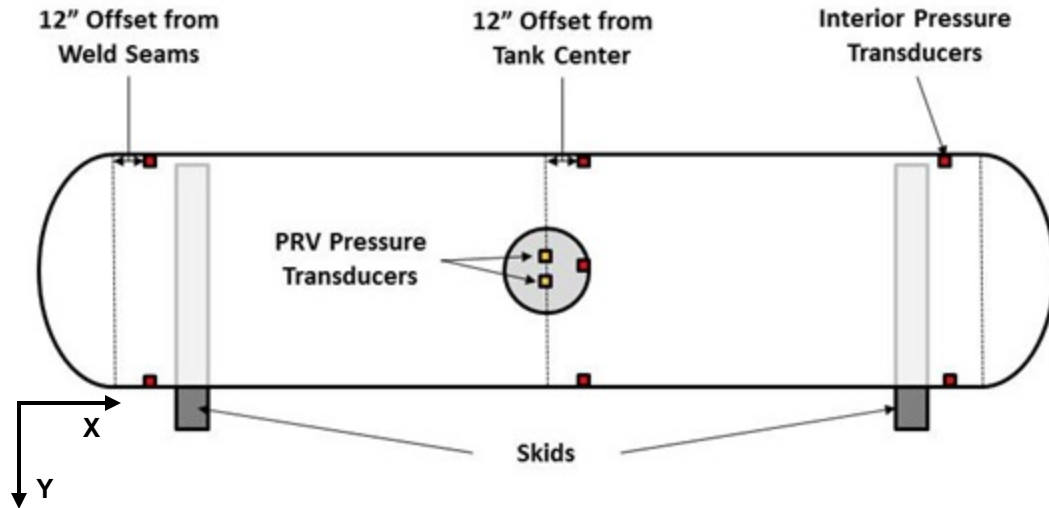
Figure 8. Tank car pressure transducers (top).
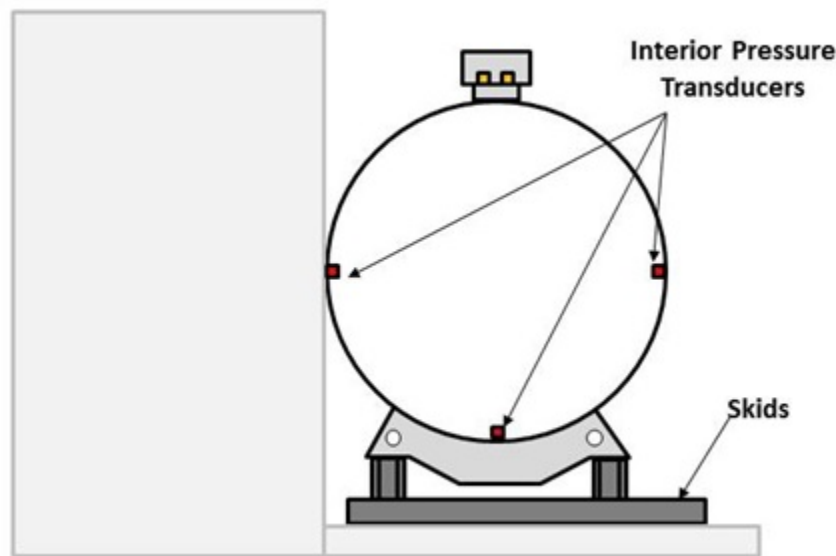
Figure 9. Tank car pressure transducers (side).

2.4 Real Time and High Speed Photography

Three high-speed and two real-time high definition video cameras were used to document the impact event. Appendix A contains additional photographs of the impact test, and Appendix B contains a schematic which provides the locations of the cameras and the targets.

2.5 Data Acquisition

A set of 8-channel battery-powered onboard data acquisition systems recorded the data from the ram car's instrumentation. These systems provided excitation to the instrumentation, analog anti-aliasing filtering of the signals, analog-to-digital conversion, and stored the results of each data stream. A similar set of ground-based data acquisition systems was used to record data from the pressure transducers and string potentiometers on the tank car.

The data acquisition systems were GMH Engineering Data BRICK Model III units and data acquisition complied with the appropriate sections of SAE J211. Data from each channel was anti-alias filtered at 1,735 Hz then sampled and recorded at 12,800 Hz. Data recorded on the data bricks were synchronized to time zero at initial impact and the time reference came from closure of the tape switches on the front of the test vehicle. Each data brick was able to withstand shock loading up to at least 100 g. Onboard battery power was provided by GMH Engineering 1.7 Amp-hour 14.4 Volt NiCad Packs. Tape Switches, Inc. model 1201-131-A tape switches provided event initial contact.

Software in the data bricks was used to determine zero levels and calibration factors rather than relying on set gains and expecting no zero drift. The data bricks were set to record 1 second of data before initial impact and 4 seconds of data after initial impact.

3. Impact Test Results

3.1 Test Conditions

As described in Section 1.3, the test involved a 14.04 mph side impact by a structurally rigid 297,125 lb ram car with a 12 inch square impactor head into the side of the 111A100W test vehicle, backed by a rigid impact barrier. The test tank car was filled to approximately 97 percent capacity with water to simulate standard commodity lading volume of a DOT-111 tank car.

3.2 Details of Test

Target speed for the test was 14 mph and the simulation predicted a puncture at that speed. The actual calculated impact speed from the speed trap was 14.04 mph and the impact resulted in large dents and penetration of both the jacket and tank shell by the ram arm. The states of the tank car and ram car after impact are shown in Figure 10(a). The impact also caused one of the weld joints on the jacket near the impact area to fail, and the back of the tank car was also deformed by the reaction against the rigid impact barrier.

The indenter head became lodged inside the tank car, requiring a 10 by 10-ft section to be cut around the center of the impact and allow for removal of the indenter head while still maintaining the deformation shape for inspection. The final shape of the punctured interior panel section after removal from the tank is shown in Figure 10(b).

3.3 Measured Test Impact Response

The data collected in the test was processed (offset corrections, filtering, etc.) by TTCI and provided to Applied Research Associates (ARA) for comparison to analyses. The offset adjustment procedure ensured that the data only contained impact-related accelerations and strains and excludes electronic offsets or steady biases in the data. In order to determine the necessary offset, the data collected just before impact was averaged. This offset was then subtracted from the entire data set for each channel. This post-test offset adjustment is independent of, and in addition to, the pre-test offset adjustment made by the data acquisition system.

The post-test filtering of the data was accomplished with a phaseless four-pole digital filter algorithm consistent with the requirements of SAE J211 [2]. A 60 Hz channel frequency class (CFC) filtering was applied to the filtered data shown in this report. A brief summary of the measured data is provided in this section.

One of the primary measurements that the team took was the longitudinal acceleration of the ram car, and multiple accelerometers were used on the ram car to capture this data. The ram car's acceleration was used to derive both the ram displacement (tank indentation depth) and the contact forces between the ram and target tank car. The ram car's average longitudinal acceleration history from all of the ram accelerometers is shown in Figure 11. Puncture of the tank car shell occurred at the point of peak acceleration (approximately 0.2 sec from trigger).

The ram car's velocity history can be calculated by integrating the average longitudinal acceleration of the ram car and using the impact speed measurement as an initial condition, as shown in Figure 12. At the moment of puncture, the ram was traveling at approximately 6 mph.

(a) Test tank car and ram car post impact

(b) Punctured tank shell

Figure 10. Post-test damage and puncture response of the test tank car.
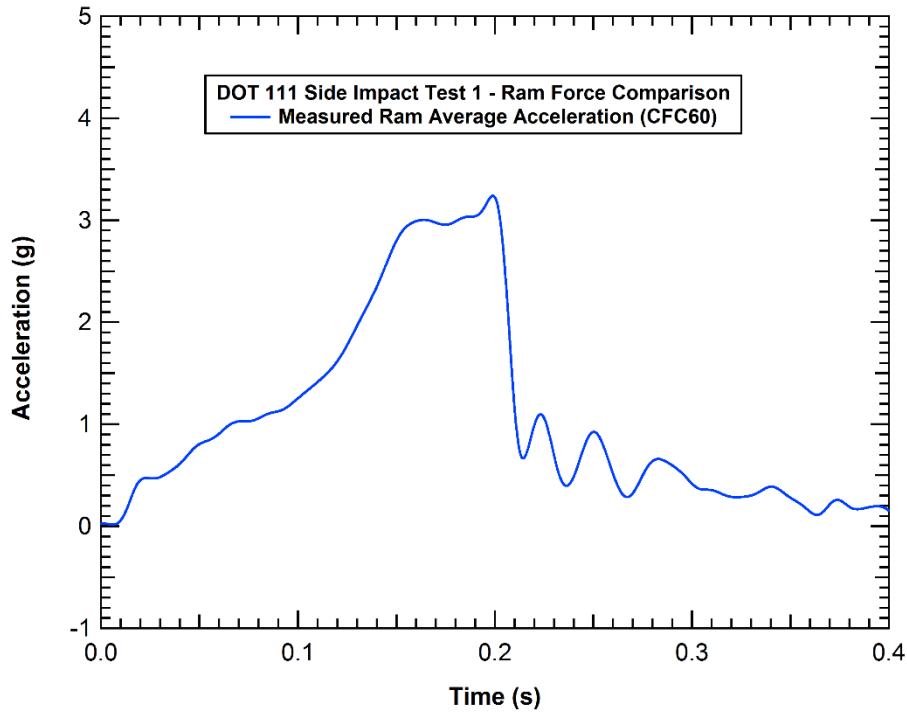
Figure 11. Longitudinal ram car acceleration data (filtered and averaged).
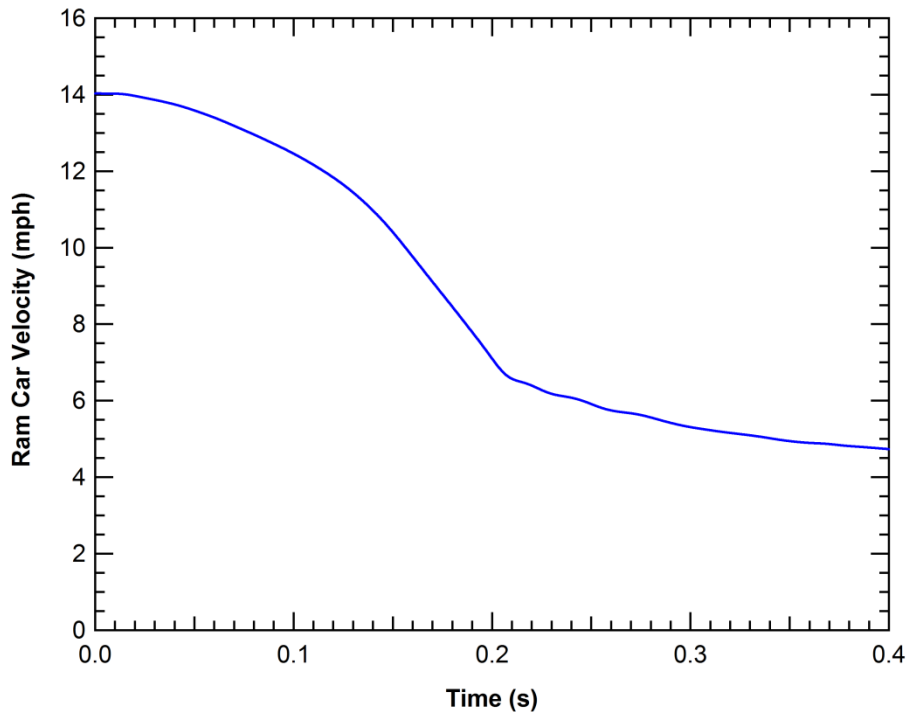
Figure 12. Ram car velocity history calculated from the measured accelerations.

The impact force can be calculated as the product of the ram car's mass and acceleration, and the ram displacement can be obtained from the double integration of the ram acceleration history. A graph of the resulting calculated ram force-displacement curve is shown in Figure 13, which

includes an integration of the force-displacement curve that calculates the impact energy dissipation and is capped at the point of the tank puncture to determine the puncture energy. The puncture occurs at a displacement of approximately 42 inches with a peak force of 962,000 lb, and a puncture energy of 1.45 million ft-lb. This is approximately 75 percent of the 19.5 million ft-lb initial kinetic energy of the ram car. Similarly, the 1.45 million ft-lb puncture energy corresponds to the energy of the ram car at an impact speed of 12.1 mph.
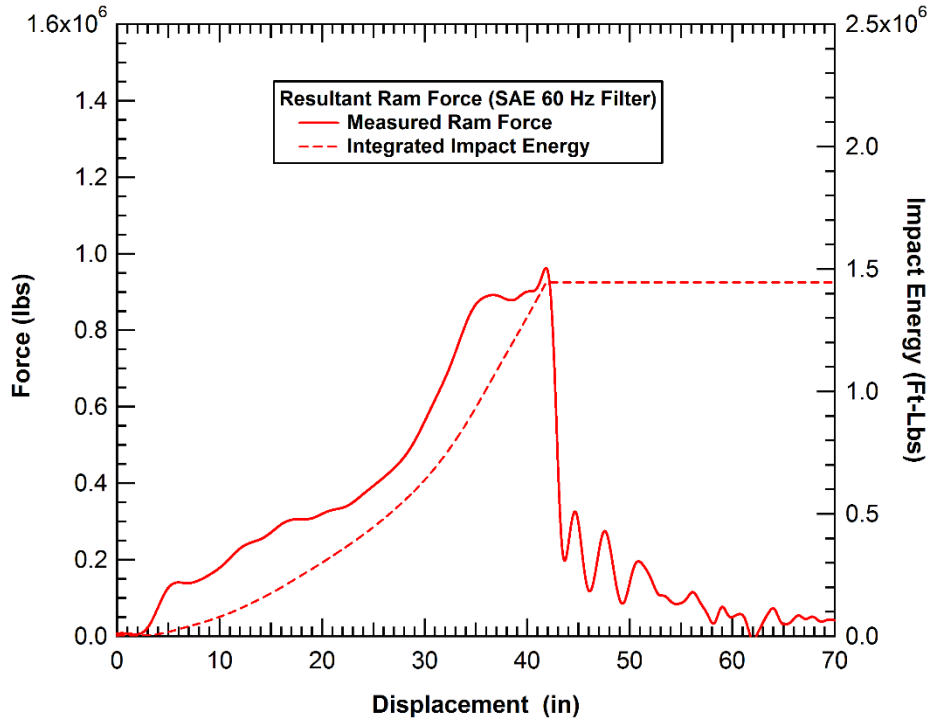
Figure 13. Test impact force-displacement behavior and puncture energy.

The team also measured the effects of the internal pressure as the tank indentation forms and reduces the volume of the tank. The tank is initially unpressurized. However, the tank was filled to approximately 3 percent outage volume with water that can be approximated as incompressible for the impact behavior. As a result, the small gas volume in the outage, initially at one atmosphere, is compressed as the dent formation reduces the tank volume and the internal pressure rapidly increases. As described in the test implementation plan [1], pressure transducers were mounted at several locations in the tank and at the pressure release valve. Figure 14 displays the data gathered from those transducers.

The positive reading on the pressure relief valve indicates when the valve was open, and the data is consistent with the relief valve activation pressure of 75 psi. Figure 15 displays a graph of the local measured centerline dynamic tank pressures, measured at locations at the front and rear walls aligned with the ram tip as well as on the tank bottom. The comparison shows that the pressure is dominated by the average hydrostatic pressure developed from the denting and volume change. However, there are additional dynamic pressures caused by the sloshing motions of the water in the tank, which add local pressure variations that can be as much as 30 psi different from the average value. It is interesting to note that a time delay can be seen as the pressure wave from the impacted front wall is transmitted through the structure and lading before it is fully felt along the tank bottom and back face.

16
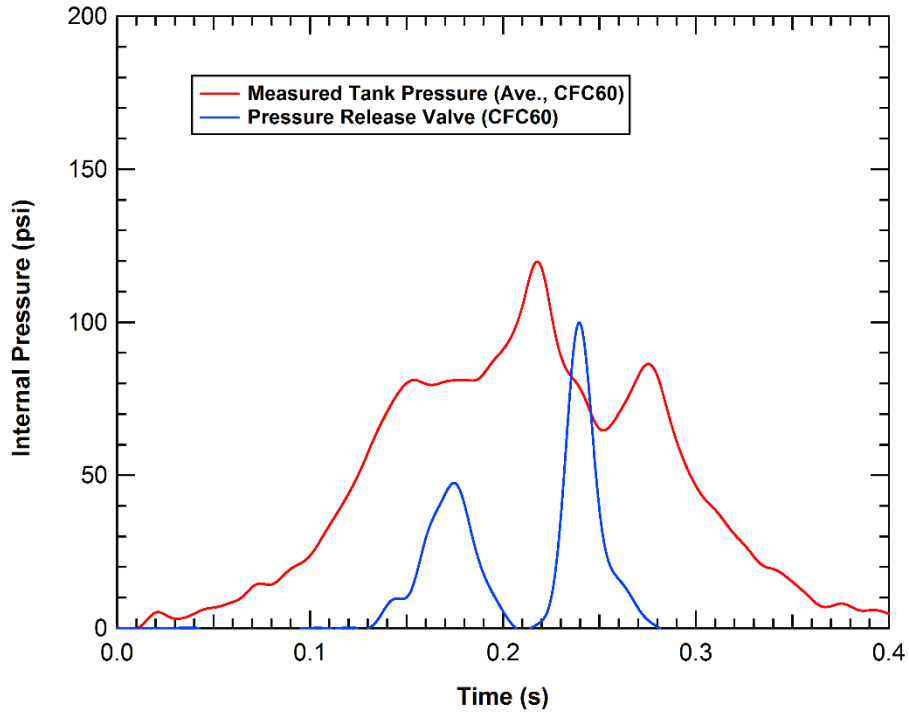
Figure 14. Measured and filtered test pressure data.
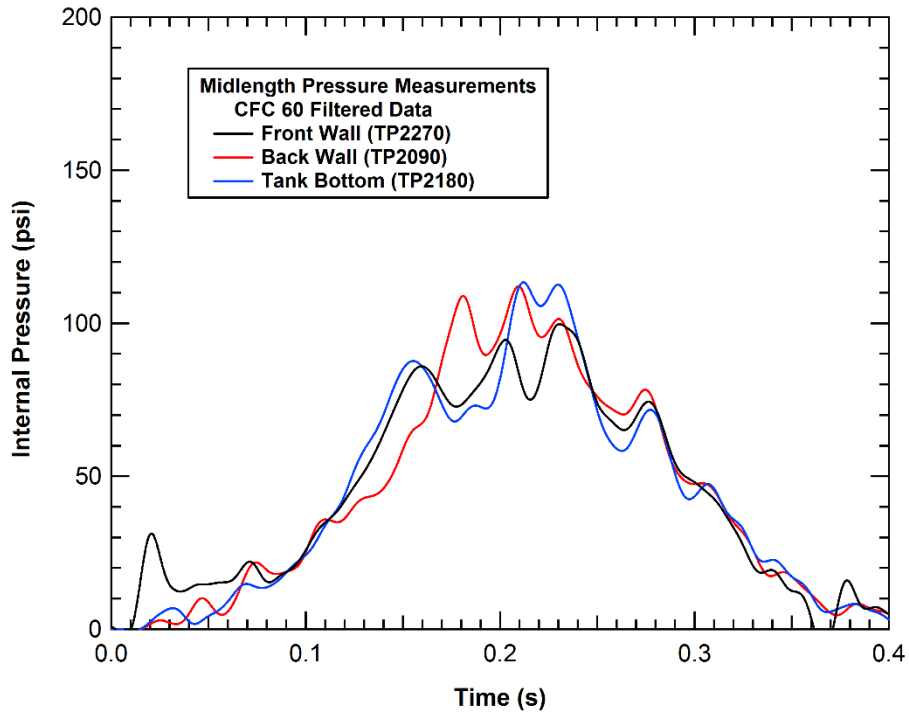
Figure 15. Filtered test local tank midsection pressure data.

The remaining quantitative measurements of tank impact behavior are displacement histories recorded with string potentiometers. These include both internal tank deformations and external

17

tank movements at both ends of the tank. The top view string potentiometer layout from the test implementation plan [1] is shown in Figure 16.
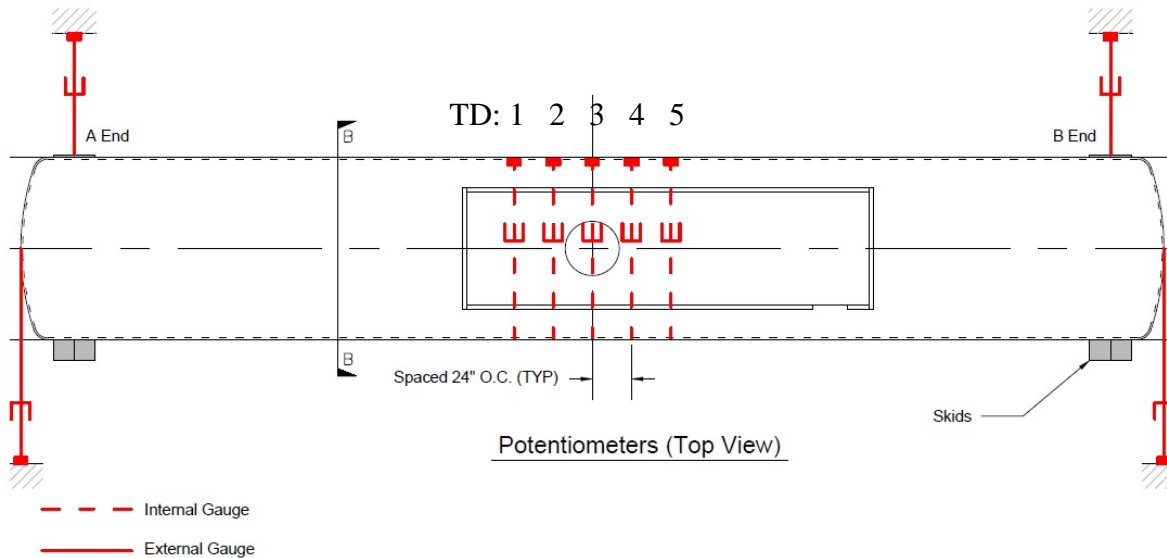
Figure 16. Tank car internal string potentiometer locations (top view) [1].

A graph of the displacements for the tank internal string potentiometers (TD1 through TD5) is shown in Figure 17. Note that the longitudinal tank crush at the centered string pot locations TD 2, 3, and 4 (Y-direction) exceed the limit of the instrumentation and the test traces max out at 24 inches. Overall, the data shows consistent measurements of the tank deflections with the largest deflection at the impact and reduced displacements at distances further from the center of the impact indentation. The ovaling deformations of the tank resulted in an approximately 13-inch maximum extension of the vertical string potentiometer at the tank centerline.

A graph of the displacements for the tank end external string potentiometers is shown in Figure 18. The displacements of the car end are significantly delayed from the motions in the impact zone; little displacement is seen for the first 150 ms of the response and approximately 4-5 inches of displacement has occurred at the time the tank is punctured (0.2 s). Note that the measurements of the car end head displacements and the skid displacements are nearly identical and the response is symmetric between the A-end and B-end of the tank until well after the tank has punctured.
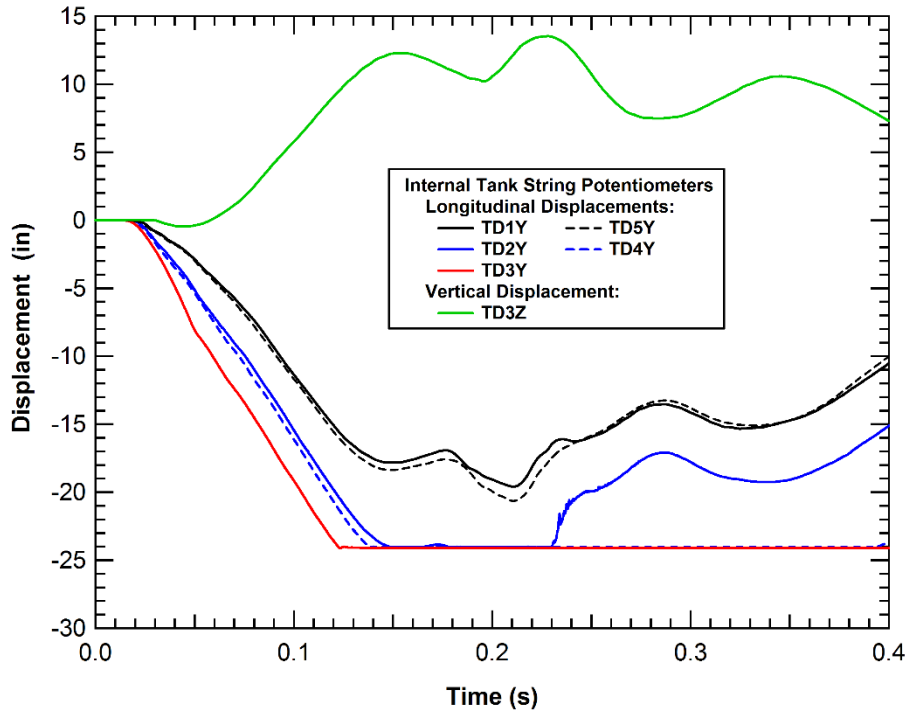
Figure 17. Measured test tank internal displacement histories.
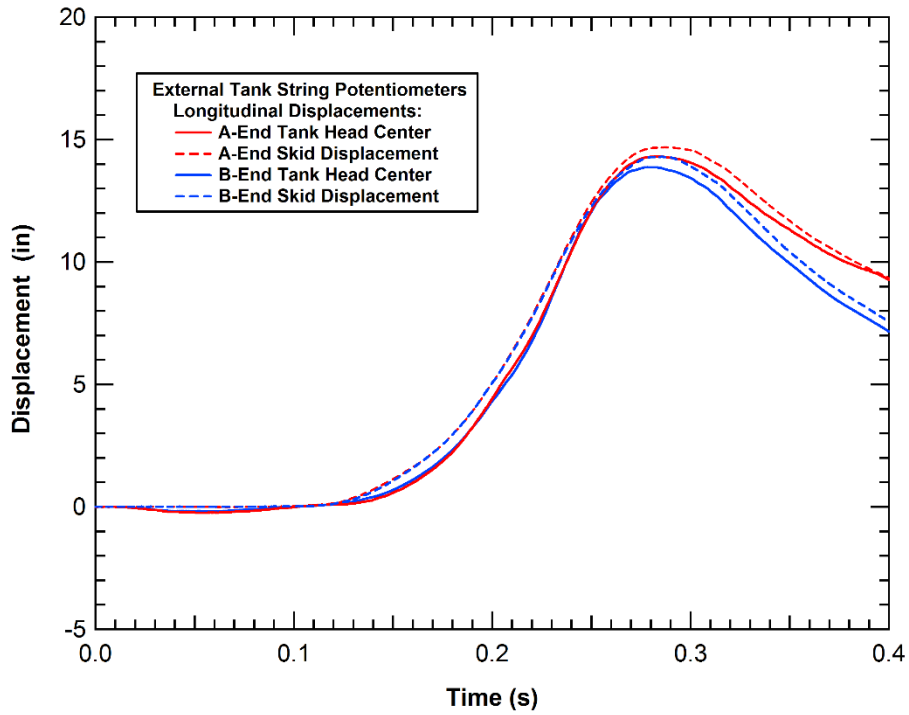
Figure 18. Measured test tank external car end displacement histories.

3.4   Material Testing

For model validation, it is important to characterize the actual material properties of the test article from tensile tests, in order to compare them to the material model inputs. After the impact test, five samples were cut from the tank shell and sent for material testing according to ASTM E8M-13a tension testing of metallic materials [22]. The results from the testing are summarized in this section. Appendix D contains additional details from the tank car material tests.

Following the impact test, cracks were observed close to the heating coil welds. Welds are stress concentrators and could initiate cracks. Also, the weld material and heat affected zone around a weld often have different mechanical properties than the base metal, which can influence the overall strength of the design. As such, two samples (Nos. 4 and 5) were taken close to the heating coil welds in an attempt to quantify the weld's influence on the tank's mechanical properties. However, inspection of the samples after tensile testing indicated that only Sample 4 included a weld fusion zone, and also, has lower ductility than the base metal. Moreover, several nonmetallic inclusions were noticed in the fusion zone of the tested sample, as illustrated in Figure 19 and Figure 20.
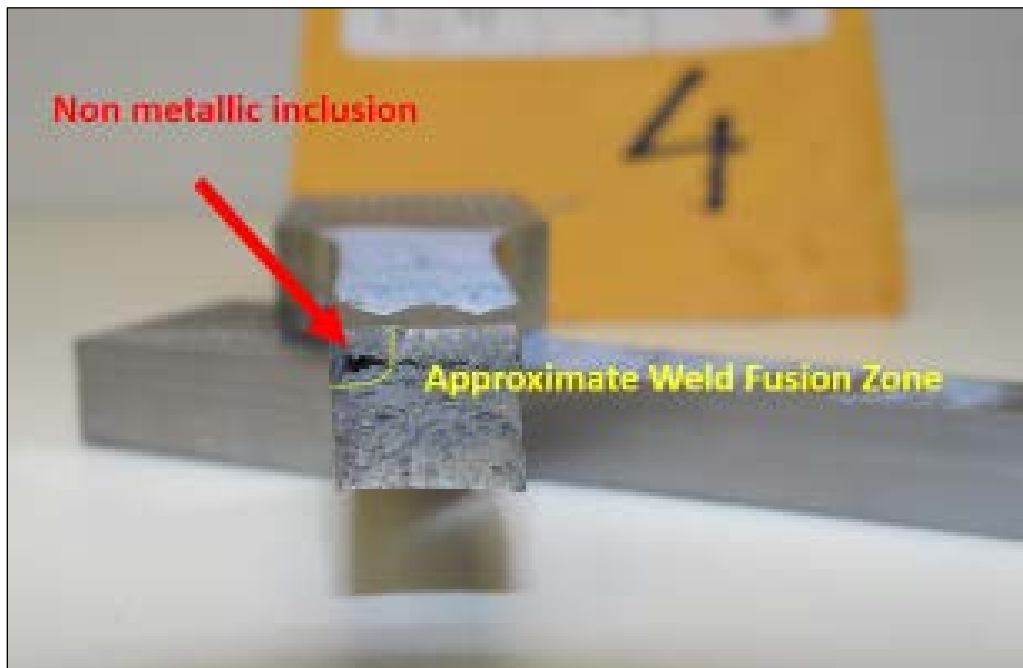
Figure 19. Material test Sample 4 — front view.
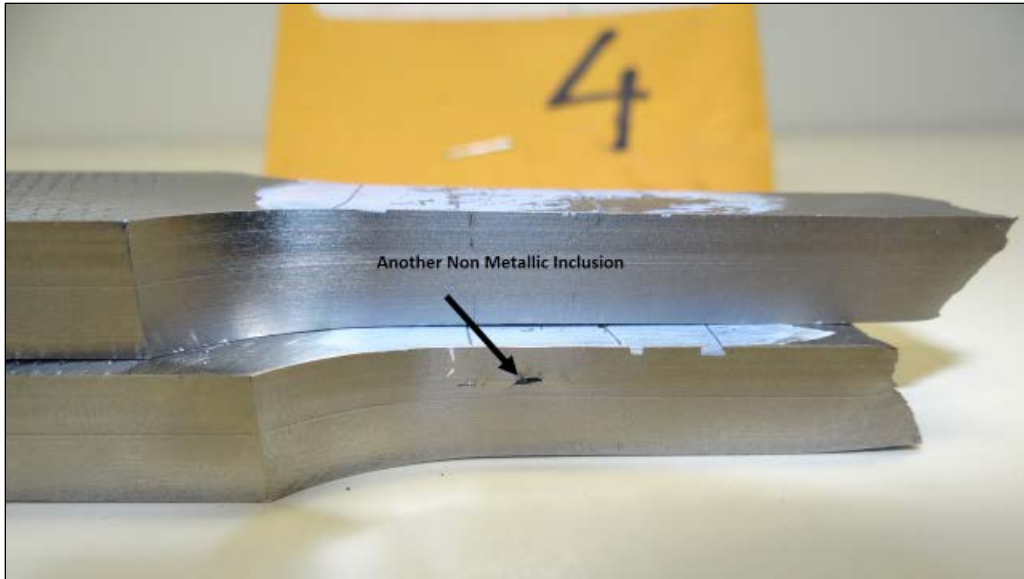
Figure 20. Material test Sample 4 — side view.

Figure 21, Figure 22, and Figure 23 compare the material properties of all tested samples. All samples meet the minimum requirements for ASTM A-515 Gr. 70 tank material: 70-90 ksi ultimate strength, 38 ksi minimum yield strength, and 21 percent elongation (for 2 inch gauge length). Sample 4 from the coil weld zone has approximately 2.5 percent higher ultimate strength, 5.5 percent higher yield strength, and 21 percent less ductility compared to the average of all the other base metal samples. While the Sample 4 data gives some indication of the influence of the weld with respect to the base metal properties, further material testing and investigation would be required to develop material properties suitable enough to refine the finite element analysis (FEA) models. In particular, tensile tests transverse to the weld direction that include the entire weld geometry would be helpful when characterizing the weld material degradation effects.
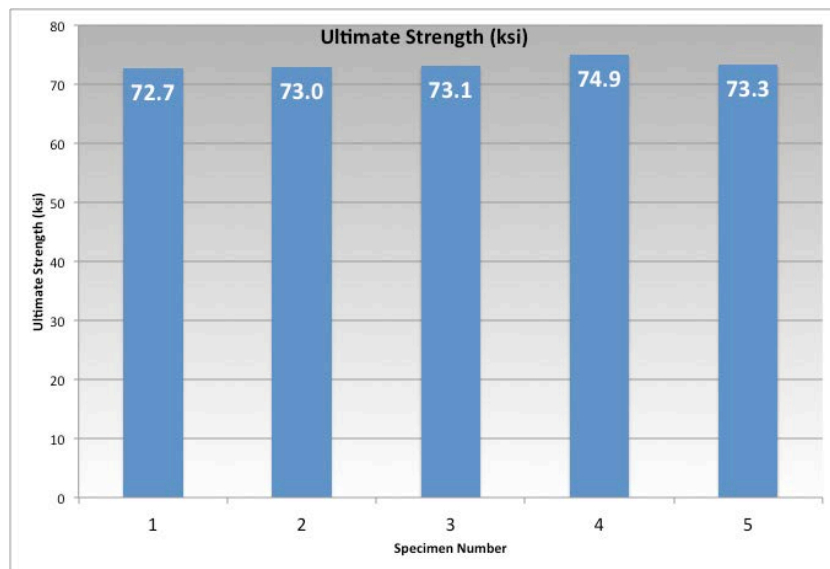
Figure 21. Material properties per sample — ultimate strength.

21
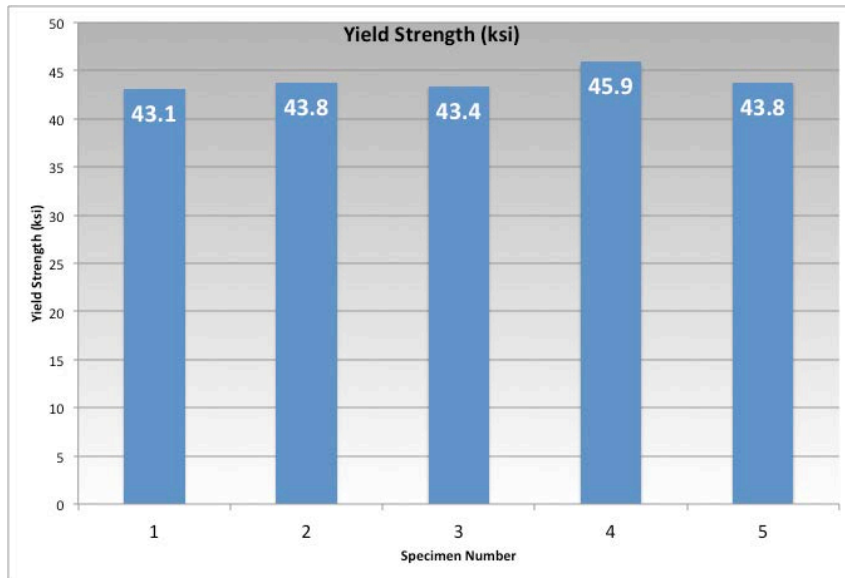
Figure 22. Material properties per sample — yield strength.
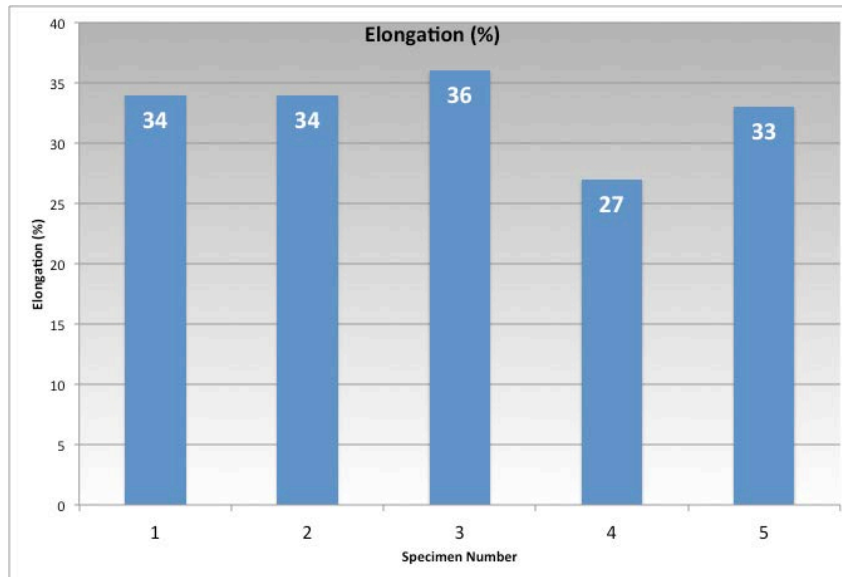
Figure 23. Material properties per sample — elongation at failure.

4. Model Development

4.1 Model Overview

The models of the DOT-111 tank car used to analyze the side impact test conditions were developed from drawings provided by FRA and by adapting models previously developed in past tank car research programs [2, 4]. The drawings used to develop the model were previously shown in Section 1.2.

Given the complexity, size, and time required to perform the analyses, several models were developed to examine different aspects of the tank's overall behavior. Two primary models were used.

The first primary model was a global model that includes a shell based model of the full tank car as well as models for the ram car and the test environment at TTCI. The purpose of this primary model was to predict the global motions and interactions of the test article, reaction wall, ground, and ram car.

The other primary model included a tank model with a detailed solid element patch in the impact zone, using a user defined Bao-Wierzbicki (BW) material model [5-7] validated for tank puncture analyses in previous research [4]. This model was simplified with far-field shell elements and had simplified boundary conditions. The purpose of this model was for detailed assessment of puncture force. The two models were considered separately to facilitate the assessment of global response and detailed puncture force calculation within the time available. All the features could not be combined into a single model due to model size, required run time, and numerical complexities, as well as the available computing resources and the limited schedule available to perform the pre-test calculations.

The models used to predict the test response are described in the following sections.

4.1.1 Material Constitutive and Damage Models

In order to accurately predict the nonlinear deformation and material behaviors under severe loading conditions, the tank car analyses required a material constitutive and damage model. A piecewise linear elastic-plastic constitutive model was used for this purpose (Material Type 24 in the modeling software package LS-DYNA). This model has been used extensively in many applications and is capable of reproducing the nonlinear stress-strain behavior of the material as it deforms into the plastic regime. The material parameters used in these constitutive models were developed from material test data on TC128B and A516-70 steel, developed under the Next Generation Rail Tank Car (NGRTC) program [4]. Reference 4 also provides a detailed description of the material constitutive model parameter development and validation against the test data.

The material constitutive model development process, described in Reference 4, starts with the engineering data collected from material characterization tests. This engineering data is converted to the true stress and true strain values that are used in the constitutive models of the finite element (FE) code. Finally, the material model is validated in a simulation of the material tests. A plot of the calculated engineering behavior compared to the test data for TC128B is shown in Figure 24. The data shows that the constitutive parameters accurately reproduce the material behaviors including the onset and development of necking in the specimen.
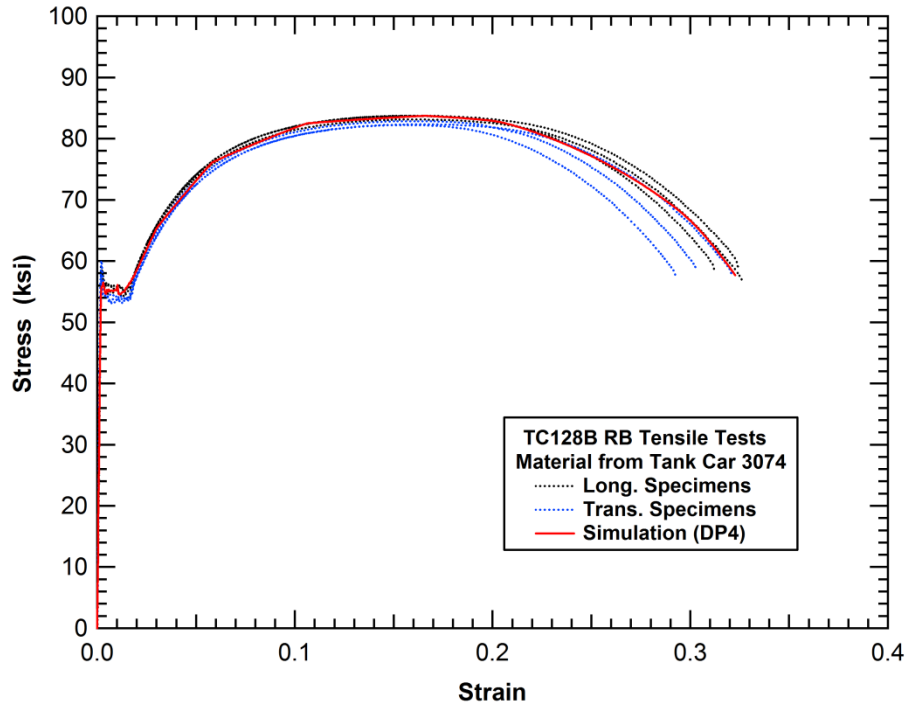
Figure 24. Comparison of the measured and calculated TC128B tensile test.

4.1.2 Bao-Wierzbicki Failure Surface

To accurately predict the puncture energies of tank cars for various impact conditions, the material model needed a detailed damage and failure assessment capability. The damage mechanics, or so-called local fracture mechanics (LFM) approach, provided enhanced capabilities for tank car design and puncture assessment.

LFM models the microstructural deformation and failure processes leading to fracture in terms of continuum parameters averaged over a small volume of material. In contrast to classical linear elastic and elastic-plastic fracture mechanics (LEFM and EPFM, respectively), which characterize fracture in terms of the conditions at the boundary of the fracture process zone while ignoring the details of the processes occurring in that zone, LFM focuses on the evolution of the process zone itself. Although LFM may initially seem more complex to formulate and more difficult to apply than LEFM/EPFM, it is more versatile and more general than the latter approaches. Local fracture mechanics methodologies are also ideally suited to implementation into finite element analyses where damage can be evaluated at the local element level.

The key mechanism in the ductile local fracture model for tank car puncture analyses is the influence of the stress state on the rate of damage development as the material undergoes plastic deformation. The primary stress state factor that controls the rate of damage development is the stress triaxiality, which is defined as the ratio of the mean stress to the equivalent stress ($\sigma_{mean}/\sigma_{eq}$). The mean stress (or hydrostatic stress) is the average of the three principal stresses (stresses on 3 orthogonal axes perpendicular to the principal planes upon which no shear stress exists). The equivalent stress, also referred to as the effective stress or the Von Mises stress, is defined as

$$\sigma_{eq} = \frac{1}{\sqrt{2}} \left[\left(\sigma_1 - \sigma_2 \right)^2 + \left(\sigma_2 - \sigma_3 \right)^2 + \left(\sigma_3 - \sigma_1 \right)^2 \right]^{1/2} \tag{1}$$

where σ_1, σ_2, and σ_3 are the three principal stresses.

There are many models that include the effects of stress triaxiality on damage development and ductility. Several of these have previously been applied within LS-DYNA to analyze various ductile fracture problems [e.g. 12-14], including the use of the Gurson-Tvergaard model [15-17] for the puncture assessment of pressure tank cars [18]. These models have the ability to include the stress triaxiality effects on ductility for tensile loading as illustrated in Figure 25. Many local damage models do not include the changes in damage development and failure for low triaxiality where the tensile damage and failure behavior transitions into a shear dominated fracture behavior. A concern that shear loads are important for tank car puncture assessments led to the selection of the Bao-Wierzbicki (BW) model in this effort [5-7].
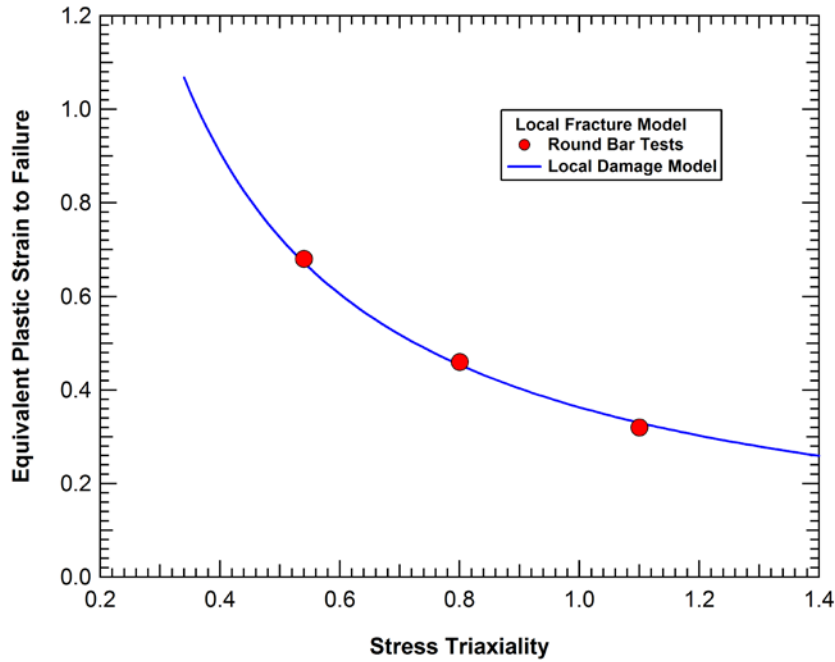
Figure 25. Local damage criterion for tensile ductile fracture analyses.

As implemented, the BW model is a basic form of a ductile fracture criterion [19]. It assumes that failure at a material location occurs when the damage within a surrounding characteristic volume (V_{MIC}) exceeds a critical value. The damage development and failure criterion can be written in the form:

$$D = \int \frac{d\varepsilon_{eq}^p}{\varepsilon_c \left(\sigma_{mean} / \sigma_{eq} \right)} = 1 \quad \text{over } V_{MIC} \tag{2}$$

where D is the normalized damage parameter, $d\varepsilon_{eq}^p$ is an increment in equivalent plastic strain, and $\varepsilon_c \left(\sigma_{mean} / \sigma_{eq} \right)$ is the critical failure strain as a function of the stress triaxiality. The characteristic volume (V_{MIC}) in this application is the element size, which was maintained with a characteristic element length of approximately 0.040 inch (1 mm) in the fracture zone. Damage

accumulation occurs with plastic deformations and the damage is tracked locally in each element in the model. When the damage level in any element exceeds the failure criterion (*D*=1), the local failure is propagated in the model by element erosion.

The critical strain function is proposed in the BW criterion and contains multiple branches depending on the range of the stress state as shown in Figure 26. The critical strain in each branch is governed by the equation

$$
\varepsilon_c\left(\sigma_{mean}/\sigma_{eq}\right) =
\begin{cases}
\infty & \left(\sigma_{mean}/\sigma_{eq}\right) \le -\dfrac{1}{3} \\[2ex]
\dfrac{A}{1+3\left(\sigma_{mean}/\sigma_{eq}\right)} & -\dfrac{1}{3} \le \left(\sigma_{mean}/\sigma_{eq}\right) \le 0 \\[2ex]
9(B-A)\left[\left(\sigma_{mean}/\sigma_{eq}\right)\right]^2 + A & 0 \le \left(\sigma_{mean}/\sigma_{eq}\right) \le \dfrac{1}{3} \\[2ex]
\dfrac{B}{3\left(\sigma_{mean}/\sigma_{eq}\right)} & \dfrac{1}{3} \le \left(\sigma_{mean}/\sigma_{eq}\right)
\end{cases}
\tag{3}
$$

And the parameters *A* and *B* can be determined by a series of tests under different stress conditions including notched tensile tests with specimens of varying notch radii [20] and tensile-shear tests with different ratios of tension to shear stress.
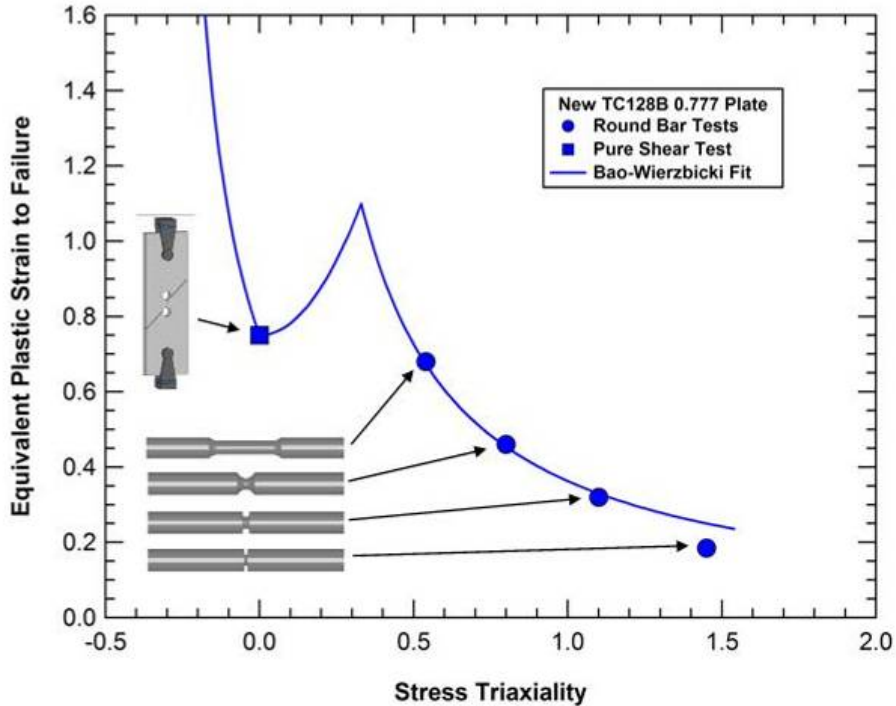
Figure 26. Bao-Wierzbicki failure surface and tests used for model calibration.

4.1.3 Global Response Model

The global response model represents the TTCI test setup used for the side impact test. As shown in Figure 27, the model includes a shell element-based DOT-111 tank car model mounted on skids, the full ram car, and the reaction wall, as well as ground and rail. The ram car, wall, ground, and ski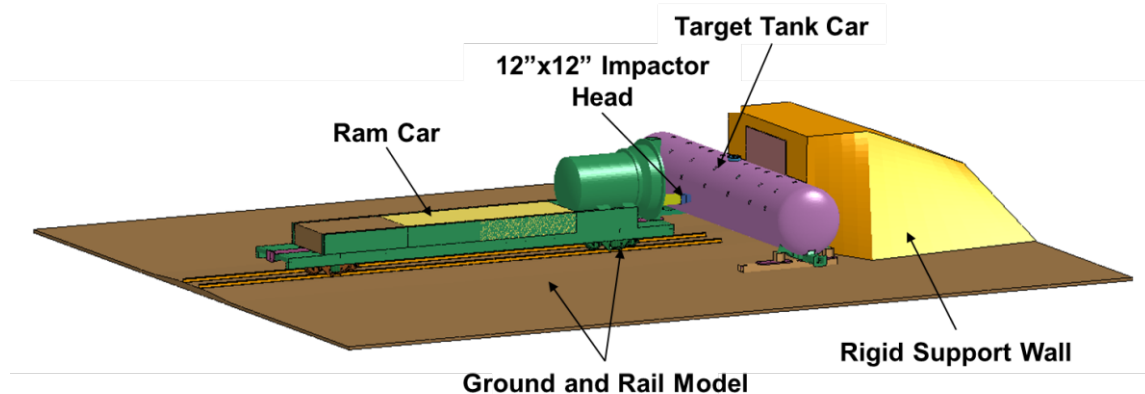d models were previously developed for other tests using the same equipment and facilities [10, 11] and were repurposed for this effort. Previously developed models for those components [4] were adapted for these analyses.

Figure 27. Global response model of DOT-111 tank car side impact test.

Figure 28 displays the model of the DOT-111 tank car that was used in the overall global response model. The DOT-111 model was adapted from previously created skid-mounted side impact tank car models, accounting for the length, diameter, and materials of the of the DOT-111 car. Note that the slight taper along the bottom of the DOT-111 was not accounted for in this model. It was assumed that treating the tank and jacket with a cylindrical geometry was adequate. Separate analyses were performed with other simplified models to assess the effect of the taper, which was found to be negligible.

For this global response model, the manway/top fitting model was reworked per the DOT-111 specification. Also, heater coils were added to the tank shell with a shell-edge-to-surface interface. Variation in material properties through the weld and heat affected zone (HAZ) were not explicitly treated in the model.
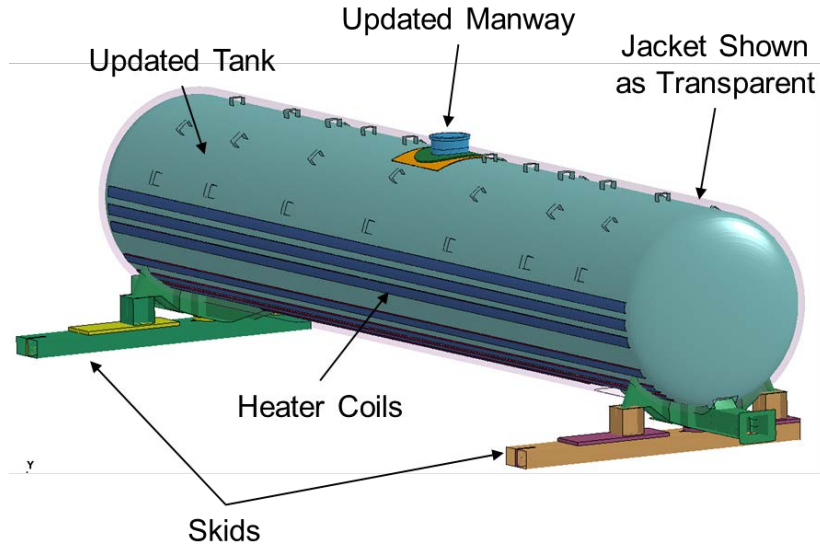
Figure 28. Skid mounted DOT-111 tank car model used in global response model.

To optimize run time, this tank car model was constructed entirely with shell elements, including in the impact zone. ARA's existing database of piecewise linear plasticity material models (LS-DYNA Material Type 24) was applied to the respective materials in the tank car. The model jacket, coil, and inner tank shell meshes were refined in the impact zone, with a typical element size of 0.5 inches. Elements transitioned to approximately 2 inches outside the impact zone. A detailed view of the inner tank and coil mesh in the impact zone is shown in Figure 29.
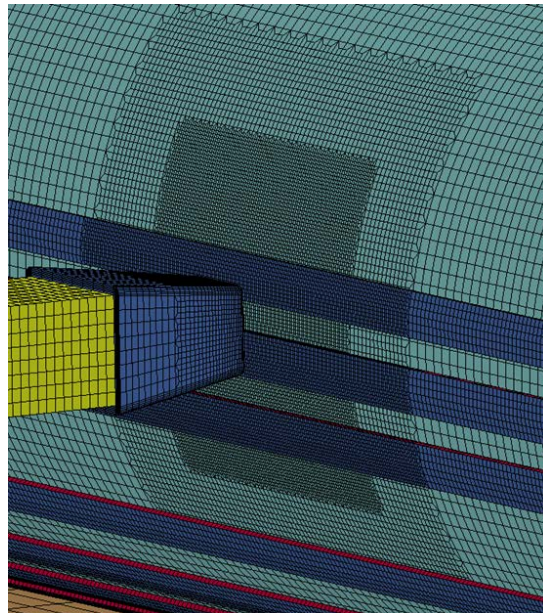
Figure 29. Impact zone of shell based tank in global response model.

Lading was accounted for in pre-test predictions with a lumped mass approach by increasing tank density. Subsequent sections will discuss how an explicit approach to modeling the lading with the global response model was investigated in post-test analyses. Regardless of the lading model approach, tank pressurization was modeled by defining a pressure-volume relationship for

a given outage volume. The relationship is based on the assumption that the outage volume has an ideal gas behavior at an initial pressure of one atmosphere and is compressed by the change in volume of the tank, with the lading having an incompressible fluid behavior. An example of the input pressure versus relative volume curve for the unpressurized tank with a 3 percent outage volume is shown in Figure 30. In the calculations, as the tank volume changed, the internal tank pressure was updated according to this defined relationship. The pressure was applied to all inner tank elements. At its initial volume, the tank pressure was set to 0 psig.
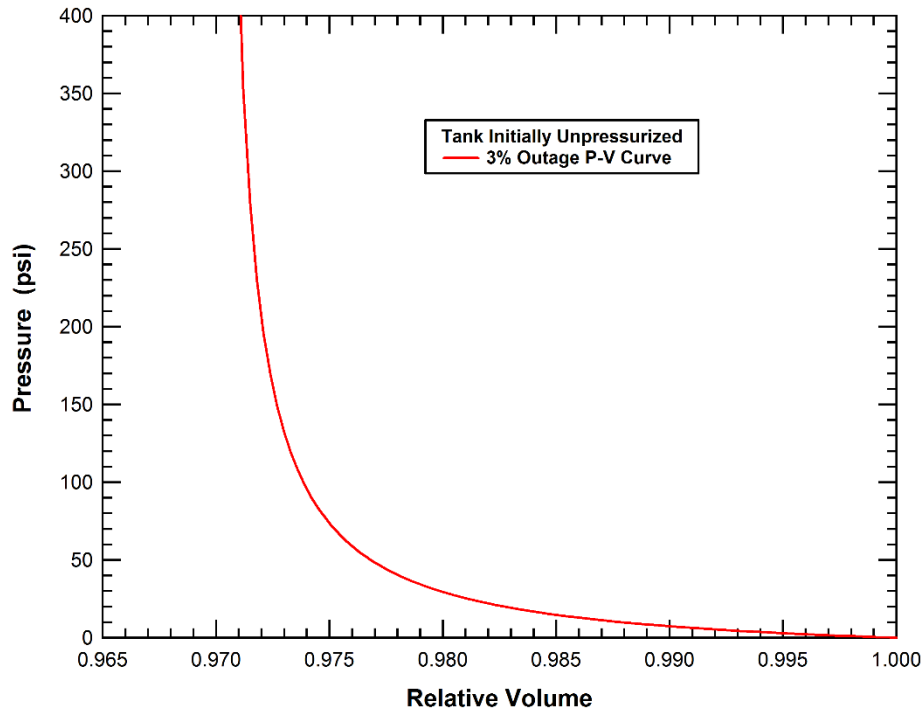
Figure 30. Pressure-volume curve for an unpressurized tank with 3 percent outage.

4.1.4 Puncture Model

A similar but separate model for the DOT-111 was developed for accurate puncture mechanism modeling and puncture force prediction. An overview of the puncture model is shown in Figure 31. This model employs an ARA-developed methodology that has been demonstrated to accurately predict tank puncture [2, 4]. The method involves using a highly refined solid element based mesh in the impact zone. User defined BW material models are used with the solid elements to accurately predict the stress-strain development, damage accumulation, and material failure. For this model, refined BW solids were used through the inner tank, heater coils, and outer jacket impact zone. A detail view of the impact zone with the solid inner tank and heater coil BW patch is shown in Figure 32.
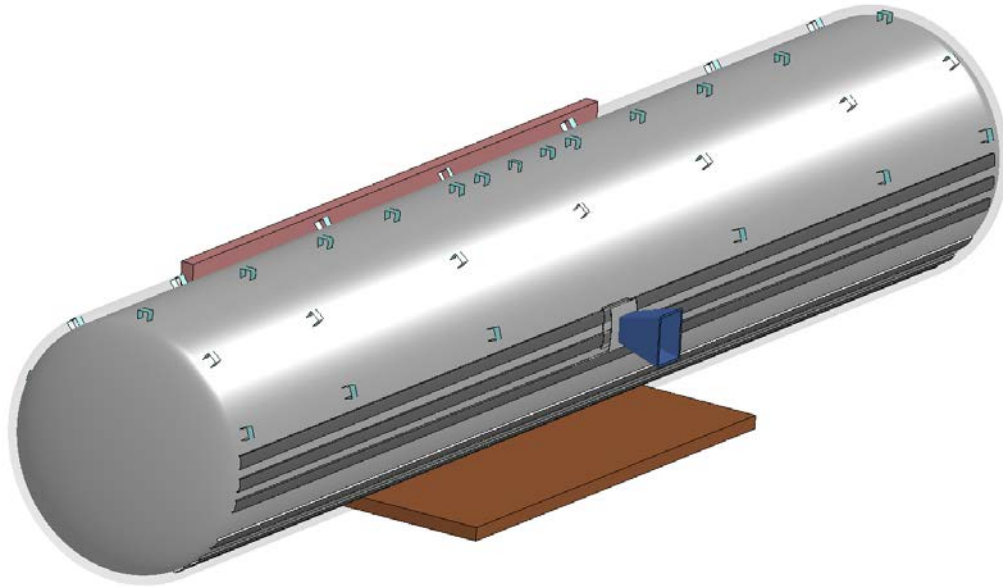
Figure 31. Puncture model overview.

Solid-shell constraint at Bao-Wierzbicki (BW) patch edge

Refined solid element BW patch in impact zone for jacket, tank, and coils.

Transition to larger elements in farfield
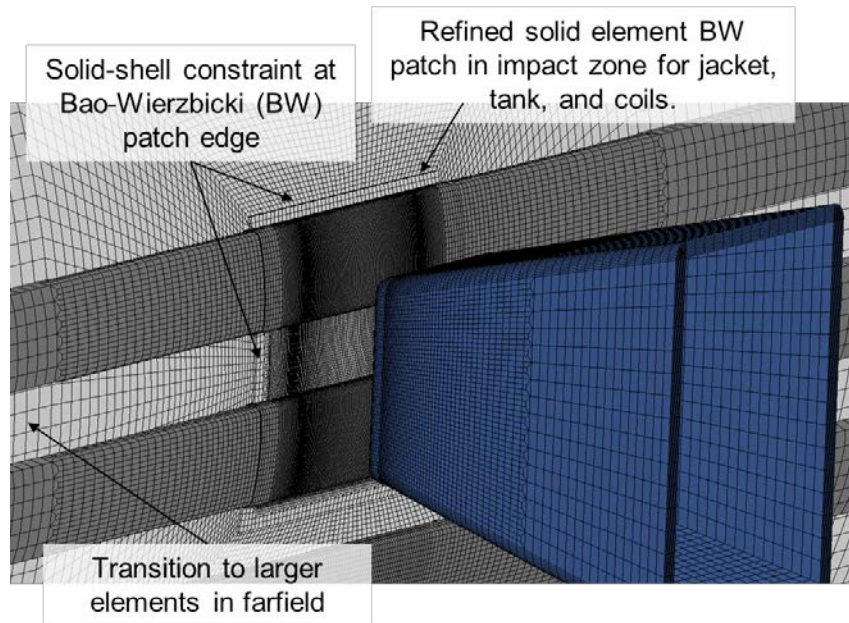
Figure 32. Close-up of impact patch in detailed puncture model.

The process of modelling the rest of the tank and jacket is similar to the shell based mesh approach developed for the global response model. To accurately predict puncture force, this level of refinement is needed though it comes at a high computational cost. Typical element sizes for the tank jacket and coils are as follows:

- Solid element BW impact zone: 0.05-0.1 inch (weighted toward impactor edges)

- Near-field shell transition zone: 0.25 to 1.0 inch

- Far-field shell elements: 2 inch

To optimize the calculation efficiency, other aspects of the model were simplified. For example, the ram only included the 12 x 12 impactor tip and the density of the tip was increased to account for the mass of the entire ram car. A simple rigid support wall was added behind the tank to represent the contact area with the reaction wall at TTCI. The pad below the tank (seen in Figure 31) was added after the team noted a concrete pad near the tank jacket. Initial calculations didn't have the vertical boundary. The stub sills, skids, and vertical support were not included, as they were far away from the impact zone. Likewise, gravity was neglected in the puncture model. The same volume-dependent tank pressurization approach was used again for the puncture model.

4.1.5 Simplified Shell Model

A simpler variation of the puncture model was used to quickly assess the contribution of various effects such as outage volume, tank geometry, impact speed, and so on. The significant change, compared to the puncture model, was that the impact zone was made up entirely of shell elements (Figure 33). The mesh is refined in the impact zone (0.4 inch element) to adequately model the pre-rupture response. The element count and overall complexity was kept low for more rapid assessment of variations than with the previous two models. These quick turnaround calculations were used to guide the inputs for the more complex and longer running models.
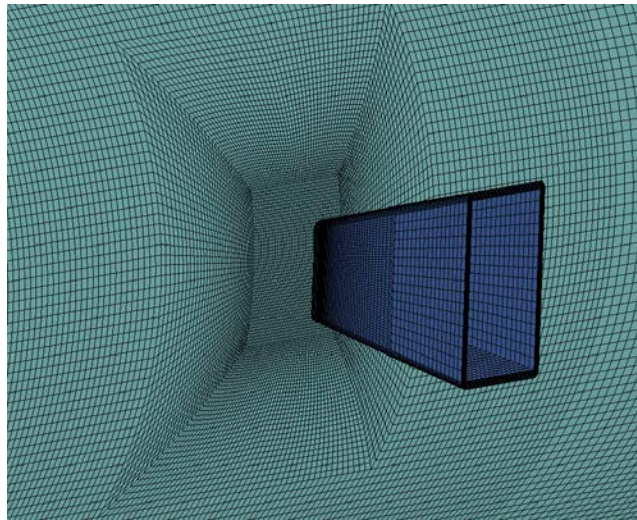
Figure 33. Close-up of simplified shell model impact zone.

Two variations of the simplified shell model used to study the effect of including the funnel flow geometry on the tank are shown in Figure 34. Other variations were set up to study the effect of heater coils and outage volume on impact force response.
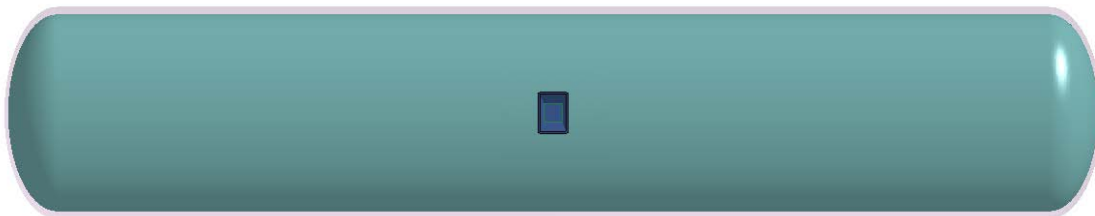
a) Straight cylinder (R34N)

31

Level line illustrates funnel flow geometry

b) Funnel flow, tapered profile at bottom of tank (R34P)

Figure 34. Simple shell model variations.

4.2   Pre-test Predictions

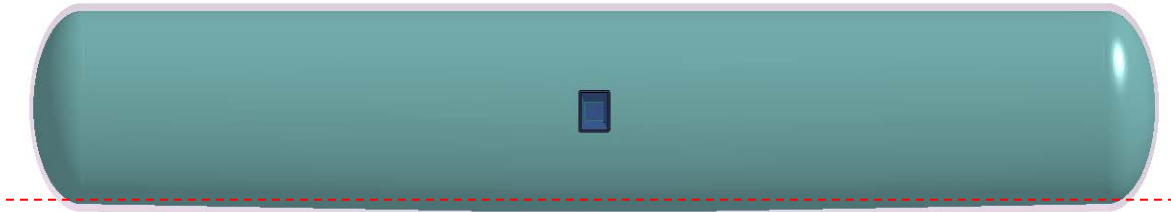A series of calculations were performed prior to conducting the side impact test. These calculations were used to guide the test conditions and to understand the expected response. Early calculations were performed with the simplified shell model to study the effects of various test parameters.

The first parameter to be examined was impact speed. The calculated impact force-displacement curve and dissipated impact energy are shown in Figure 35 for 12.5 and 15 mph impact speeds. As expected, impact speed has an influence on the tank car impact response. The higher speed collision has more inertial resistance and the overall force-displacement curve is shifted upward, which results in a corresponding increase in absorbed energy for the higher impact speed. The different impact speeds also have an influence on the timing and characteristics of the late time tank dynamics that cause the double peak behavior of the impact forces between 40 and 55 inches of displacement.

The second parameter to be investigated was the effect of the tapered bottom tank geometry (Figure 34b). The calculated impact force-displacement curve and dissipated impact energy are shown in Figure 36 for this geometry variation. The tapered geometry had much less influence on the overall response. As such, given the added complexity of mesh development when adding heater coils to the inner tank shell, the tapered geometry was neglected in the puncture and global response models.
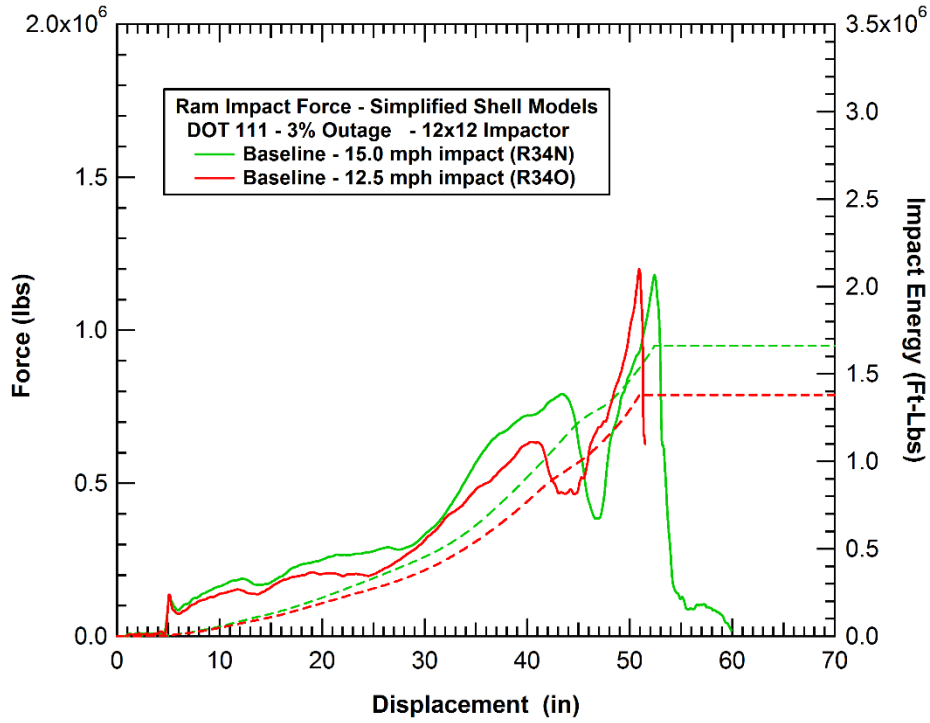
Figure 35. Comparison of impact response for different ram impact speeds.
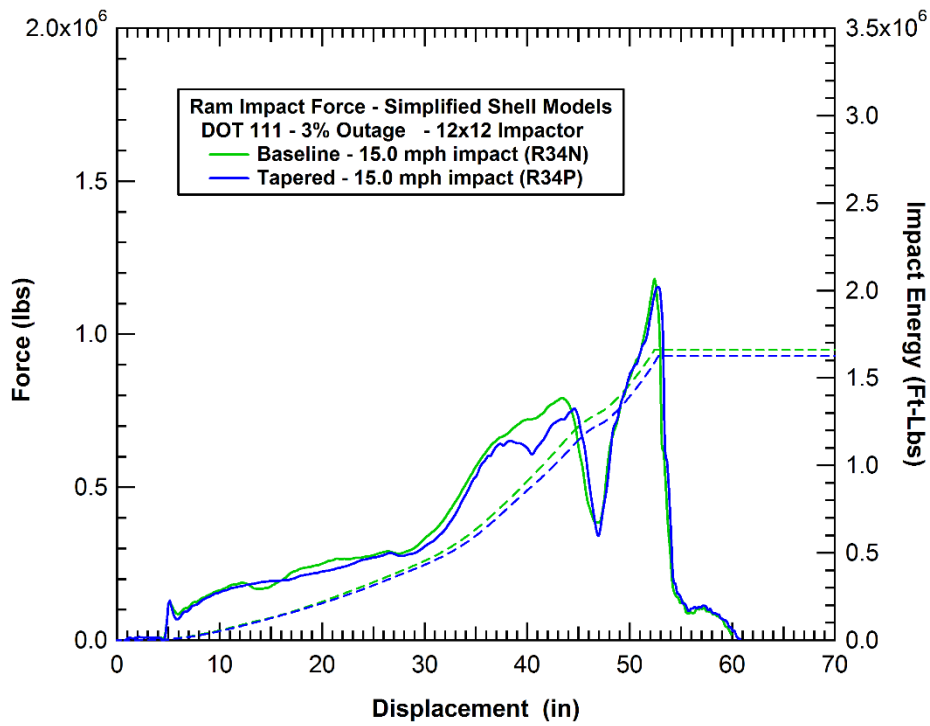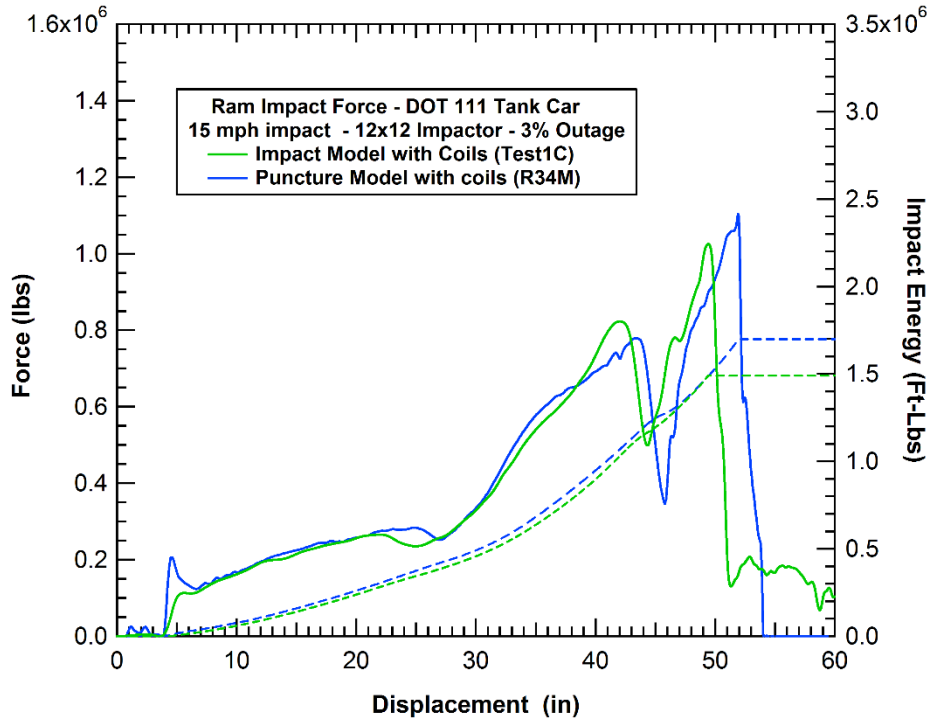

Figure 36. Comparison of impact response for straight and tapered bottom profiles.

The contribution to impact force and energy absorption from the heater coils was also evaluated. Figure 37 shows the effect evaluated by the detailed puncture model with and without heater coils. The predicted difference is relatively small but the added material and resistance from the coils adds about 5-10 percent to the predicted energy absorption compared to the bare tank/jacket variation. As a result, the coils were deemed a significant feature and were carried through subsequent analyses. One feature of the coils not included in these analyses is any potential reduction in ductility or damage tolerance as a result of the heater coil welds in the impact zone.
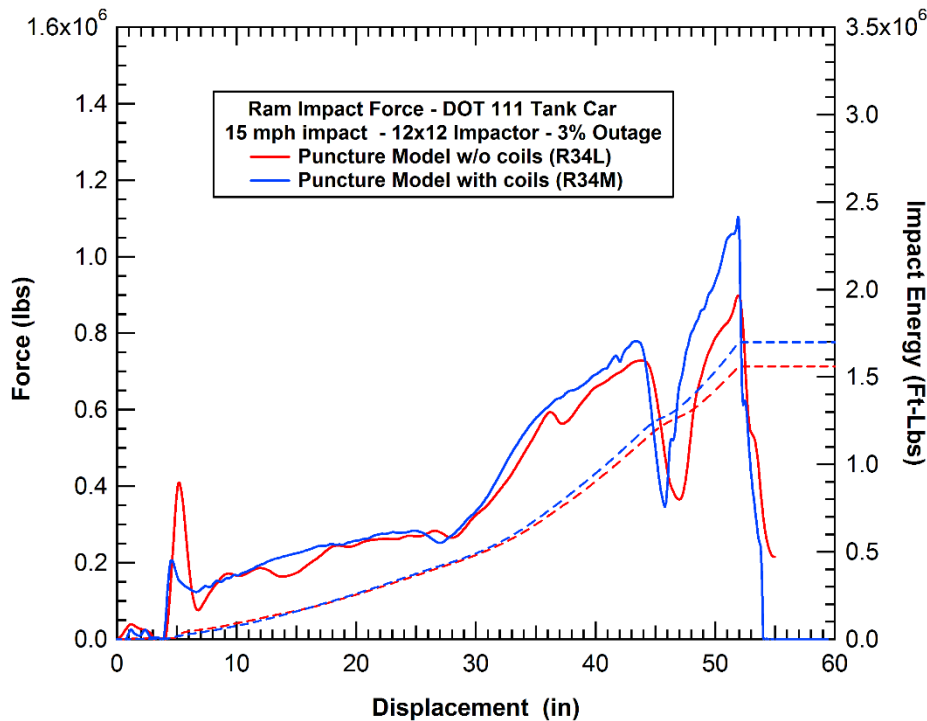
Figure 37. Assessment of the contribution of heater coils on the tank impact response.

The predicted impact force-displacement and integrated absorbed energy for a 15 mph impact with 3 percent outage volume is shown in Figure 38. Calculations were made using the global response model and the puncture model of the tank. The two models agree well up to about 40 inches of ram displacement where the predictions diverge slightly in the later time tank dynamic response. These dynamics could be influenced by factors such as the mass of the bolsters, sills, and skids attached at the ends of the tank. The shell-based global model has a slightly stiffer response and ruptures at a slightly reduced force with approximately 2-3 in less displacement than the puncture model. As a result, the more ductile puncture model predicts 13 percent more energy absorption. From the puncture model, for a 15 mph impact with 3 percent outage volume, the predicted rupture force was 1.1 million lbs and the energy absorbed was 1.7 million ft-lbs. This puncture energy corresponds to the kinetic energy of a 13.1 mph impact speed for the ram car.

Figure 38. Predicted force-displacement behaviors (15 mph impact at 3 percent outage).

5. Comparison of Test Response to Analysis

5.1   Test Observations

ARA personnel were on-site for the side impact test (summarized in Section 3.3) and documented several post-test observations for later comparison to the pre-test and post-test analyses. This section describes the observations, highlighting similarities and differences found between the observed test article and the predicted response.

5.1.1 Noted Features on Underside of Tank

Prior to the test, a few features were noted on the underside of the test tank that were not in the pre-test models. Figure 39 shows a heater coil fitting and what appears to be a cutout in the outer jacket in the vicinity of the fitting. These features were to the left of the tank centerline by about 2 ft. These features were not expected to significantly influence the test response and were not included in the pre- or post-test FEA models. Lastly, it was noted at the test site that the concrete pad shown in Figure 39 is in close proximity to a significant portion of the bottom of the tank center. This pad was not included in pre-test predictions. Evidence of tank/pad interaction was not clear from reviewing the test video and it was unclear whether contact and support from the concrete had any influence on overall tank motion. The pad was added to post-test simulations, which indicated that it had a slight interaction with the jacket near the tank centerline but the effect on overall response was negligible.

5.1.2 Inner Tank Failure Observations

Shortly after the test, the outer jacket was cut away from the impact zone to expose the punctured inner tank. Figure 40 and Figure 41 show the puncture zone from the left and right side of the impactor head, respectively. Looking at the post-test impressions and fracture patterns, it can be deduced that the tank rupture initiated on the right side of the ram head. The denting on the heater coils from the initial impact seen in Figure 40 slid to the left, relative to the ram tip, as a vertical tear opened on the right edge of the impact face. The tear, which extends above and below the impactor head, is shown in Figure 41.

The modeled rupture initiation, shown in Figure 42, is quite similar to observed test behavior. The rupture is a vertical crack corresponding to the edge of the impact head. Also, similar impact face denting is observed in the model and test article.

5.1.3 Buckle Modes Outside of Impact Zone

Localized cracking was observed at several locations along the heating coils, as shown in Figure 43. It initiated near the tank shell welds at points where the tank and coils plastically deformed. The relatively brittle weld and HAZ along with plastic hinge formation led to crack propagation extending to the coil and tank shell. While similar heater coil and tank shell buckling was seen in the pre-test models, the model's approach and refinement away from the puncture zone was not sufficient to capture these material failures. However, the absence of cracking in the models would not significantly influence the puncture force or other metrics of interest for this test. It was also noted from observing the test article that the heater coil welds appear larger than the 3/16 in specification (estimate closer to ½ in).
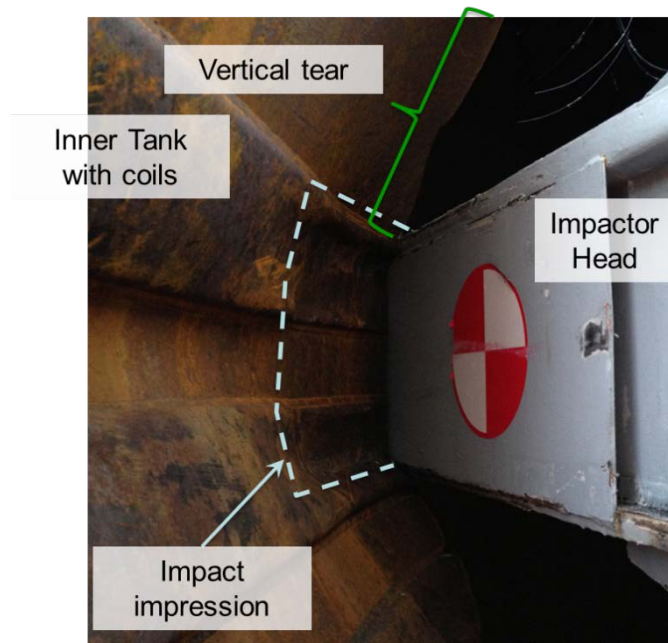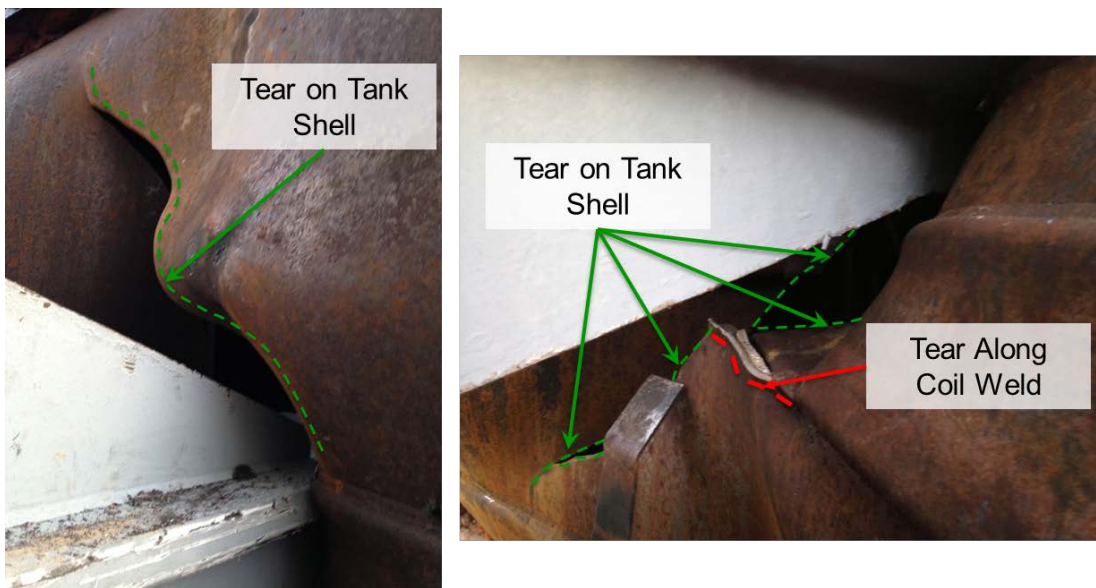
a) Localized jacket/tank transition
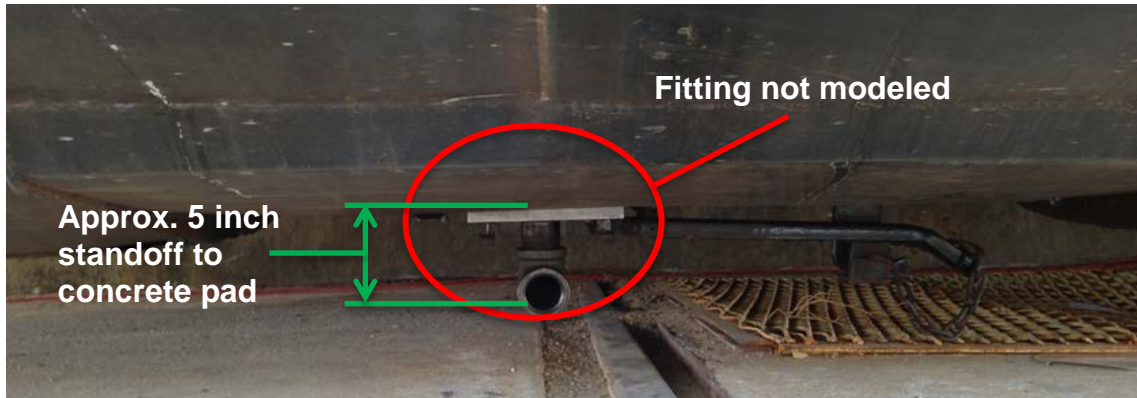
b) Concrete pad in close proximity to tank underside

Figure 39. Observed details on tank underside, not included in pre-test models.

Figure 40. Post-test impact face and tank rupture detail—left side of ram

a) View above ram

b) View below ram

Figure 41. Post-test impact face and tank rupture detail—right side of ram
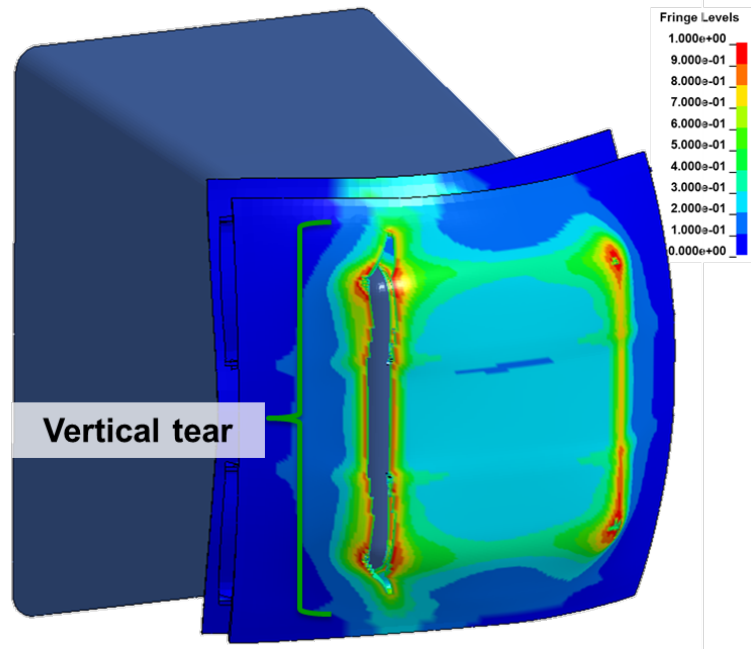
Figure 42. Modeled tank rupture response. View of Impact patch including jacket, coils, and inner tank, with fringes of damage (1=fully damaged).
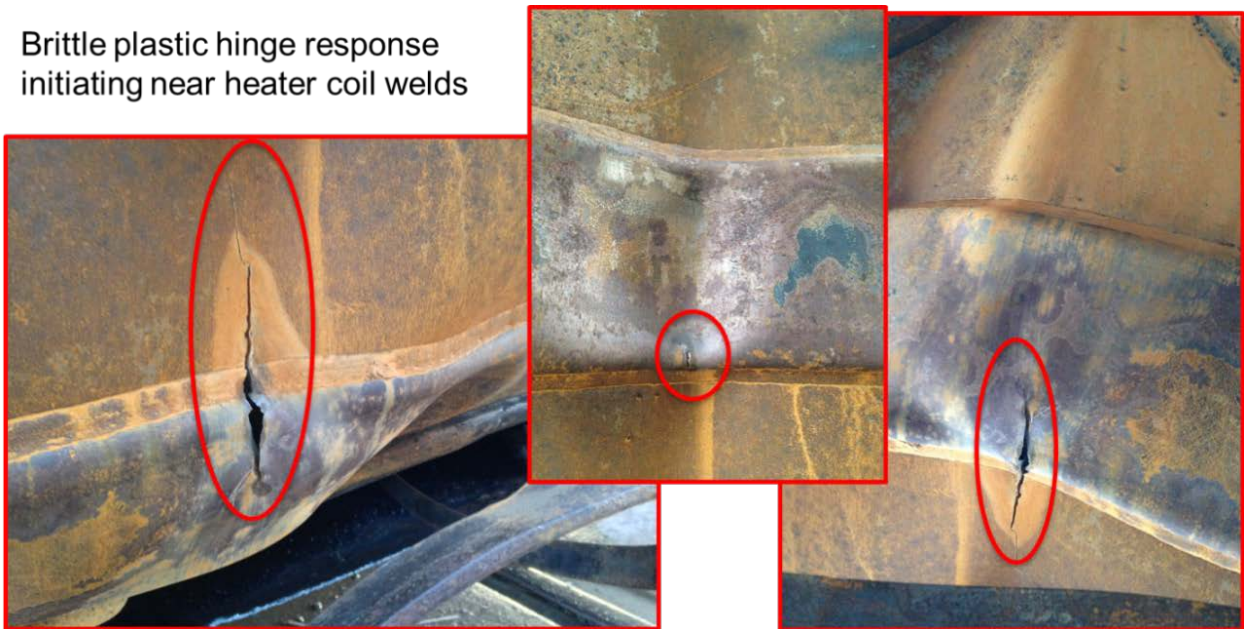
Figure 43. Localized cracking at coil-tank interface, away from impact zone.

Figure 44. Localized tank buckling between coils at tank center, near base of tank. Jacket cut away locally to expose inner tank.
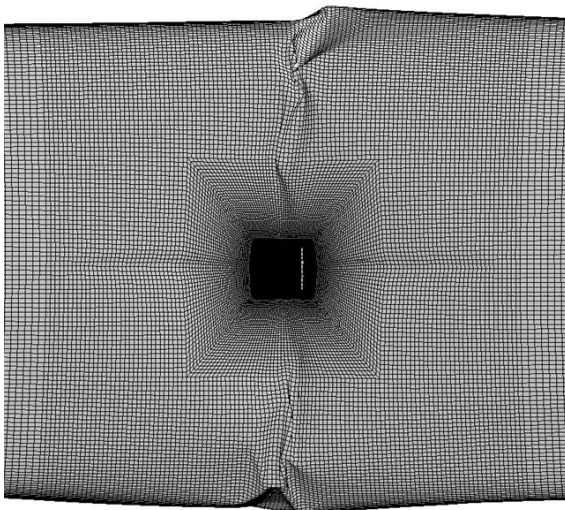
a) View with jacket   b) View without jacket

Figure 45. Modeled tank-centered buckling mode extends vertically across tank shell.

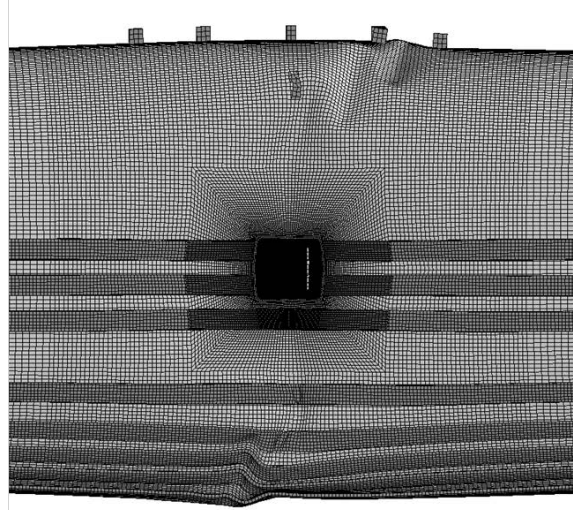Figure 44 shows another example of localized tank wall buckling that occurred between a pair of relatively stiff tank-centered underside coil return bends. While these centerline heater coil return bends were not modeled, Figure 45 shows that the pre-test model predicted similar overall tank-centered buckling patterns. Since the predominantly vertical buckling was captured by the models, as was the measured tank displacement (see Section 6.2), refining the models with details such as the return bends was not thought to be important in subsequent post-test modeling.

5.2 Comparison of Test Data to Pre-Test Analysis

5.2.1 Force-Deflection Response

A comparison of the puncture model's pre-test predictions and the measurements of the test's force-displacement behavior is shown in Figure 46. Note that the predictions were performed with an initial ram car speed of 15 mph, while the measured speed from the test was 14.04 mph. The difference in speed would lead to slightly different traces but not enough to explain the discrepancy. The peak puncture force seen in the test was 962 kips at 42 inches of displacement. The pre-test predictions with and without coils bounded the tested puncture force but at about 10 in more displacement. As a result, the predicted energy absorption was higher than tested.
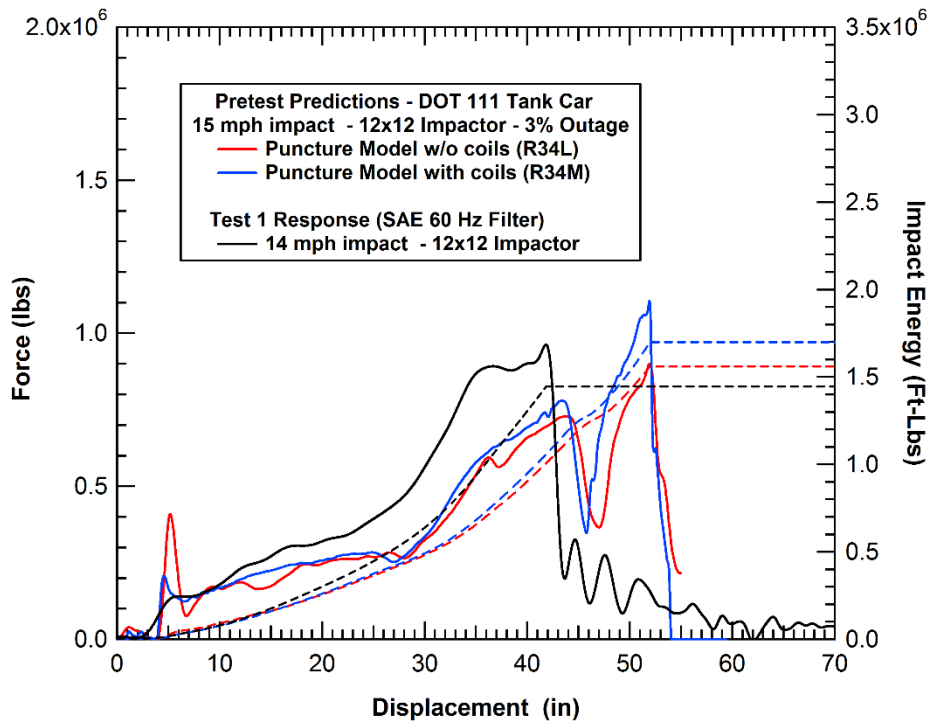
Figure 46. Comparison of predicted and measured force-displacement behavior.

The pre-test puncture model simulation with heater coils over-predicted the puncture force by approximately 14 percent. Note that the coil-tank welds were not included in these models. It is likely that much of the difference in puncture force resulted from the strength reduction caused by the heater coil welds extending through the puncture zone. Multiple fractures were observed near the coil welds, and they reflect the effects of stress concentrations and reduced ductility compared to the base metal properties. In the absence of material data to model the welds and

HAZ, the effect of the heater coil welds on failure initiation in the puncture zone was not considered directly. Characterizing weld materials in the vicinity of the impact zone on future test articles will help improve pre-test prediction accuracy.

From the data, it is evident that the response of the tank is significantly stiffer than predicted. This was suspected to be a result of a lower than expected outage volume, which led to more rapid tank pressure development and tank stiffness as the tank volume decreased under impact loading. At the low outage tested, the impact and puncture response is quite sensitive to variations in the outage volume.

To further investigate this discrepancy, the team compared the predicted tank internal pressure with an average of the measured tank pressure transducer traces (as shown in Figure 47). From the plot, it is evident that the measured test pressure leading up to puncture is higher than predicted. This is consistent with a lower than expected outage volume, and might explain why the tank was stiffer than predicted, resulting in a higher than predicted puncture force. Also note that a relief valve is not modeled, thus, the effects of any pressure venting are not included in the analyses (although these are expected to be small in the time scale of the impact event).
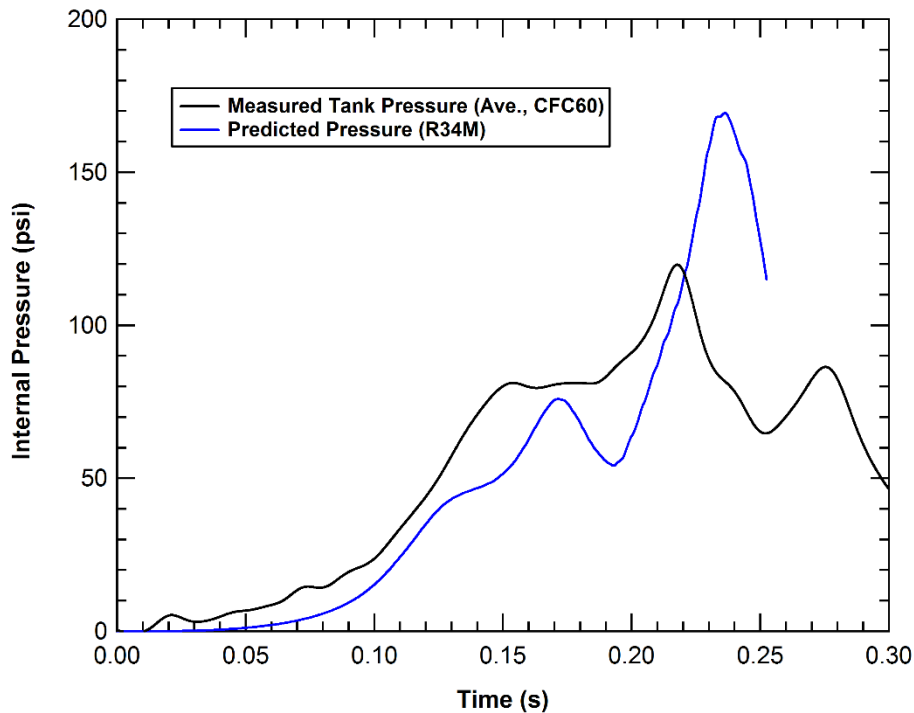
Figure 47. Comparison of the predicted and measured tank pressure histories.

Another significant discrepancy between the pre-test predictions and the measured responses is the double force peak that was predicted past 40 inches of displacement in the pre-test calculations (Figure 46) but was not observed in the test. In the calculations, a reduction in impact force was seen as the tank accelerated on its skids from the imparted ram load and before the reaction wall gave the deforming tank sufficient support to resist further displacement. Recall that the pre-test predictions combined the lading mass into the tank wall. Under these conditions, impact force and displacement is resisted by the stiffness of the jacket and tank material as well as the inertial effect of the lumped lading coupled into the tank wall. In reality,

42

the fluid lading would also create a load path between the front and rear tank walls and into the reaction wall. This effect is enhanced at low outage volumes like the one tested. In addition, the lading mass is not rigidly coupled to the tank structure. Thus, the magnitude and character of the dip in the pre-test force response predictions is influenced by the modeled treatment of lading as a lumped mass within the tank shell. Subsequent post-test modeling tested this theory with an explicit model of the fluid lading, which is discussed in more detail in Section 6.2.

5.2.2 Test Outage Volume Assessment

The pre-test analyses all assumed the outage was exactly at the 3 percent target value. The outage volume control in the test preparation was based measuring the volume of water added to the tank via a flow gauge and comparing it to the tank capacity (24,081 gallons stenciled on the tank head). In hindsight, this method was too crude to accurately measure the volume. A 1 percent error in the flow rate measurement would result in a 33 percent error in the final outage volume. Thus, precisely measuring the lading volume should improve pre-test predictions in the future.

To confirm that the outage volume was lower than expected, a post-test calculation was performed. Fortunately during the test preparations, the distance between the top of the water lading and the top of the tank (at the nozzle location) was measured at 6.0 in. Using calculations of the tank geometry, this outage height indicates that the actual outage in the test was between 2.1 percent and 2.3 percent. Post-test analyses, discussed in Section 6.1, indicate that the impact response is consistent with an outage volume between 2-2.5 percent.

5.3   Post-Test Observation Conclusions

Overall, the tank puncture and secondary buckling modes were close to pre-test predictions. The impact force history was similar to predictions with some specific areas identified for improving the correlation. Stress concentrations and reduced ductility around the heater coil welds observed in the test probably accounted for the discrepancy between the predicted and measured puncture force.

It was noted that the impact force response is sensitive to variation in the outage volume, especially for low outage percentages. Based on the test plan, pre-test predictions assumed the outage to be 3 percent. Subsequent post-test analysis, discussed in Section 4, indicated that the actual tested outage volume was likely closer to 2-2.5 percent. Precise measurement of the lading volume is required to improve pre-test predictions of future tests.

Another primary conclusion was that the lading should be modeled explicitly for more accurate force-displacement prediction. It is expected that if explicitly modeled, the partially coupled lading-tank response would smooth out the dip in predicted force response, which was not observed in the test. This approach was analyzed and is discussed further in Section 6.

Several other mostly geometry-related differences listed below were observed while comparing the models to the as-tested hardware. These differences are expected to have relatively minor effect on analysis accuracy and, in most cases, were not explored extensively with further post-test analysis.

- Tapered geometry for funnel flow tank

- o Simplified as cylindrical in most models and demonstrated to have little effect on the response with simplified shell models.

- Proximity of concrete pad to tank underside

    - o Approximately 5 in. gap in test setup, interaction of pad and tank during test is a minor effect based on post-test modeled response. Included in final post-test models.

- Simplifications to coil geometry in model

    - o Semicircular end treatments neglected in model.

    - o Circumferential spacing differs from actual, especially closer to the tank heads, due to non-tapered modeled tank geometry.

    - o These details occur well outside of the puncture zone and do not have a significant influence on puncture force or energy.

6. Post-Test Analysis

6.1 Effect of Outage Volume

Several post-test calculations were performed to explore the sensitivity of the impact force response to variations in the outage volume. As discussed in the previous section, it was suspected that the stiffer test article behavior and higher internal tank pressure, compared to pre-test predictions, could be partially be attributed to the tested outage volume being lower than expected. With less outage volume, the gas would compress to higher pressure faster as the tank dented and reduced in volume, thereby offering more outward support against the impacting ram.

The initial series of analyses used simple shell impact models of the tank at various outage volumes to investigate the influence on the force deflection behaviors. A series of pressure versus relative tank volume curves were developed for various outage volumes between 2 and 3 percent (Figure 48). The calculated force deflection response from the simplified analyses with outage volumes between 2 and 3 percent are compared in Figure 49. After comparing the test to the response of these variations, it was estimated that 2.0-2.25 percent outage will best match the test. This is in agreement with the calculated outage for the test based on the measured height of the outage prior to the test (2.1-2.3 percent). The corresponding tank pressure histories for the outage variations between 2 and 3 percent are shown in Figure 50. Again, these indicate that an outage in the range of 2-2.25 percent best matches the test. As a result, an outage volume of 2.25 percent was used for the explicit lading investigation discussed in the next section.
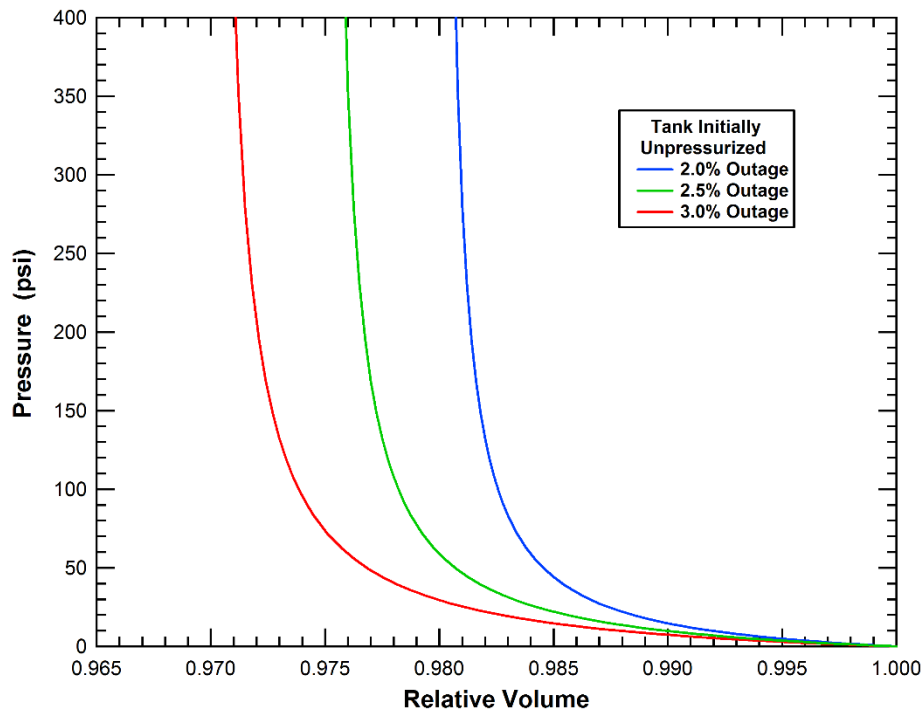
Figure 48. Pressure-volume curves for unpressurized tanks with 2-3 percent outage volumes.
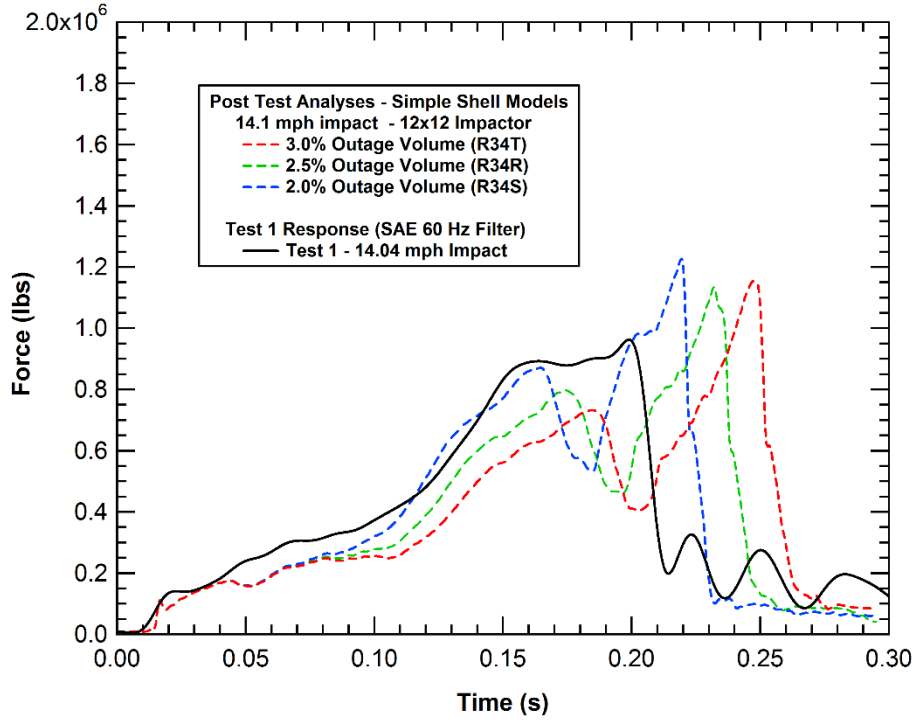
Figure 49. Effect of outage volume on impact force: 2-3 percent outage range (simple shell model without heater coils).
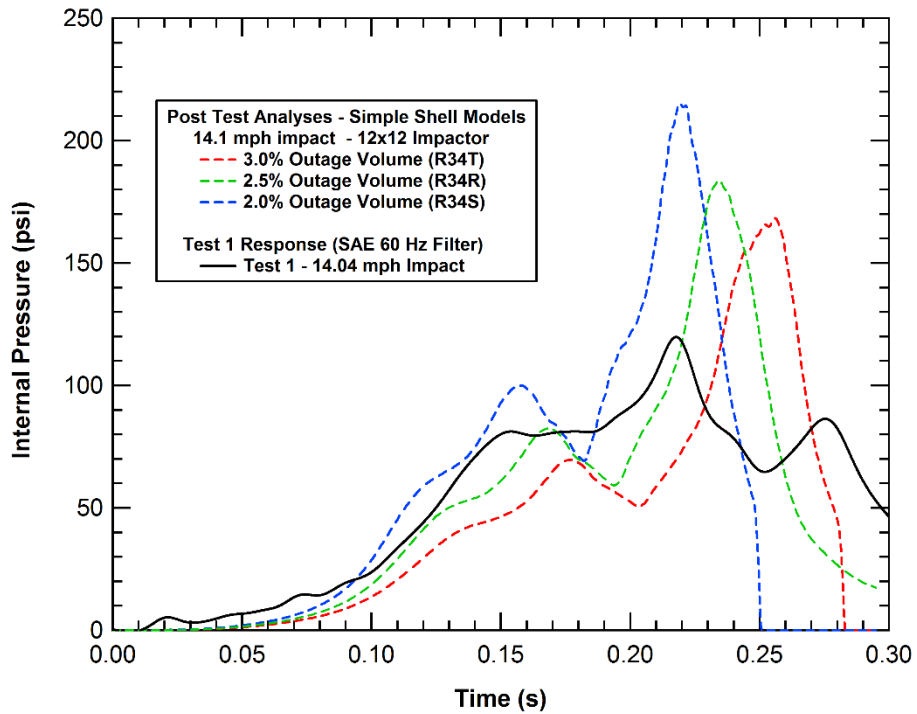
Figure 50. Effect of outage volume on impact pressures: 2-3 percent outage range (simple shell model without heater coils).

After quick calculations with the simple shell model were performed, the simulations were refined using the detailed puncture model with heater coils and at lower outage volumes. The calculated responses from 2.0 and 2.25 percent outages are shown in Figure 51. The revised calculations indicate a better agreement with the force-deflection behavior, especially in the early pre-puncture dent formation stage. Primarily, the discrepancies remain with the late time dynamics. Resolution of this detail was pursued with a detailed ALE lading model, which is discussed in the next section.
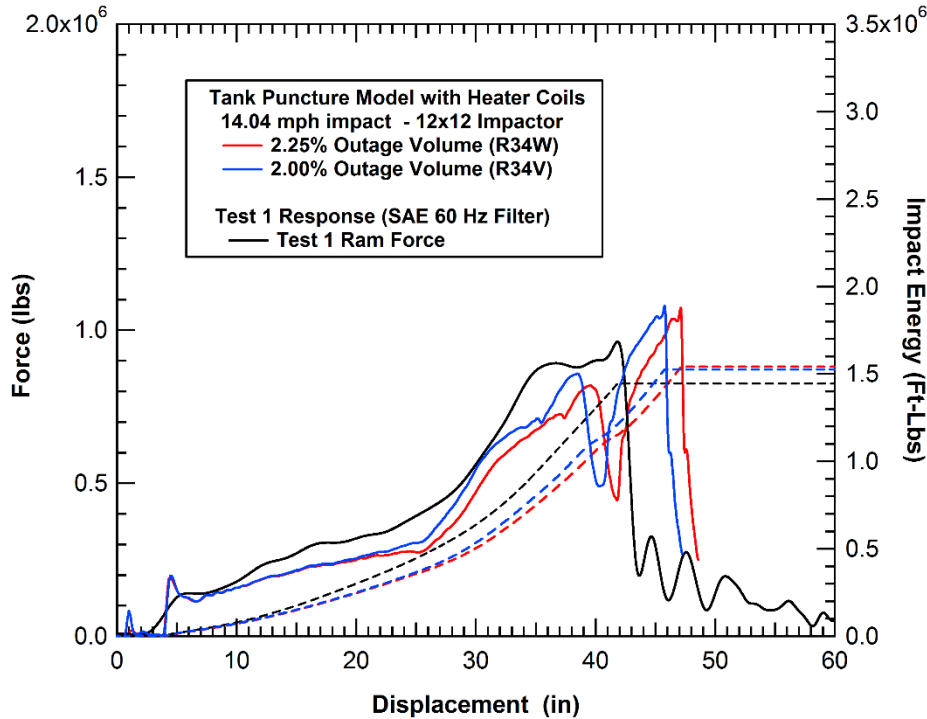
Figure 51. Effect of outage volume using simple shell models with heater coils (2.0 and 2.25 percent outage).

While the outage refinement doesn't account for all the discrepancy between the simulation and the test, it is still a significant change. The differences seen in the calculated response supports the recommendation for precise measurement of outage volume in subsequent tests to minimize pre-test model prediction uncertainty.

6.2 Explicit Treatment of Lading

In Section 5, it was concluded that the lading should be explicitly modeled to better simulate the force-deflection behavior observed in the test. The pre-test analyses used a lumped mass approach for the lading by increasing the inner tank density to obtain a combined weight of the tank and lading. It was expected that if the lading was explicitly modeled in the post-test environment, the effects of the tank lading dynamics would be accurately reproduced and smooth out the dip in predicted force response, which was not observed in the test.

To evaluate the effect of a coupled fluid-structure interaction (FSI) response, the global response model described in Section 4.1.3 was adapted to include an arbitrary Lagrangian-Eulerian (ALE) mesh to represent the fluid lading. The ALE mesh, shown in Figure 52, defines a fluid control volume that was set up to travel with the motion of the tank. In the analysis, the ALE fluid mesh

47

interacts with the existing Lagrangian tank shell. The control volume extends outside the initial tank surface to allow for the localized increase in radius as the tank dents and deforms under impact. Full enclosure of the tank shell throughout the calculation is important to capture the lading-tank interaction without leakage.
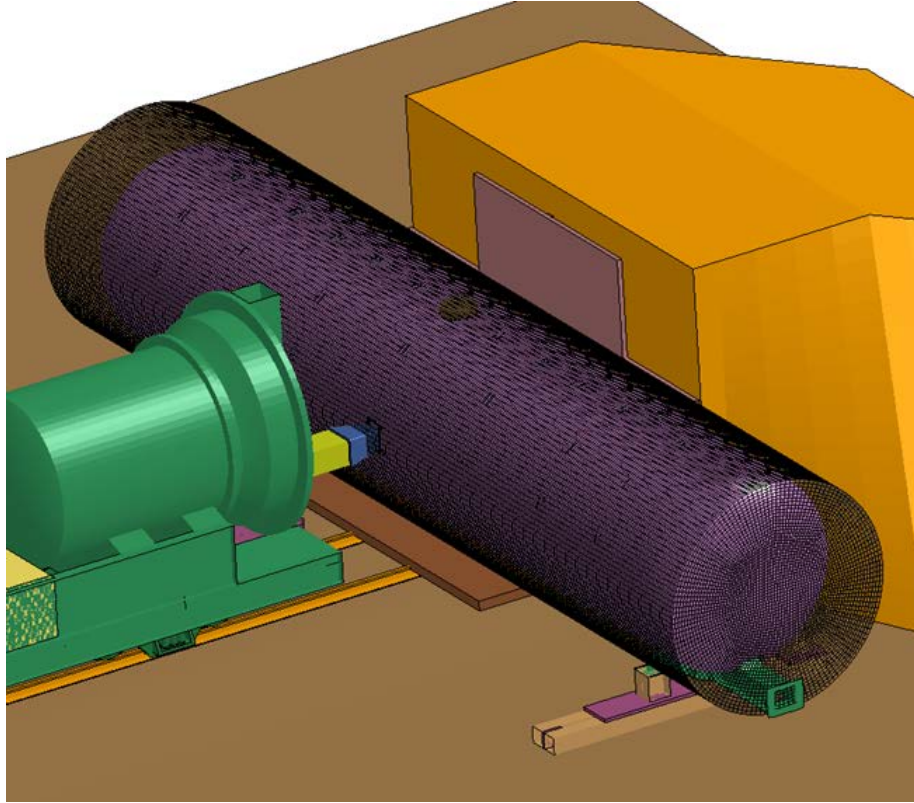
**Figure 52. ALE lading mesh added to the global response model.**

The fluid lading, shown in Figure 53, is modeled with the properties of water, which are summarized in Table 5.

Table 5. Fluid Lading Material Properties

Density, ρ	9.353e-5	lbf-s^2/in^4
	1000	kg/m^3
Dynamic Viscosity, μ	1.260e-7	lbf-s/in^2
	8.735e-4	Pa-s

Tank pressurization has been implemented independently of the lading modeling methodology through the *AIRBAG functionality in LS-DYNA, while a Pressure-Volume (P-V) relationship is specified and applied to the control volume defined by the initial undamaged tank shell. As the volume of the tank changes due to impact, the internal pressure changes according to the P-V relationship. Initially, the model was set up to calculate the P-V response directly through the ALE-structure coupling. In this approach, an ALE multi-material group would include the fluid lading as well as separate outage and outside air volumes in the ALE mesh. However, early calculations using this configuration showed that the ALE approach tends to diffuse the internal tank pressure across the FSI boundary (the tank wall). In other words, the tank didn't

48

realistically hold pressure as the volume decreased under impact load. Therefore, the airbag approach was the preferred pressurization method for both ALE and lumped mass lading model approaches. For this modified ALE approach, FSI coupling occurred only between the fluid lading and the tank. The ALE air materials effectively acted as a void volume into which the lading can flow, as governed by the dynamically changing tank and fluid free surface boundaries.


a) point of impact (0.10 s in simulation)   b) 0.24s after impact, at point of tank rupture
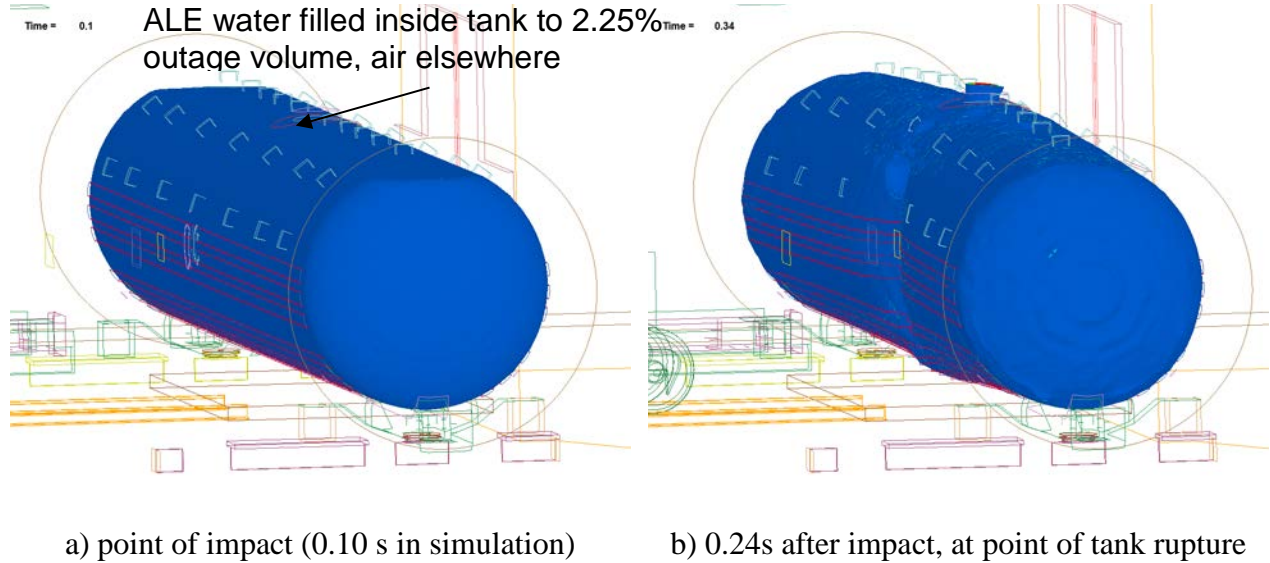
Figure 53. Illustration of impact induced deformation of ALE fluid lading within tank shell.

Although the internal tank pressure is not calculated directly with the ALE fluids, the lading dynamic pressure is still calculated as it flows and interacts with the tank shell. The modeled lading, outage gas, and outside air pressure were initially set to one standard atmosphere (14.7 psi). The fluid lading was set to cavitate when the pressure dropped by two atmospheres. Figure 54 shows snapshots of dynamic fluid pressure at various times (through a horizontal section at the tank and ram tip center). The pressure contours range from -14.7 psi (cavitation) to 100 psi. Note that gravity and tank pressurization is initialized over the first 100 milliseconds of the simulation. The time stamps on the images in Figure 53 and Figure 54 are in simulated time, including the initialization phase. Times relative to the point of impact point are also noted.
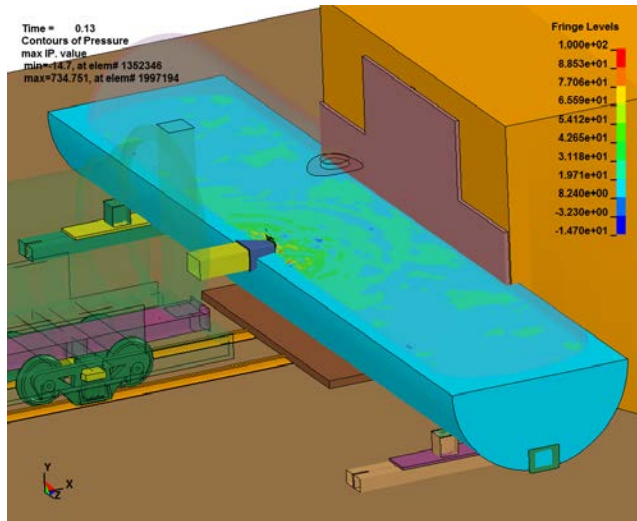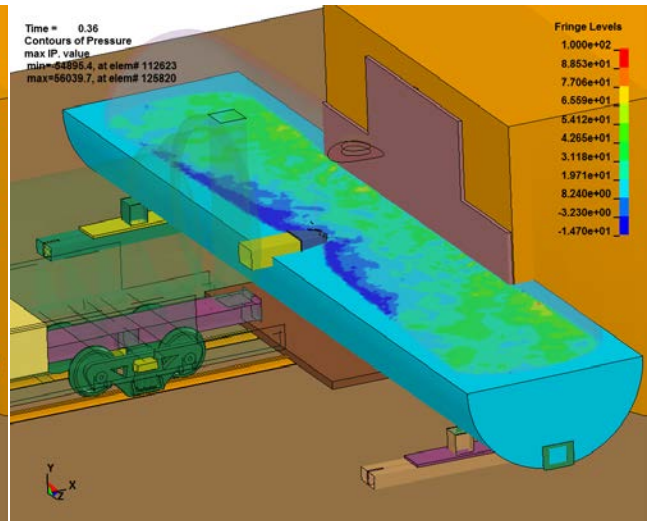
a) **Just after ram contacts inner tank (0.03 s after model initialization phase)**
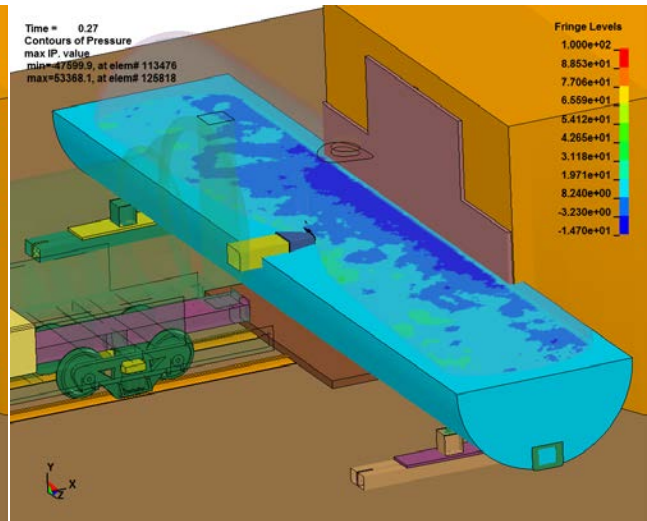
b) **Suction in fluid as rear tank wall moves toward reaction wall (0.17 s)**
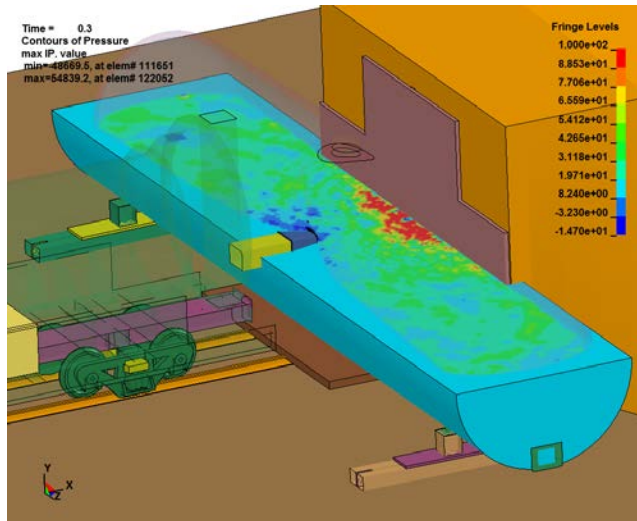
c) **Rear of tank impacts reaction wall, fluid drives into wall causing positive dynamic pressure in lading (0.20 s)**

d) **Just after tank rupture, front tank wall rebounds toward ram car causing negative dynamic pressure in lading (0.26 s)**

Figure 54. Illustration of dynamic lading pressure within ALE control volume. (ALE sectioned to show fluid pressure, some tank and ram parts transparent)

Figure 55 compares the measured and calculated force-displacement behaviors with the ALE lading model. In this figure, the force-displacement response is a much better match than previous analyses with a lumped mass lading approach. From the early displacement, through the tank stiffening that occurs around 30 inches, and to the elimination of the sharp unloading seen in previous simulations, the model tracks with the tested response quite well. As seen in previous comparisons, the rupture force and ductility are expected to be over-predicted in this shell based global model. The higher ductility of this model results in higher energy absorption compared to the side puncture test, though most of the energy-displacement curve tracks very well. It is expected that the detailed puncture model with the solid BW patch would be more accurate at pinpointing rupture. Unfortunately, the added numerical complexity of combining the puncture model with the ALE model would significantly increase runtime for models that are already computationally expensive. This combination was not undertaken for this post-test investigation but should be considered for future efforts.
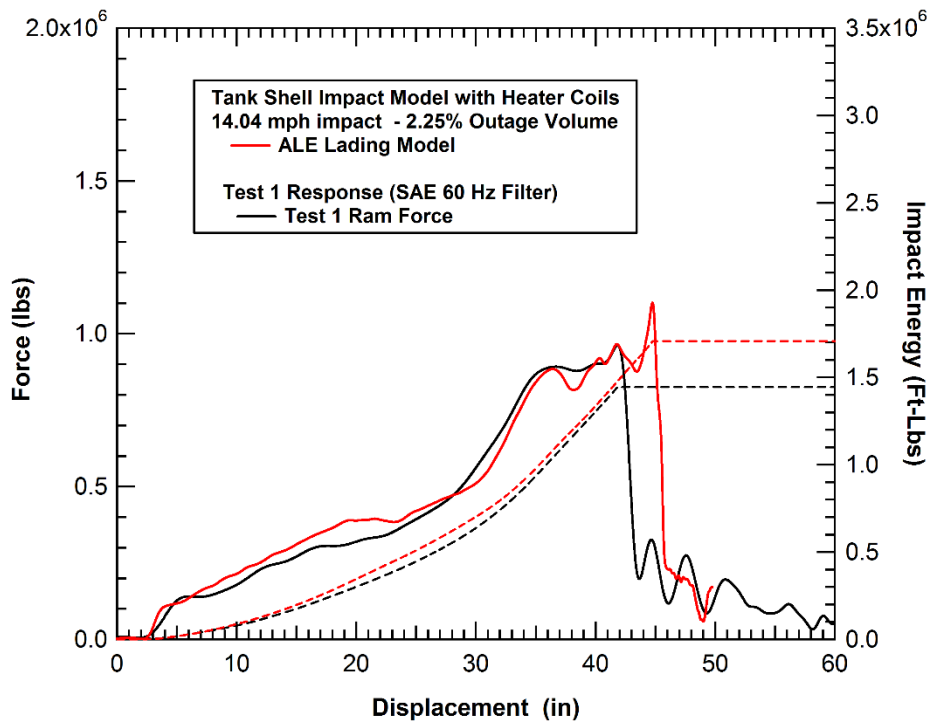
Figure 55. Predicted force and energy response with explicit lading model.

Figure 58 compares the internal tank pressure as it is predicted by the ALE lading with the measured pressure as a function of the ram displacement. The model tracks reasonably well with the average test pressure, except for the final pressure spike near rupture and post-rupture response. Note that some discrepancies are expected because the pressures compared in the figure were obtained somewhat differently; the test trace is an average of dynamic pressure measurements at discrete points, while the calculated trace is the hydrostatic pressure obtained from the P-V methodology in the analysis. The peak pressure discrepancy seen in the figure is due to slightly delayed rupture behavior and elevated puncture strength in the analyses. In this region of the tank response, the rapidly decreasing tank outage volume near peak compression causes a correspondingly rapid rise in tank pressure. The post-puncture release of pressure is also not accurately simulated with the control volume approach used in the analysis, which led to

51

differences in observed behavior. However, accurate post-puncture response modeling in this regard was not an objective of the analysis.
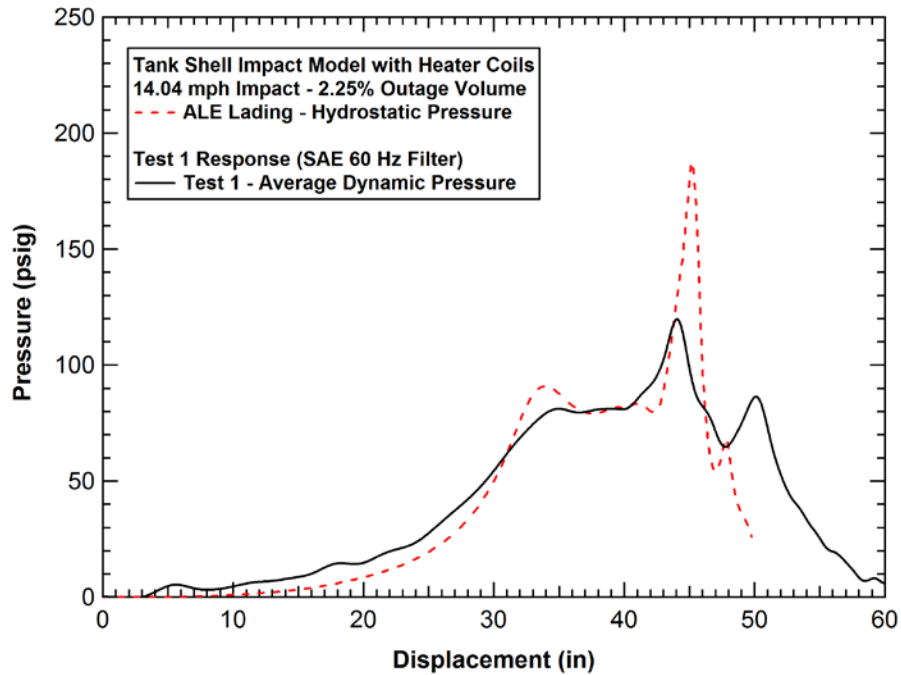
Figure 56. Predicted tank pressure with explicit lading model.

Figure 57 compares the predicted and measured displacements for the tank internal string potentiometers TD1 through TD5. Again, the calculated response shown is for the shell impact model with ALE fluid and a 2.25 percent outage. Note that the tank crush at the centered string pot locations TD 2, 3, and 4 (Y-direction) exceeded the limit of the instrumentation and the test traces max out at 24 inches. Overall, the comparison shows good agreement between the calculated and measured tank deflections. There are some small discrepancies in secondary dynamic oscillations. However, any oscillations in the post-puncture response (after 0.2s) would not necessarily be expected to be accurately captured. Again, the simulations match the test displacements well overall.
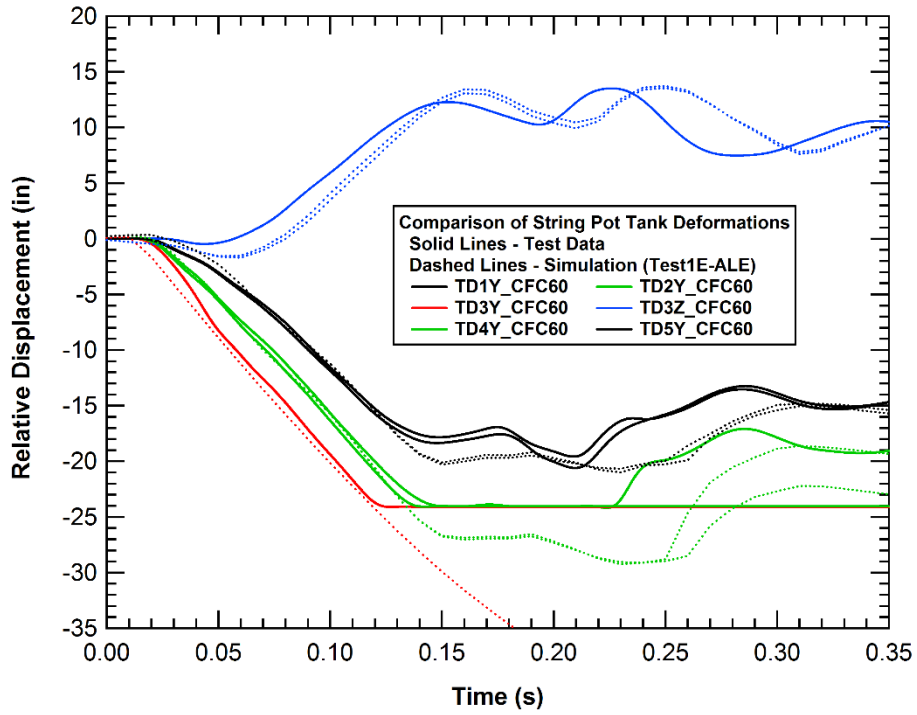
Figure 57. Comparison of calculated and measured tank displacements with explicit lading model.

7. Summary and Conclusions

This report documents the combined efforts of TTCI, and ARA to perform a side impact puncture test, to determine the baseline performance of a DOT-111A100W tank car. This research supports FRA's tank car research program to provide the technical basis for rule-making on enhanced and alternative performance standards for tank cars.

The side impact test was conducted to evaluate the performance of a legacy DOT111 car and to provide data for verifying and refining corresponding computational model(s). On December 18, 2013 at TTCI in Pueblo, Colorado, the tank car was impacted at 14.0 mph by a 297,125 lb ram car equipped with a 12-in x 12-in ram head. The ram head impacted the tank center and punctured both the external jacket and tank shell. The impact resulted in large dents of both the jacket and tank shell by the ram arm. The impact also caused one of the weld joints on the jacket near the impact area to fail, and the back of the tank car was also deformed by the reaction against the rigid impact barrier. All test requirements were met.

Cracks were observed close to the heating coil welds, which are stress concentrators and could initiate cracks. Further material analysis demonstrated that the tank car shell metal directly under the heating coil weld had lower ductility than the base metal. Moreover, several nonmetallic inclusions were noticed in the fusion zone. To better capture the effects of the welds and weld zone material properties in the finite element models, additional material characterization of weld zone properties may be beneficial. ARA performed both pre-test predictions and post-test analyses of the impact response to evaluate, validate, and improve puncture modeling capabilities. While the pre-test simulations predicted lower forces than measured over much of the impact period, the peak simulated force levels were about 14 percent higher than the measured force levels. However, it is likely that much of the difference resulted from the strength reduction caused by the heater coil welds extending through the puncture zone. The predicted puncture also occurred on the second peak of the force-displacement curve at about 10 inches more displacement than measured in the test. As a result, the predicted energy absorption was higher than measured.

In the post-test environment, an evaluation of the test conditions and modeling assumptions was performed to determine the sources of the discrepancy between the pre-test predictions and measured response. One source of potential variation was the tank outage assumed. When the test was planned and pre-test predictions were performed, a tank outage volume of 3 percent was assumed; the true outage volume in the test was approximately 2.1-2.3 percent. The pre-test prediction models were refined using the measured impact speed and the lower outage volumes. The revised predictions indicate better agreement in the force-deflection behavior, especially in the early pre-puncture dent formation stage. However, discrepancies remained in the late time dynamics.

Additionally, the pre-test approach in which the fluid mass was lumped together with the tank shell mass was enhanced by explicitly modeling the lading to evaluate the effect of a coupled FSI response, which allows the dynamic pressure of the lading's sloshing behavior to be calculated as part of the tank impact response. It was seen that this approached offered a much better match with the measured force deflection characteristics.

Overall, the comparison of the analyses and the test results demonstrates that impact behavior of tank cars can accurately be modeled. Lading slosh is probably more significant for this test condition than in previous tank side impact tests on pressure tank cars [4]. In the previous tests, the thicker tank structures and higher internal pressure produce a much higher initial structural stiffness that dominates the behavior, compared to the lading's sloshing loads.

8. References

1. Federal Railroad Administration. (9 December 2013). *Test Implementation Plan for FRA Tank Car Side Impact*.

2. SAE J211/1 Standard 1995. (2007). *Instrumentation for Impact Test – Part 1: Electronic Instrumentation*. SAE International.

3. Federal Railroad Administration. (March 2013). *Detailed Puncture Analyses of Various Tank Car Designs - Analysis of Different Impactor Threats and Impact Conditions*, Report No. DOT/FRA/ORD-13/17.

4. Applied Research Associates. (January 2009) "Detailed Puncture Analyses of Various Tank Car Designs,", Prepared for the Next Generation Railroad Tank Car (NGRTC) Project.

5. Bao, Y., & Wierzbicki, T., "On Fracture Locus in the Equivalent Strain and Stress Triaxiality Space," *International Journal of Mechanical Sciences*, 46, 81-98.

6. Bao, Y., & Wierzbicki, T., "A Comparative Study on Various Ductile Crack Formation Criteria," *Journal of Engineering Materials and Technology*, 126, 314-324.

7. Lee, Y-W., & Wierzbicki, T. (August 2004). *Quick Fracture Calibration for Industrial Use*, Massachusetts Institute of Technology Impact & Crashworthiness Laboratory, Report No. 115.

8. *Steel Construction Manual*. (2005). American Institute of Steel Construction, 13th Edition.

9. *Machinery's Handbook*. (1990). Industrial Press, 23rd Edition.

10. Transportation Technology Center, Inc, (8 October 2007). *Fully Instrumented Side Impact Test of Tank Car 3069*, Report No. P-07-033.

11. Transportation Technology Center, Inc. (8 October 2007). *Second Fully Instrumented Tank Car Baseline Side Impact Test of Tank Car 3074*, Report No. P-07-034.

12. Giovanola, J. H., & Kirkpatrick, S. W. (1992). "Applying a Simple Ductile Fracture Model to Fracture of Welded T-Joints," In J. H. Giovanola & A. J. Rosakis (Eds), *Advances in Local Fracture/Damage Models for the Analysis of Engineering Problems*, AMD Vol. 137, American Society of Mechanical Engineers, New York, pp. 285-303.

13. Giovanola, J.H., & Kirkpatrick, S.W. (1993) "Methodology for Evaluating Strength and Fracture Resistance of Weldments Using a Local Approach to Fracture," in Pennel, W.E., Bhandari, S., & G. Yagawa, (Eds), *Pressure Vessel Integrity-1993*, PVP-Vol. 250, American Society of Mechanical Engineers, New York.

14. Giovanola, J.H., Kirkpatrick, S.W., & Crocker, J.E. (9 September 1996). "Investigation of Scaling Effects in Elastic-Plastic Ductile Fracture Using the Local Approach," In *Proceedings of the First European Mechanics of Materials Conference on Local Approach to Fracture*, Euromech-Mechamat '96, Fontainebleau-France.

15. Gurson, A.L. (1977). "Continuum Theory of Ductile Rupture by Void Nucleation and Growth: Part 1—Yield Criteria and Flow Rules for Porous Ductile Media." *Journal of Engineering Materials and Technology*, Vol. 99, pp. 2-15.

16. Tvergaard, V. (1982). "On Localization in Ductile Materials Containing Spherical Voids." *International Journal of Fracture*, Vol. 18, pp. 237-252.

17. Tvergaard, V. (1990). "Material Failure by Void Growth to Coalescence." *Advances in Applied Mechanics*, Vol. 27, pp. 83-151.

18. Chlorine Institute (7 August 2006). *Quantifying and Enhancing Puncture Resistance in Railroad Tank Cars Carrying Hazardous Materials.*

19. Mudry, F. (1985). "Methodology and Applications of Local Criteria for Prediction of Ductile Tearing," *Elastic-Plastic Fracture Mechanics*, L. H. Larson (Ed.), ECSC, EEC, EAEC, Brussels and Luxembourg, Belgium, pp. 263-283.

20. Mackenzie, A. C., Hancock, J. W., & Brown, D. K. (1977). "On the Influence of State of Stress on Ductile Failure Initiation in High-Strength Steels," *Eng. Fracture Mechanics*, 9, 167-188.

21. Powers, Lucas. (9 July 2013). "Safety rules lag as oil transport by train rises - British Columbia." *CBC News*. Retrieved 10 July 2013.

22. ASTM Standard E8/E8M-13a (July 2013). *Standard Test Methods for Tension Testing of Metallic Materials*. ASTM International, doi:10.1520/E0008_E0008M.

Appendix A.   Photographs of the Impact Test

Figure A-1 Impact Wall

Figure A-2. DOT-111 Tank Car

Figure A-3. Ram Indenter Alignment and Trigger System
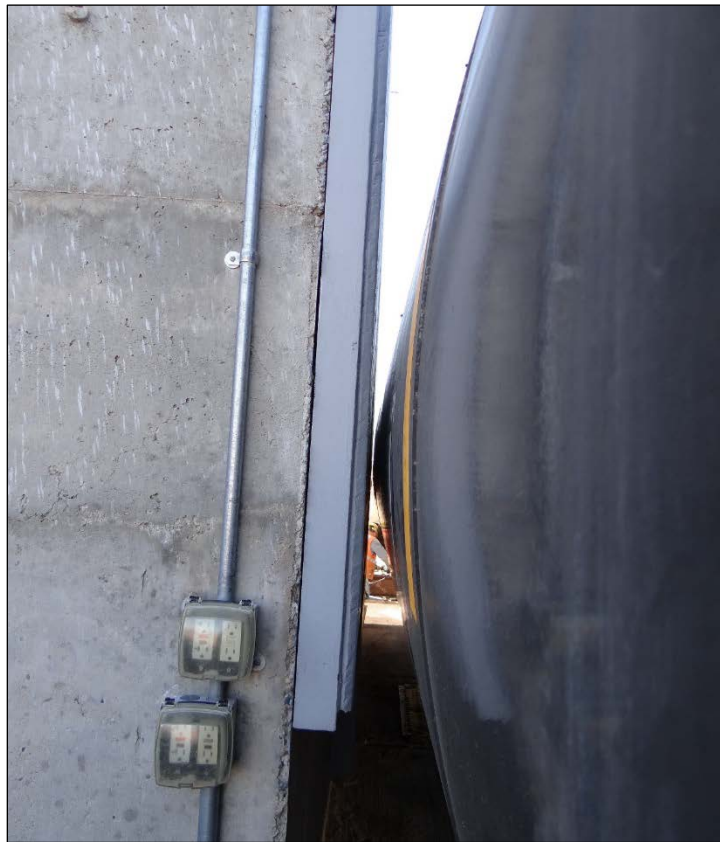
Figure A-4. Distance between Impact Wall and Tank Car (Pre-Test)
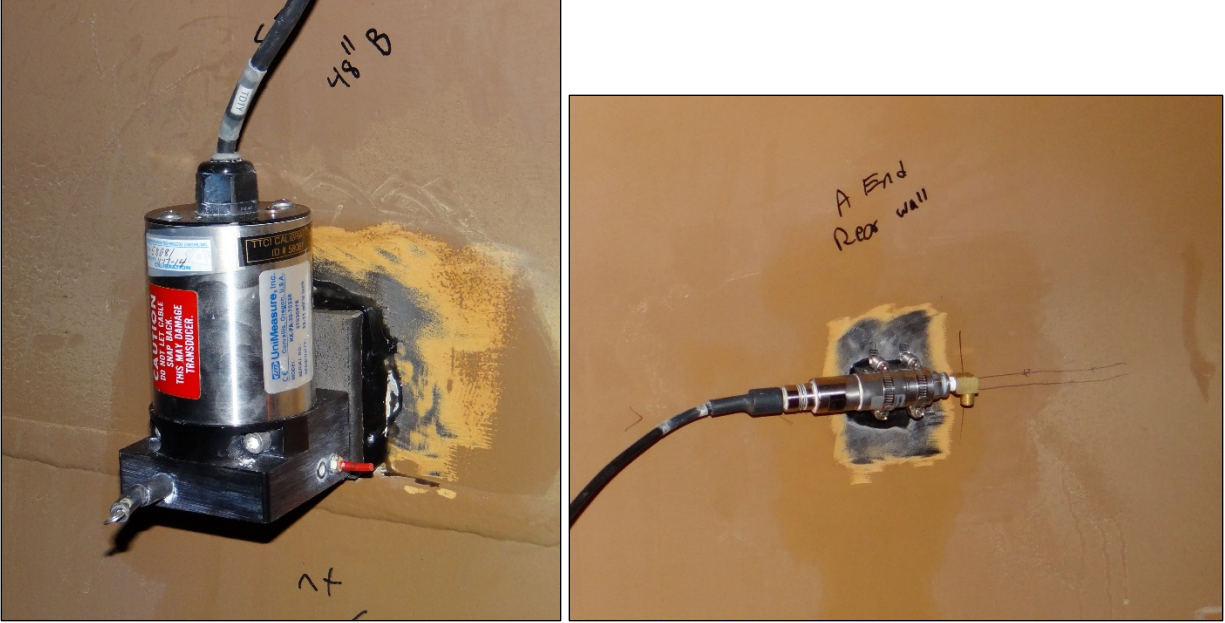
Figure A-5. Typical Mounting of String Potentiometer and Pressure Gauges (Tank Interior)

Figure A-6. Punctured Jacket after the Test

Figure A-7. Punctured Shell after the Test

Figure A-8. Punctured Shell Removed from the Tank Car (Interior Side)

Figure A-9. Cracked Shell below the Ram (Interior Side)

Figure A-10. Cracked Shell above the Ram (Interior Side)

Appendix B.   Camera and Target Positions
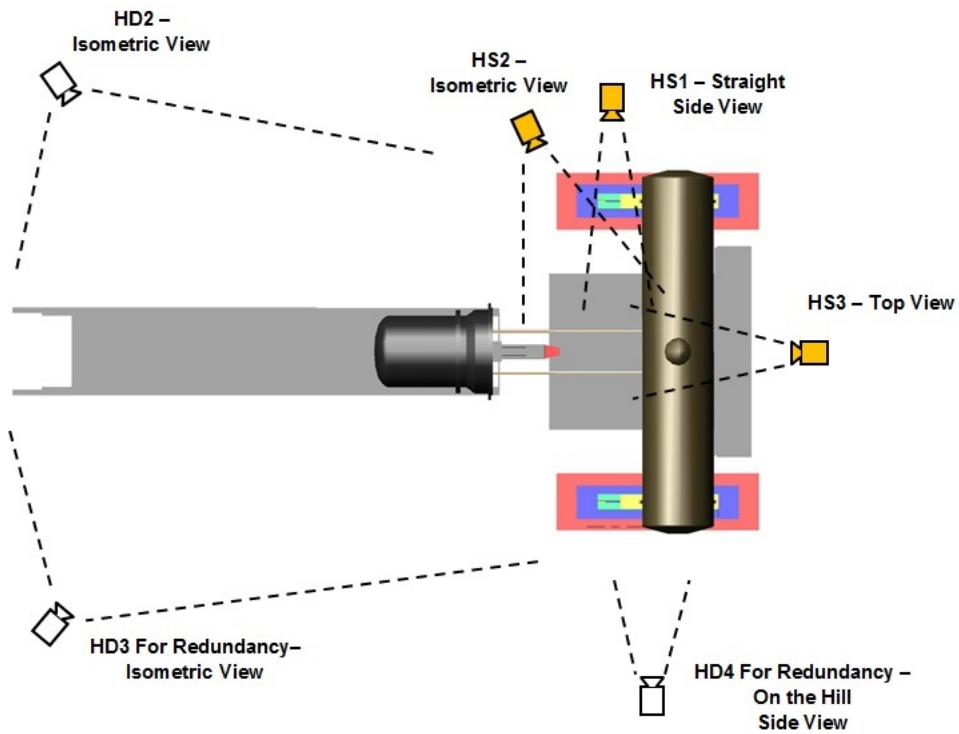
Figure B-1. Camera Positions (Top) — High Speed (HS), High Definition (HD)
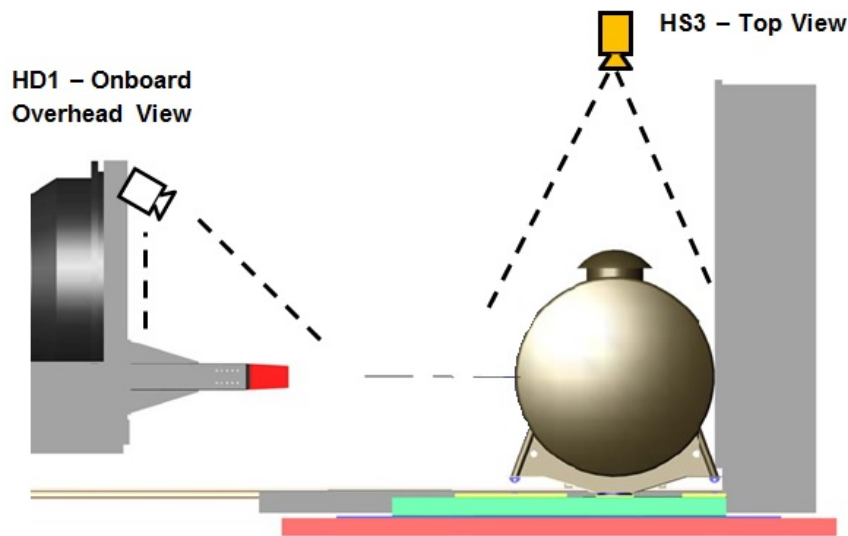
Figure B-2. Camera Positions (Side) — High Speed (HS), High Definition (HD)
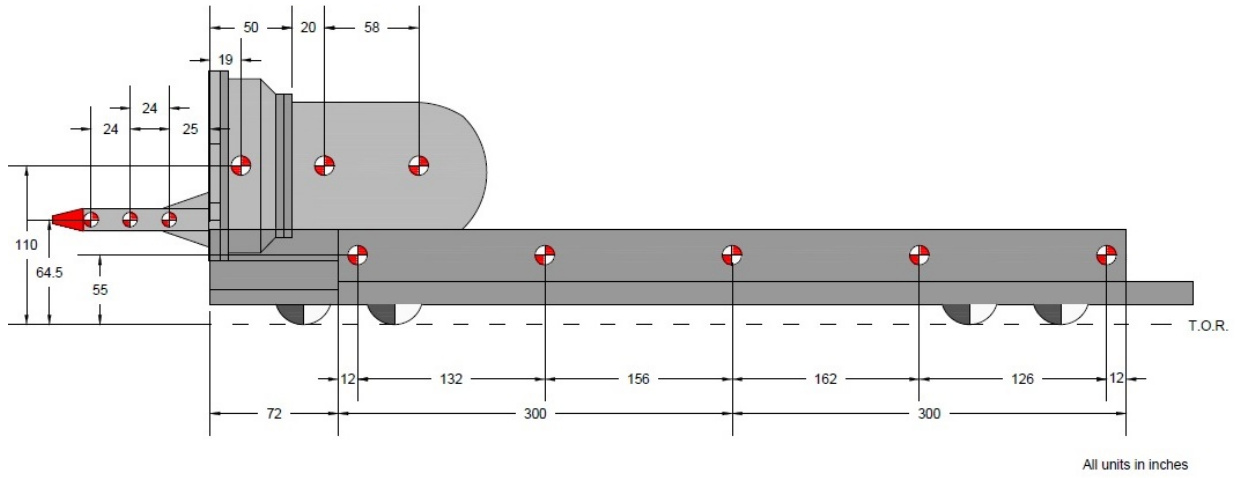
Figure B-3. Ram Car Target Positions
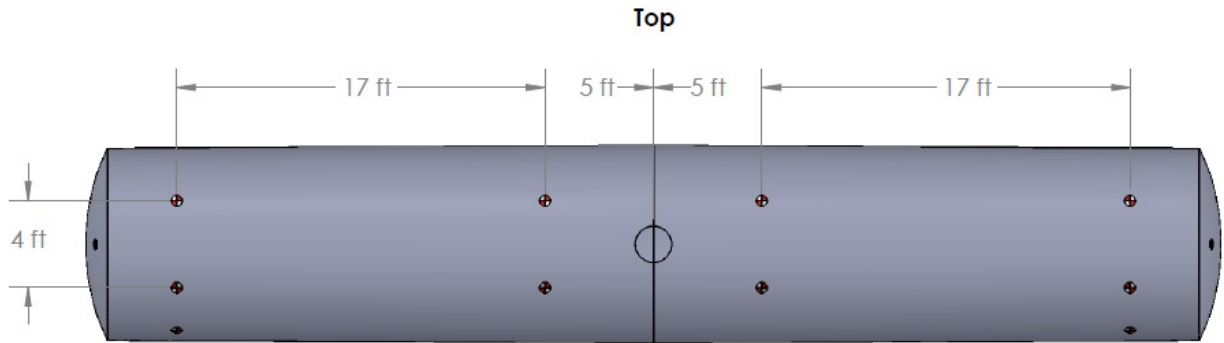
Figure B-4. Tank Car Target Positions (Top)
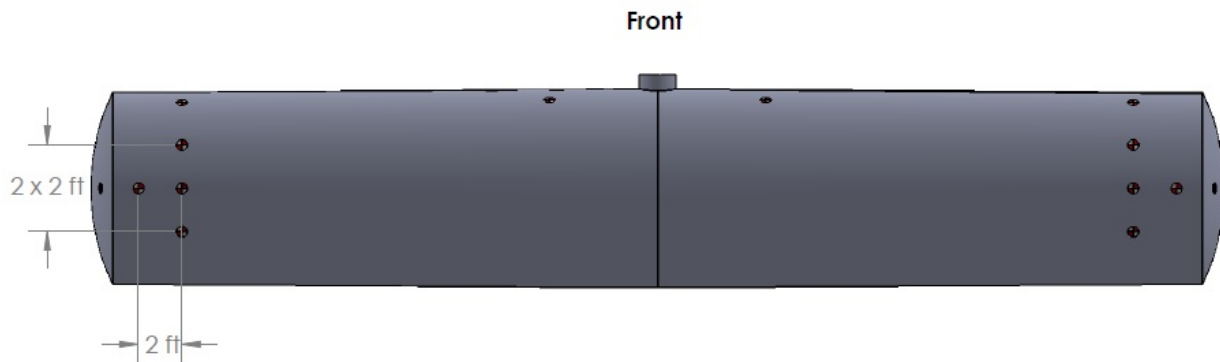
Figure B-5. Tank Car Target Positions (Front)

64
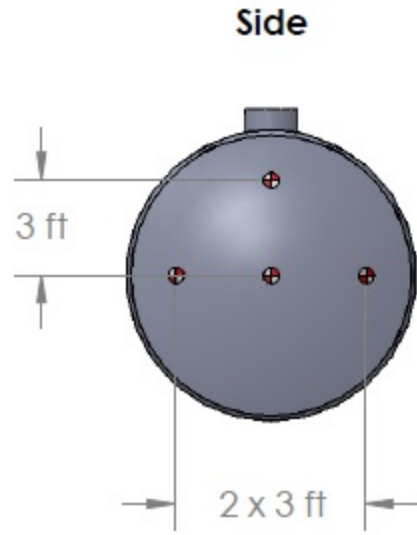
Figure B-6. Tank Car Target Positions (Side)

Appendix C.   Data
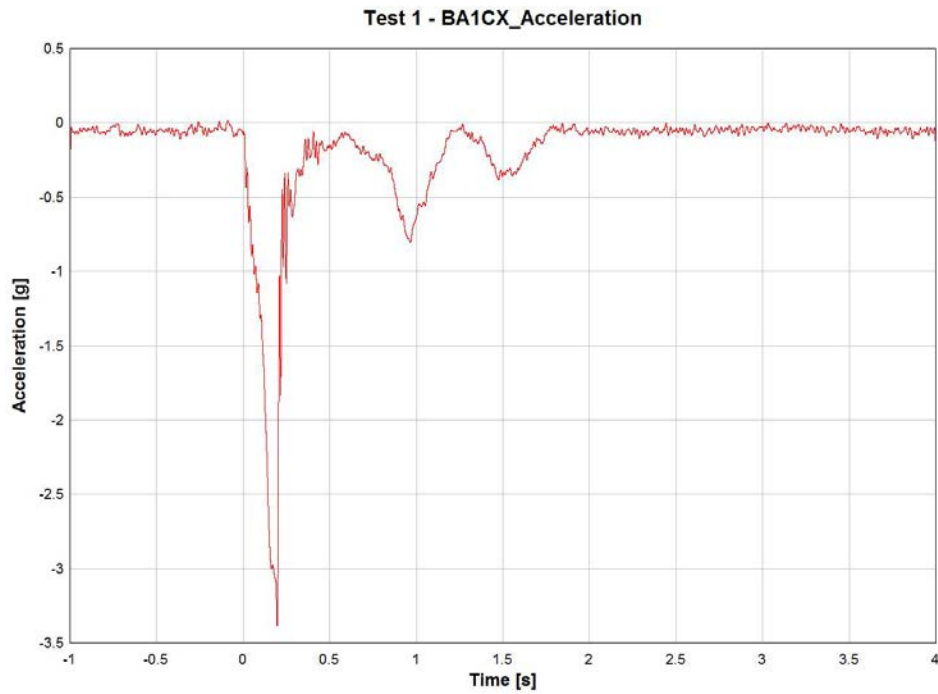
Figure C-1. BA1CX Accelerometer Data
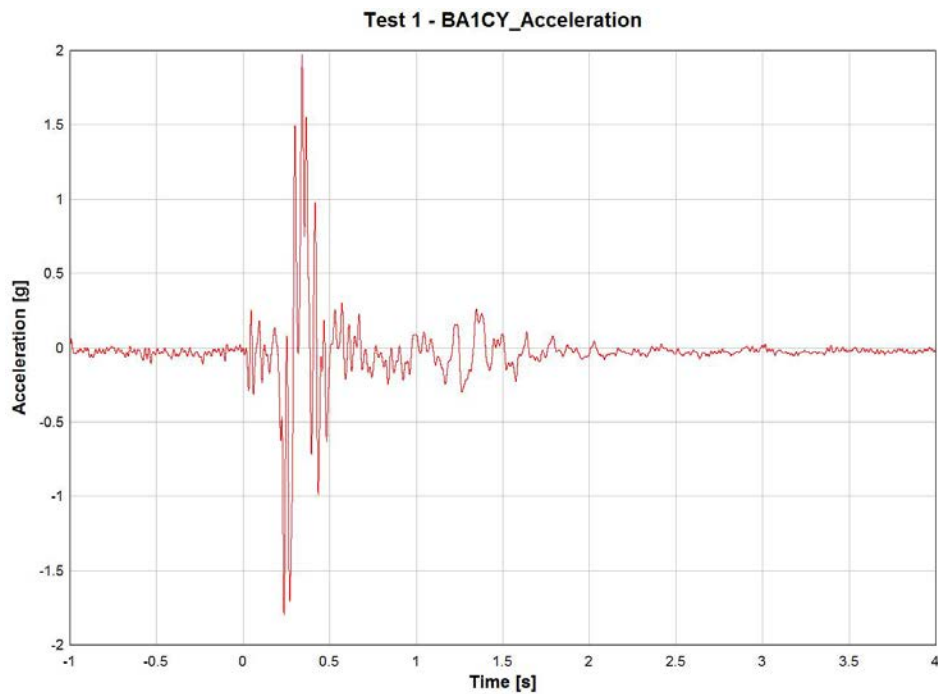
Figure C-2. BA1CY Accelerometer Data
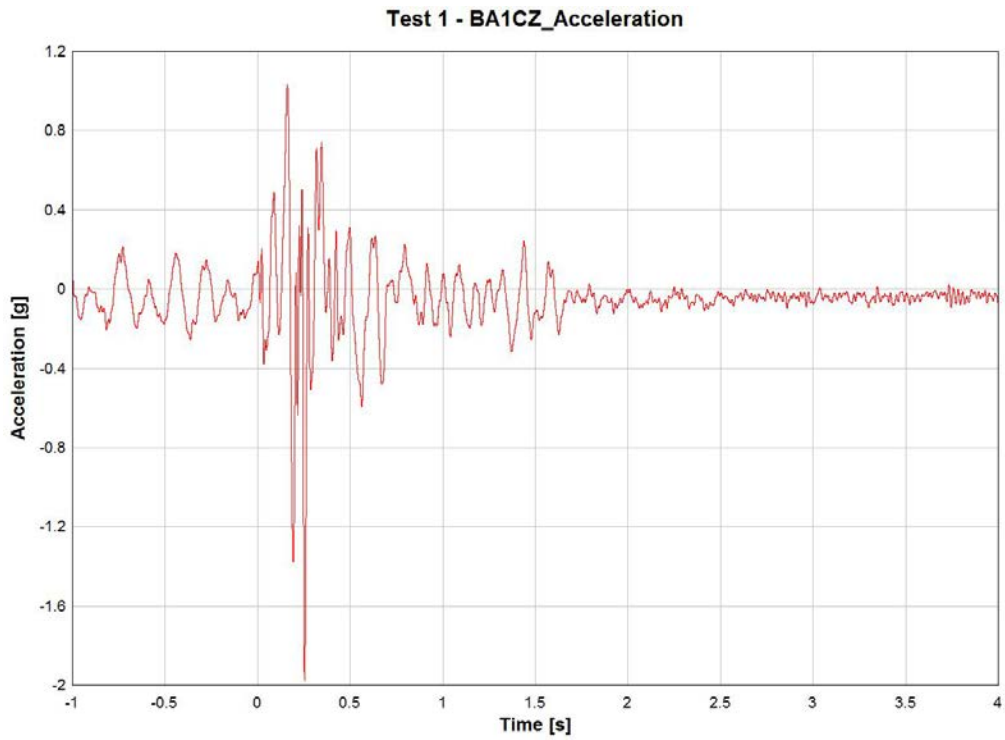
Figure C-3. BA1CZ Accelerometer Data
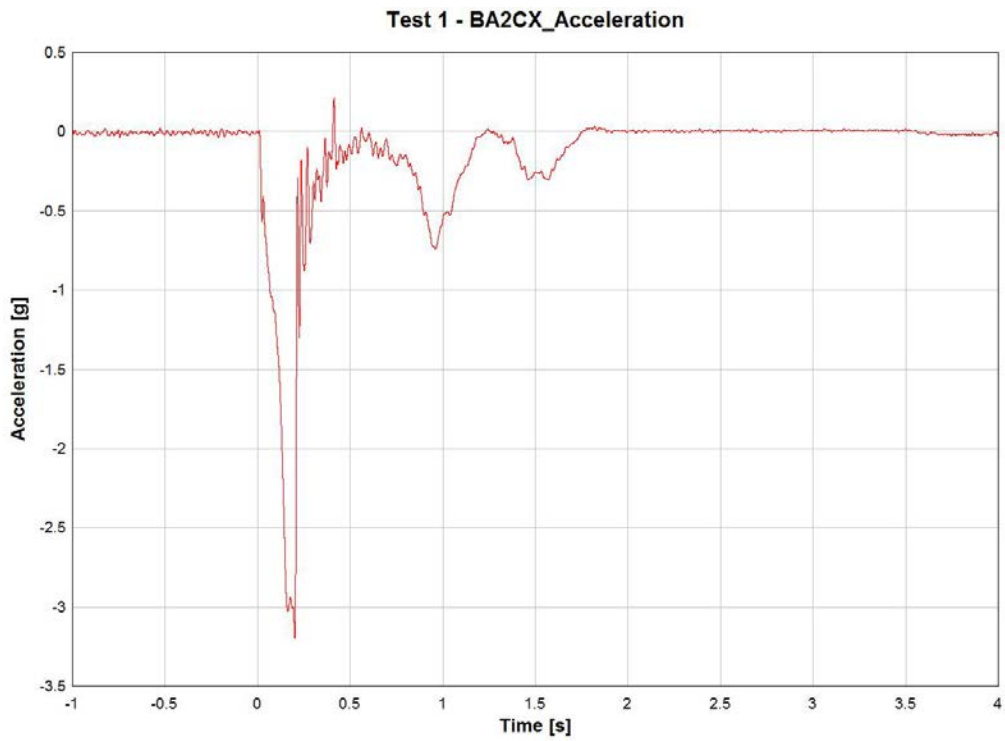
**Figure C-4. BA2CX Accelerometer Data**

67
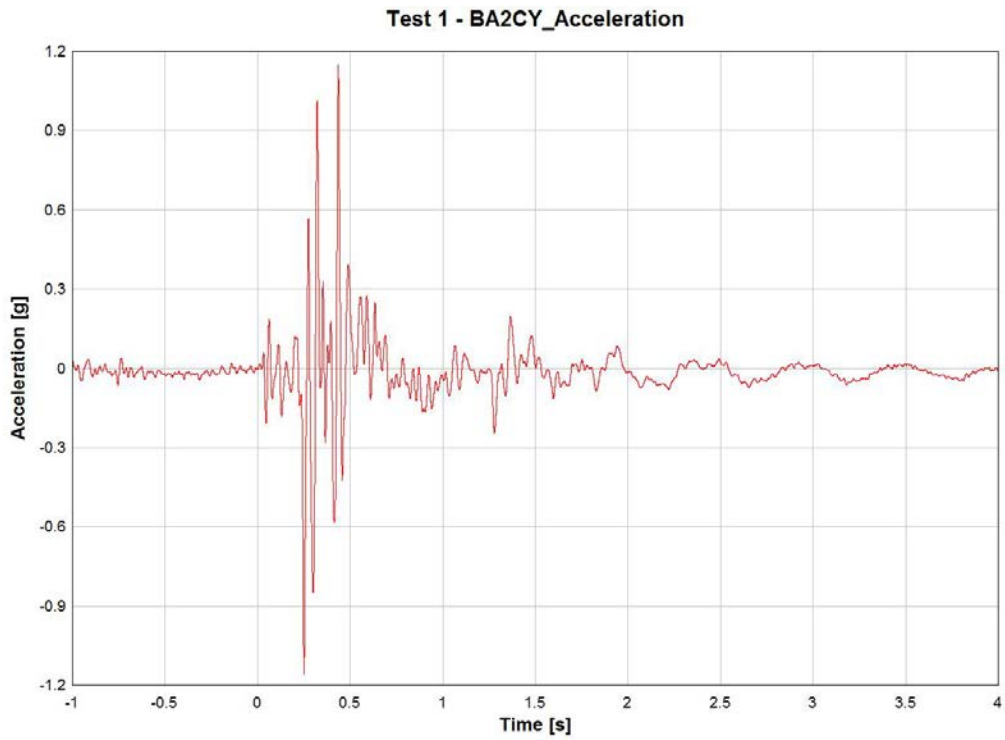
Figure C-5. BA2CY Accelerometer Data
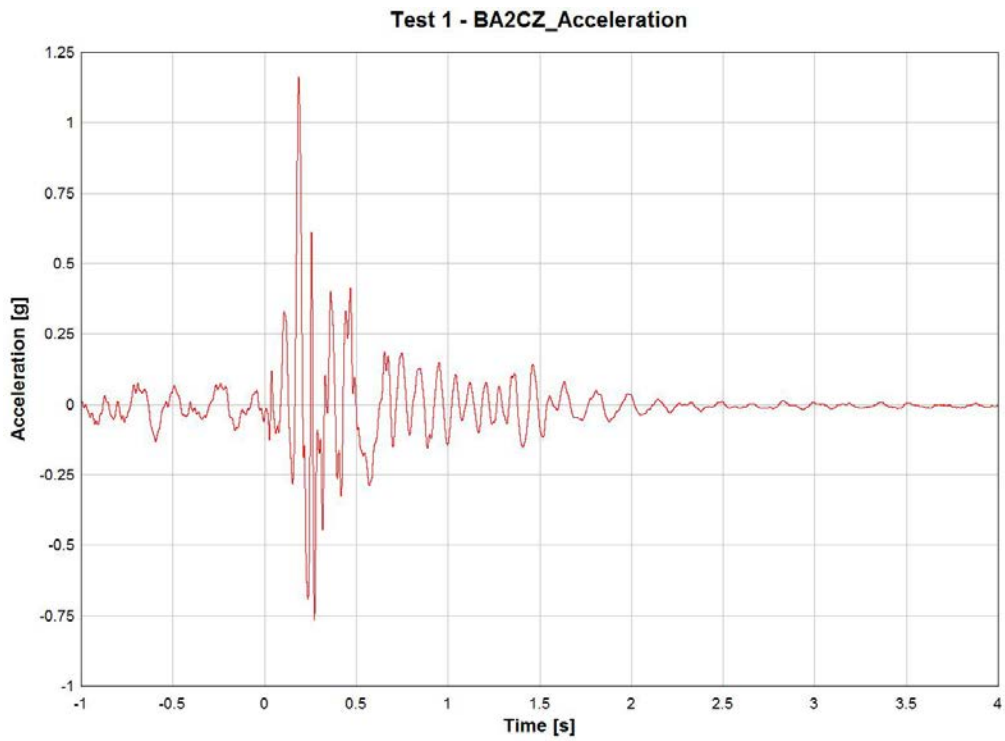
Figure C-6. BA2CZ Accelerometer Data
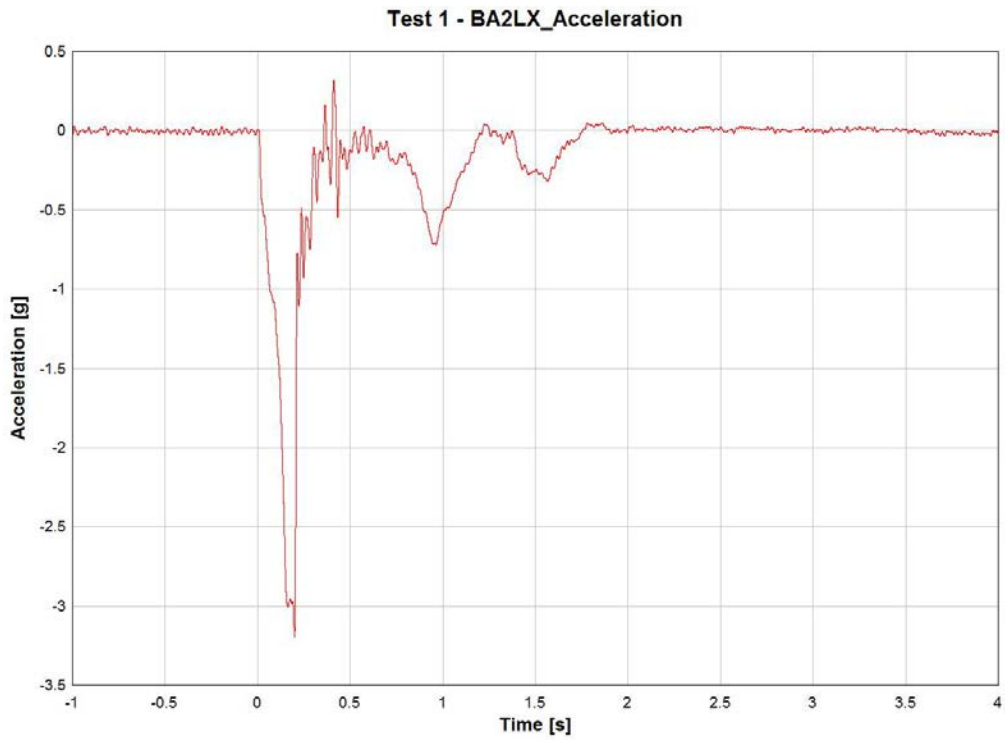
Figure C-7. BA2LX Accelerometer Data
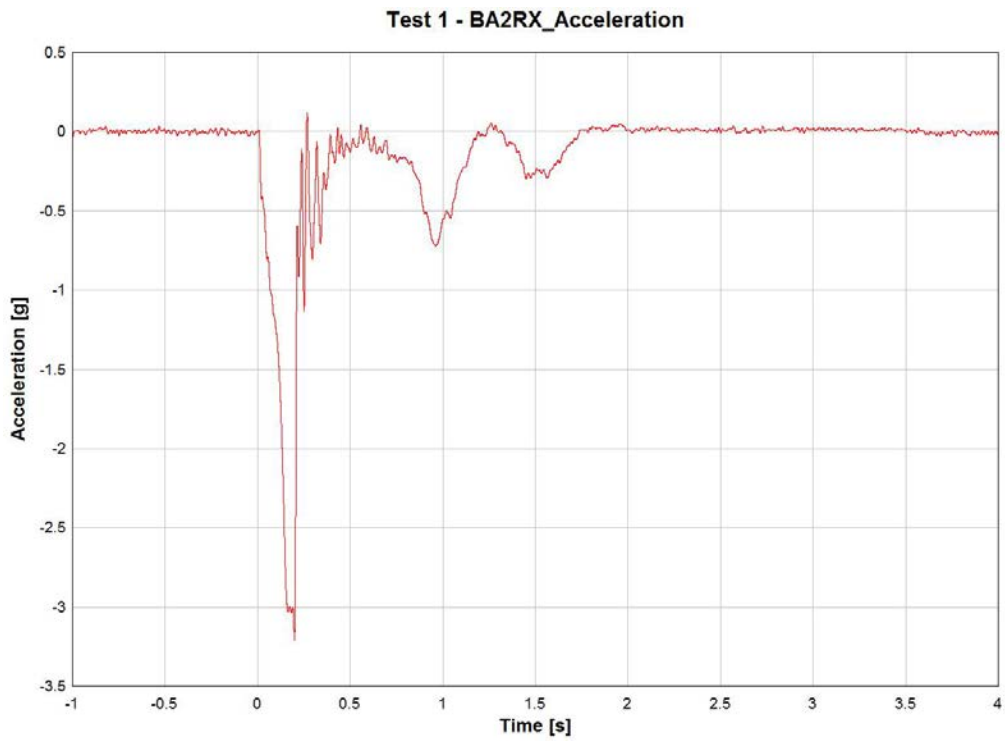
Figure C-8. BA2RX Accelerometer Data
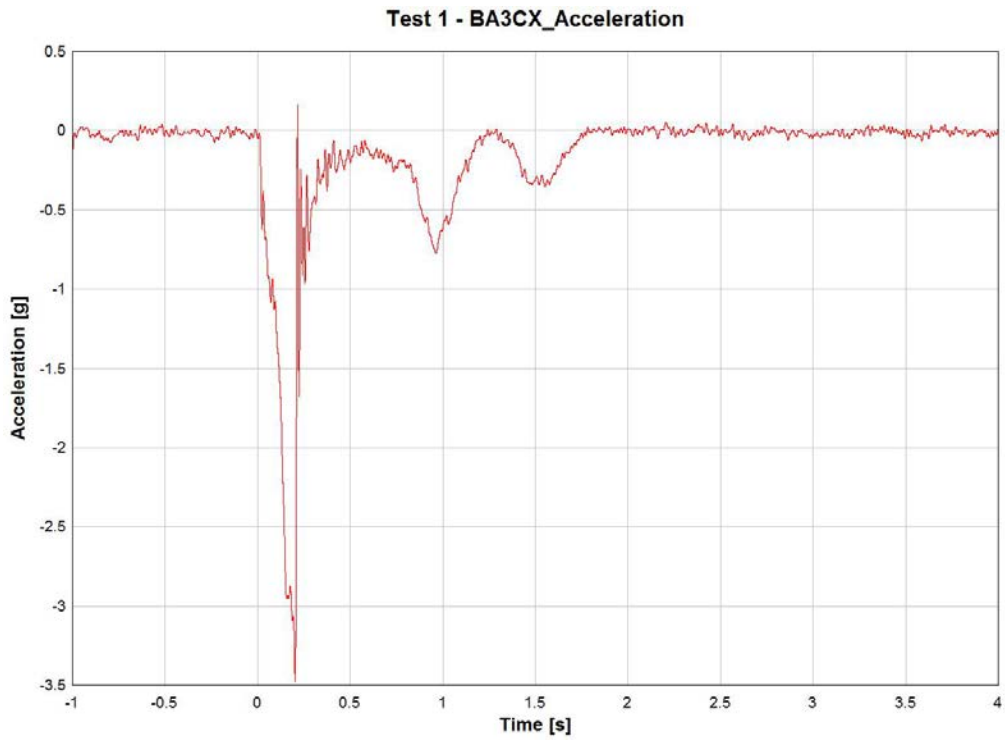
Figure C-9. BA3CX Accelerometer Data
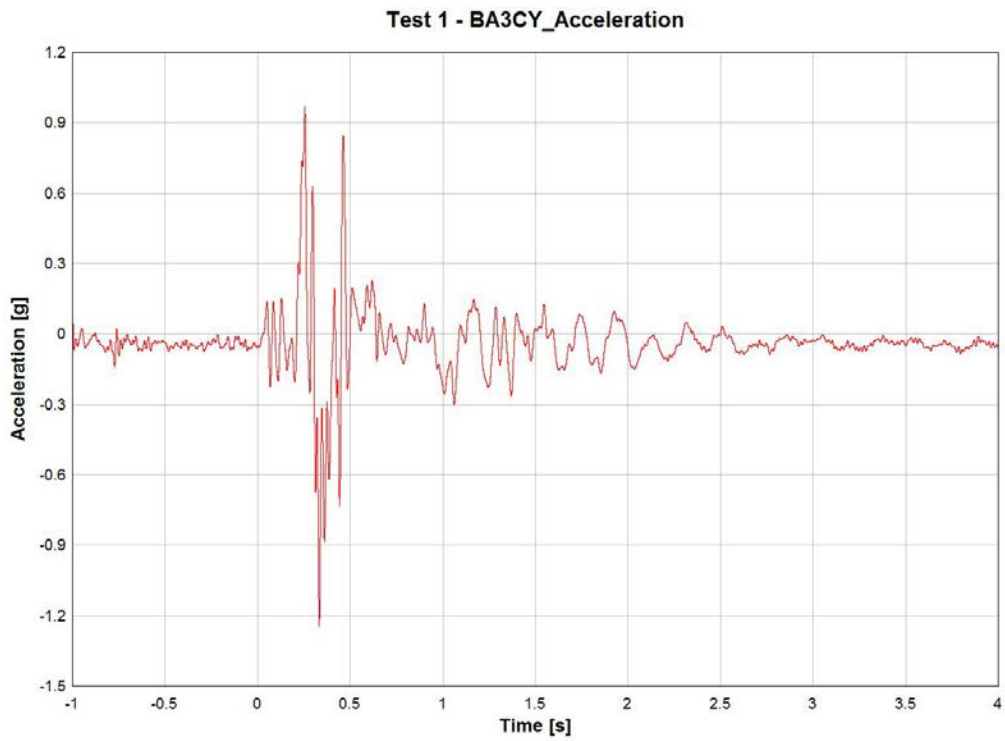
Figure C-10. BA3CY Accelerometer Data
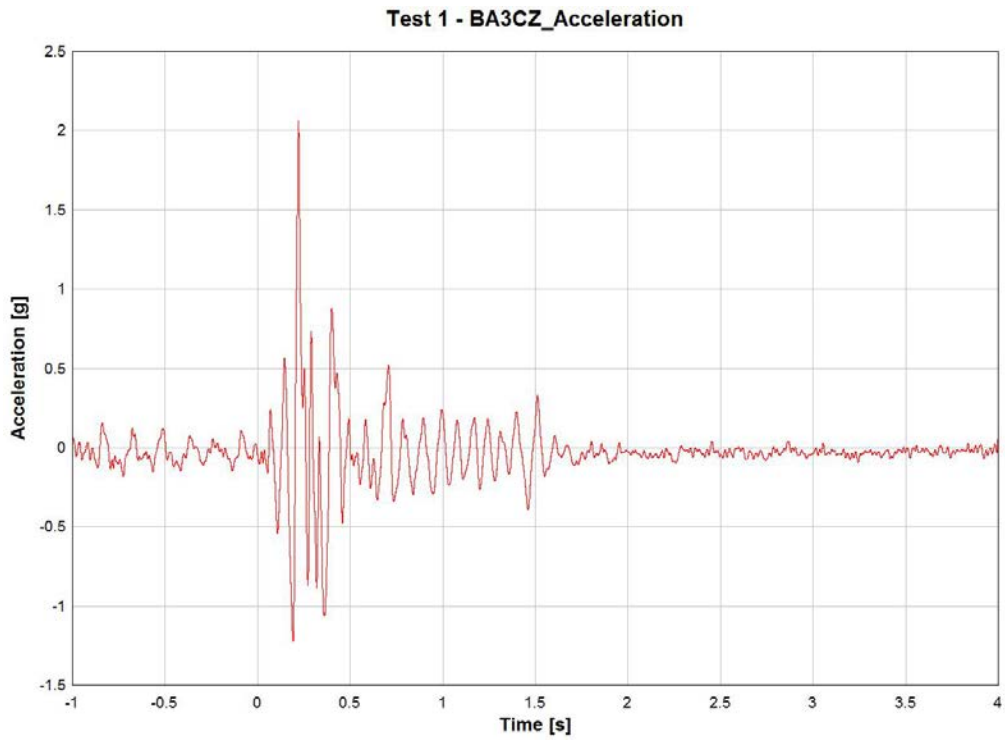
Figure C-11. BA3CZ Accelerometer Data
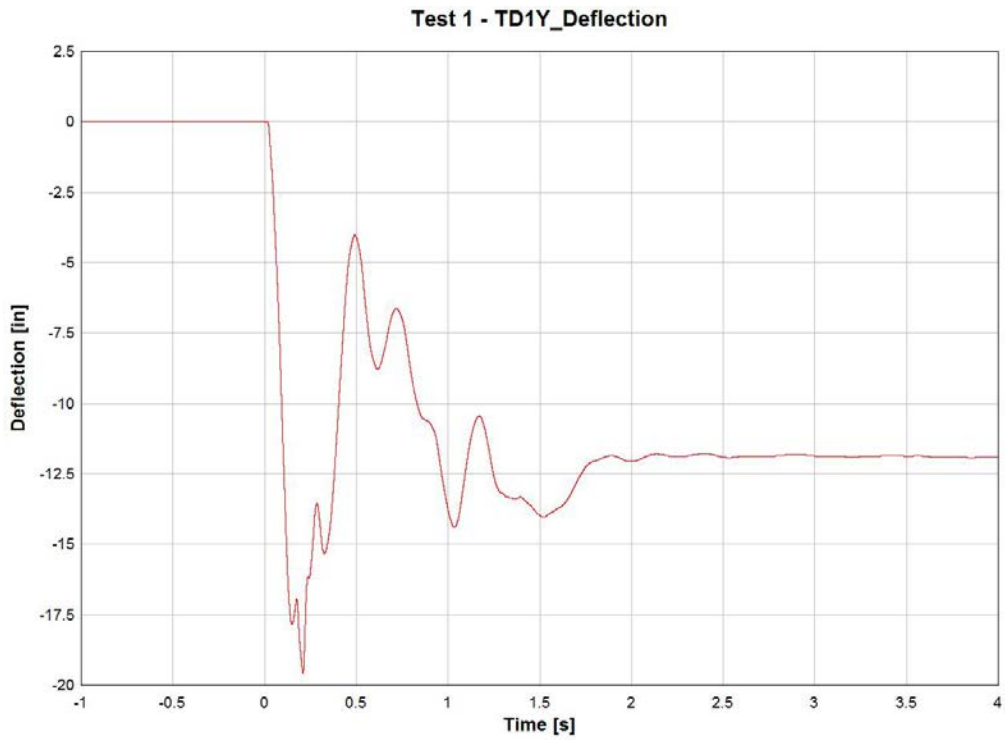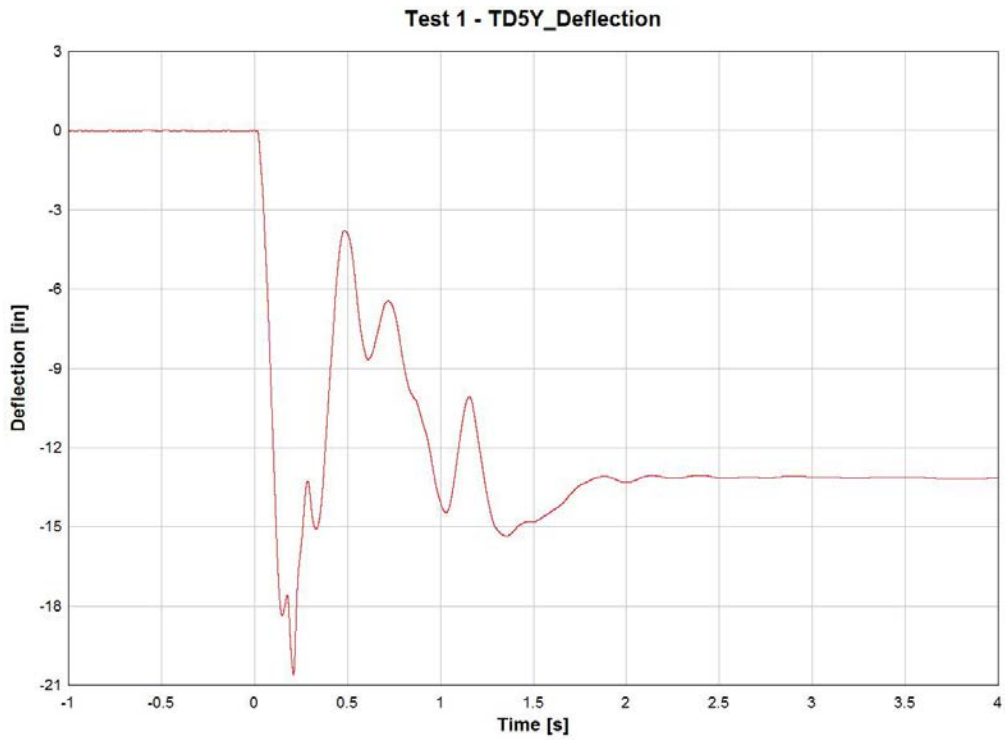

Figure C-12. TD1Y String Gage Potentiometer Data

71
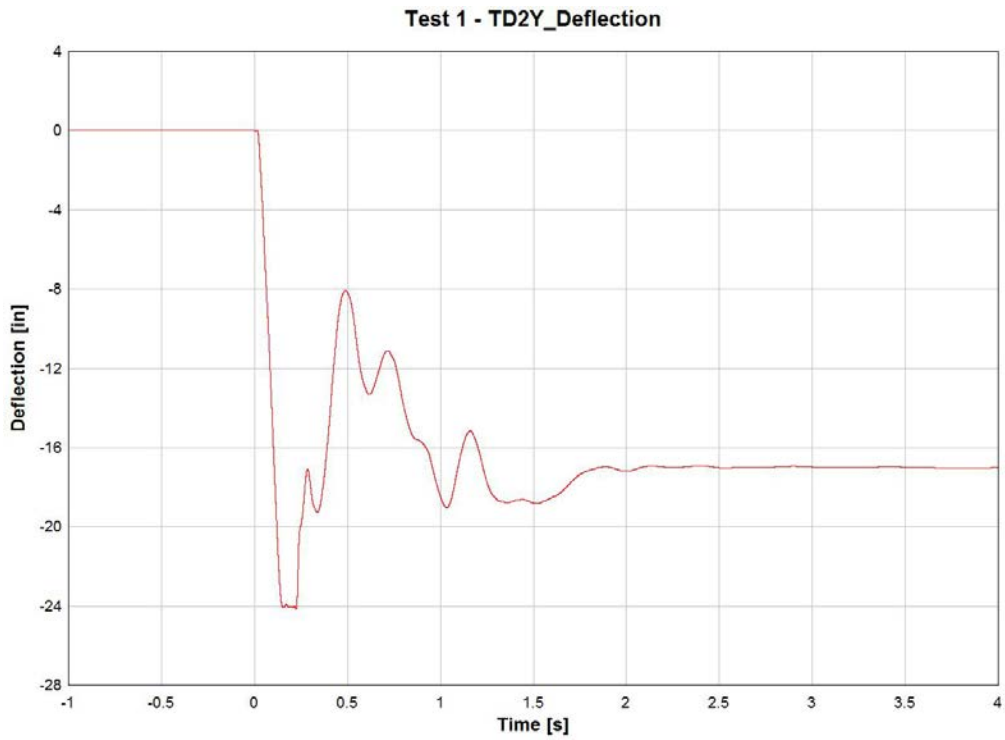
Figure C-13. TD2Y String Gage Potentiometer Data
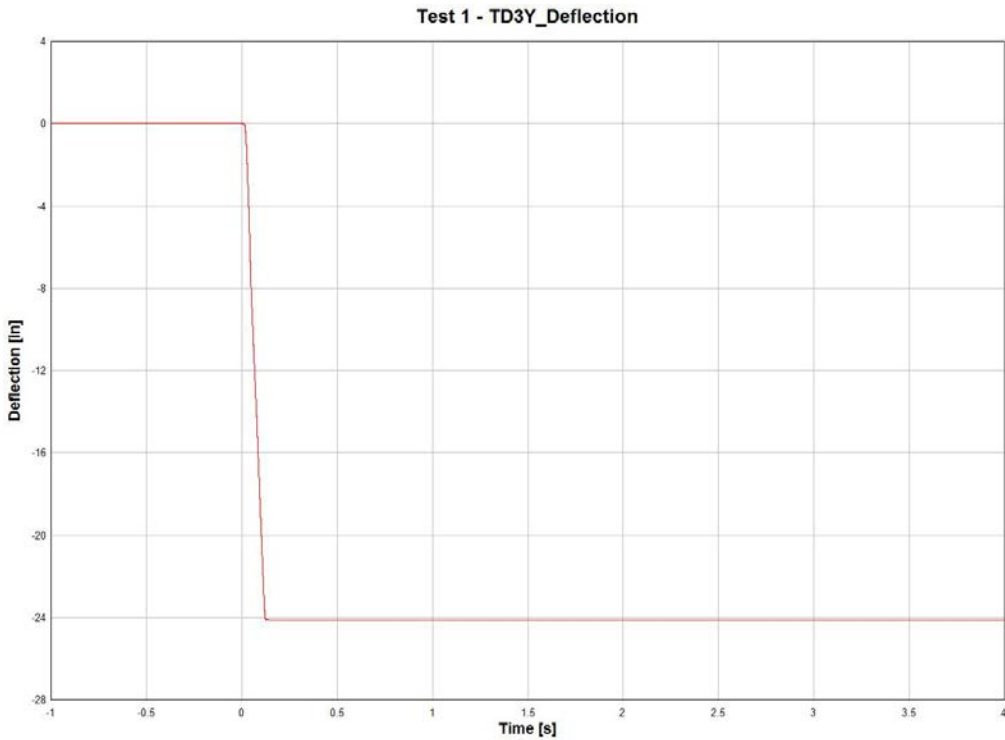
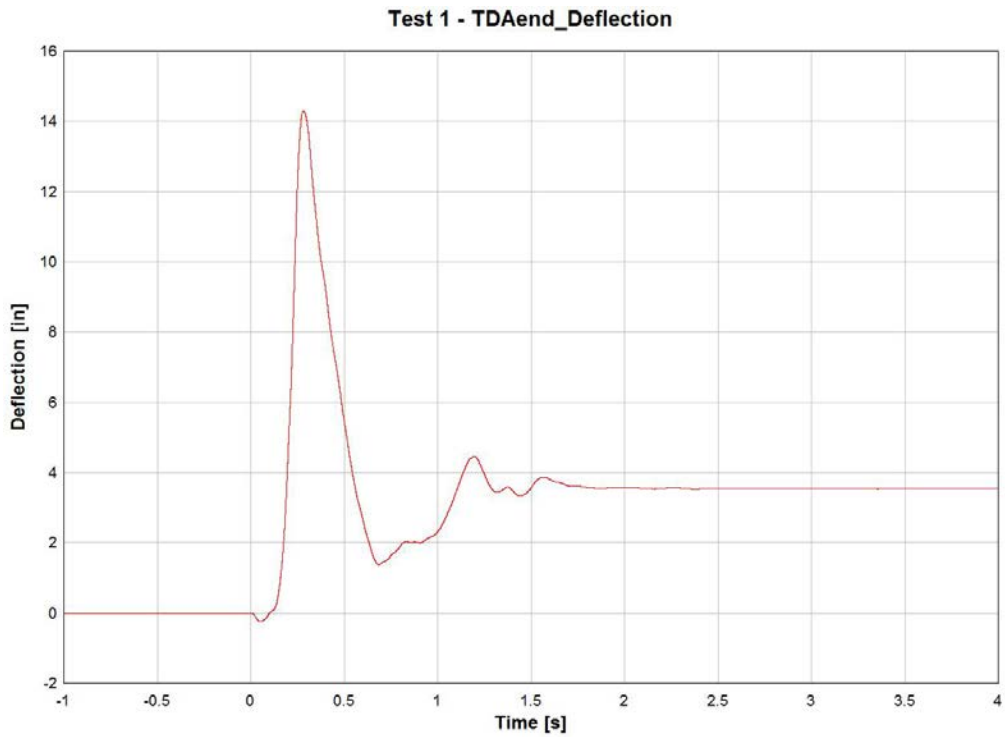**Figure C-14. TD3Y String Gage Potentiometer Data**
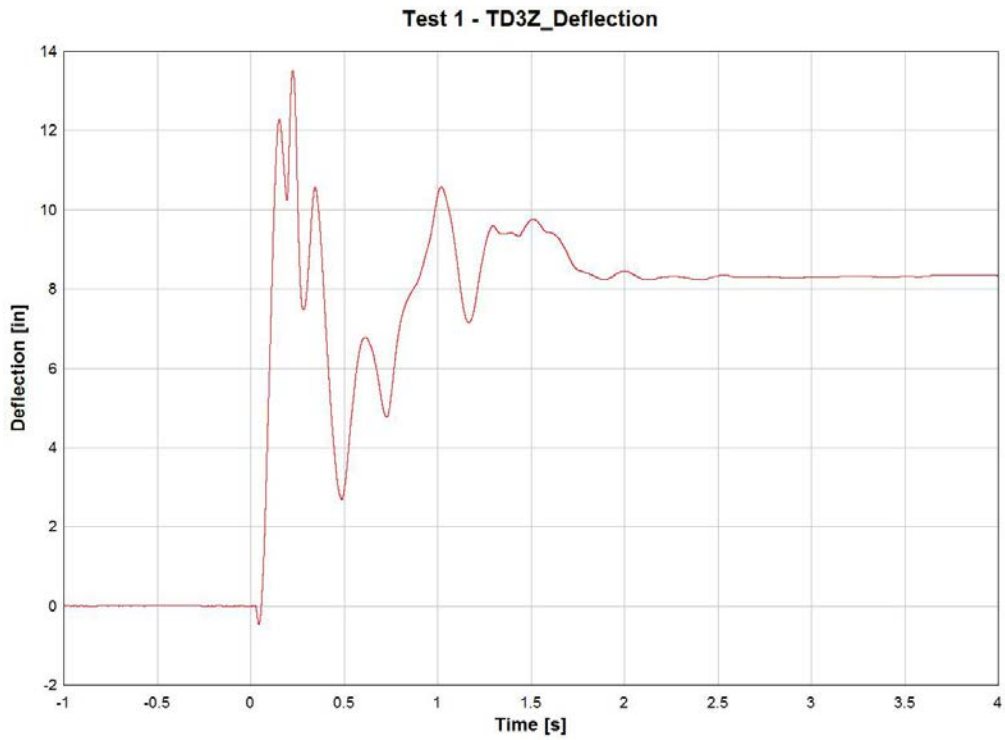
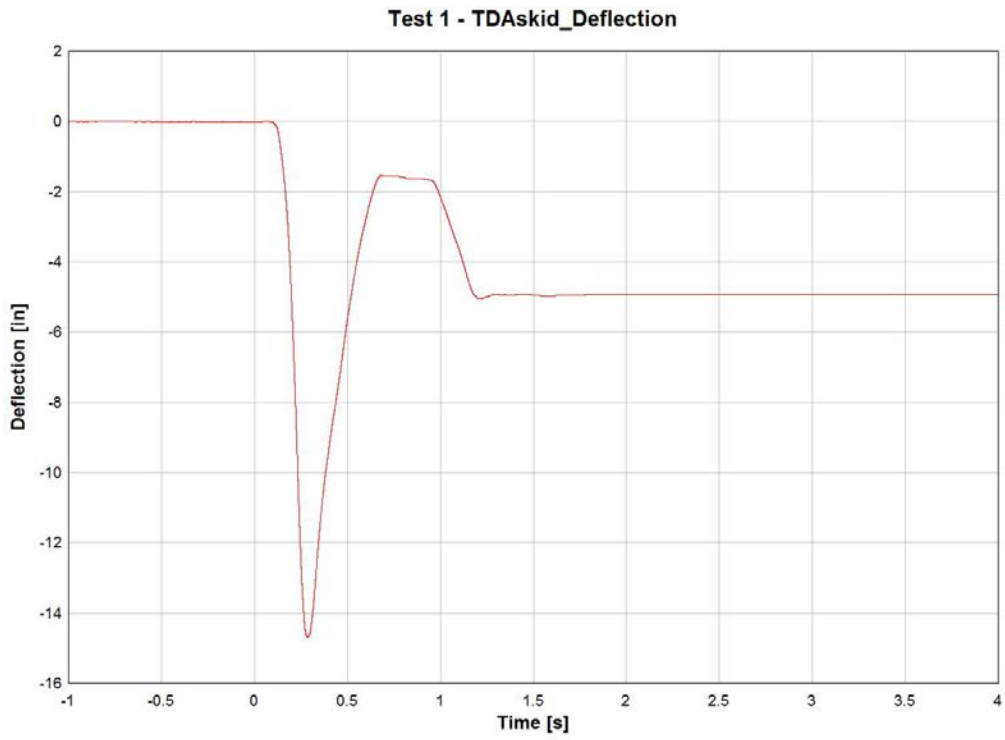**Figure C-15. TD3Z String Gage Potentiometer Data**
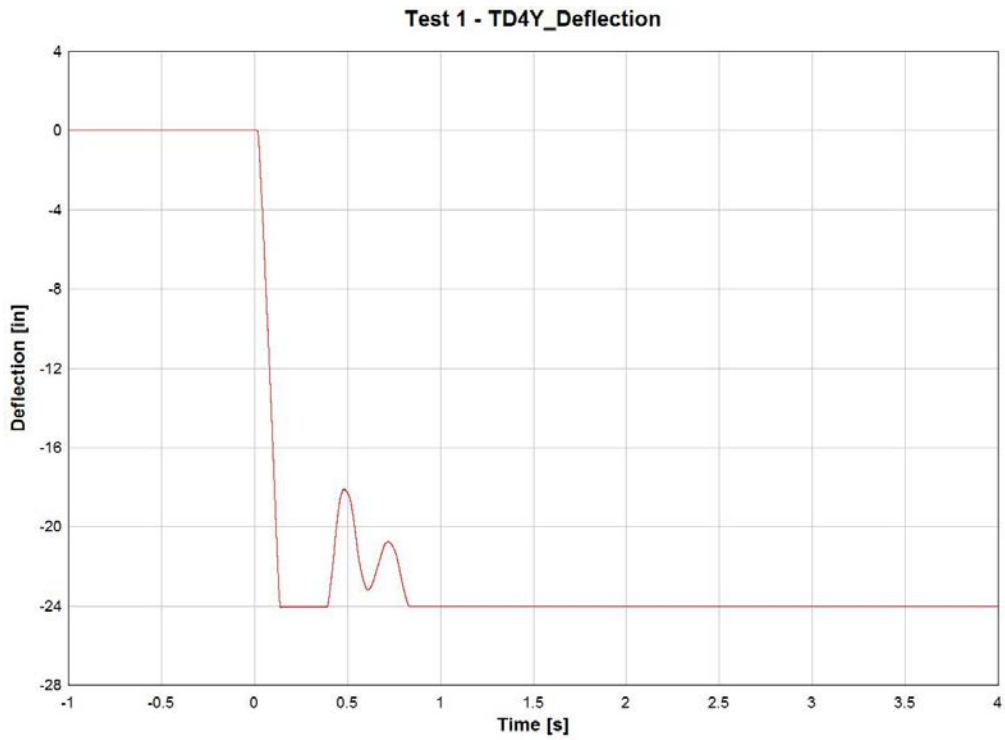
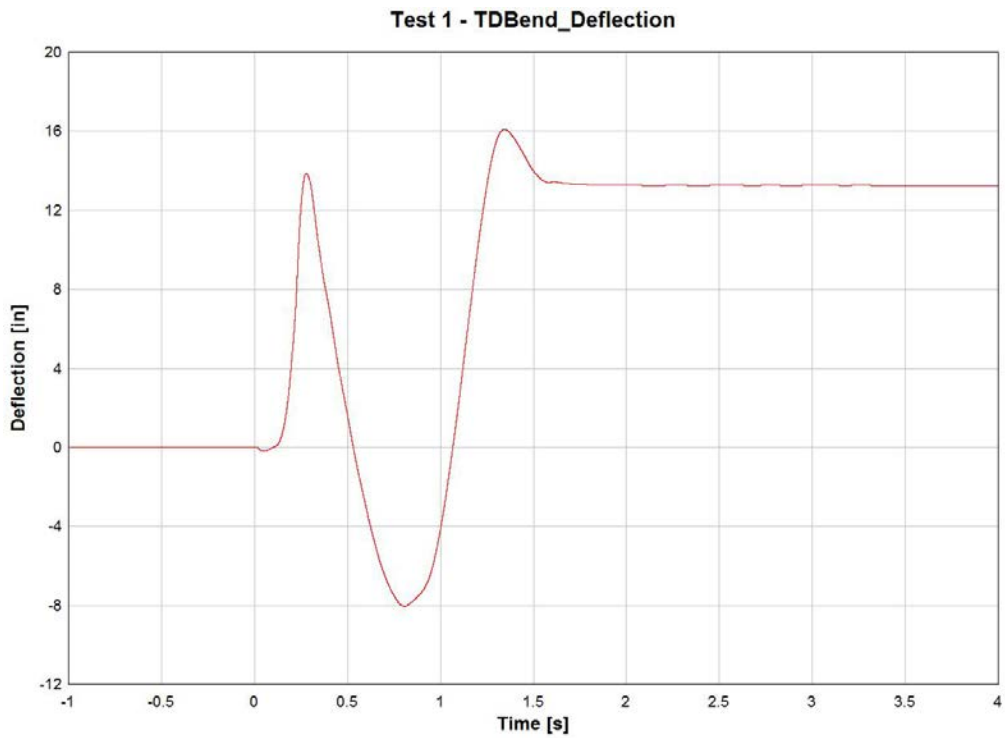**Figure C-16. TD4Y String Gage Potentiometer Data**
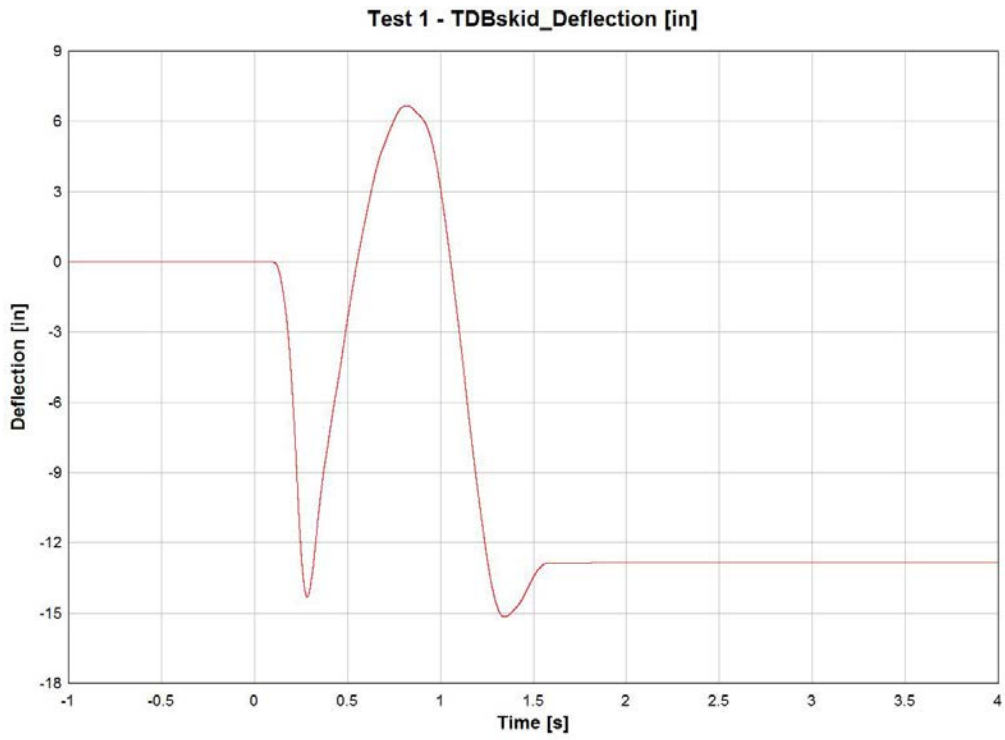
Figure C-17. TD5Y String Gage Potentiometer Data
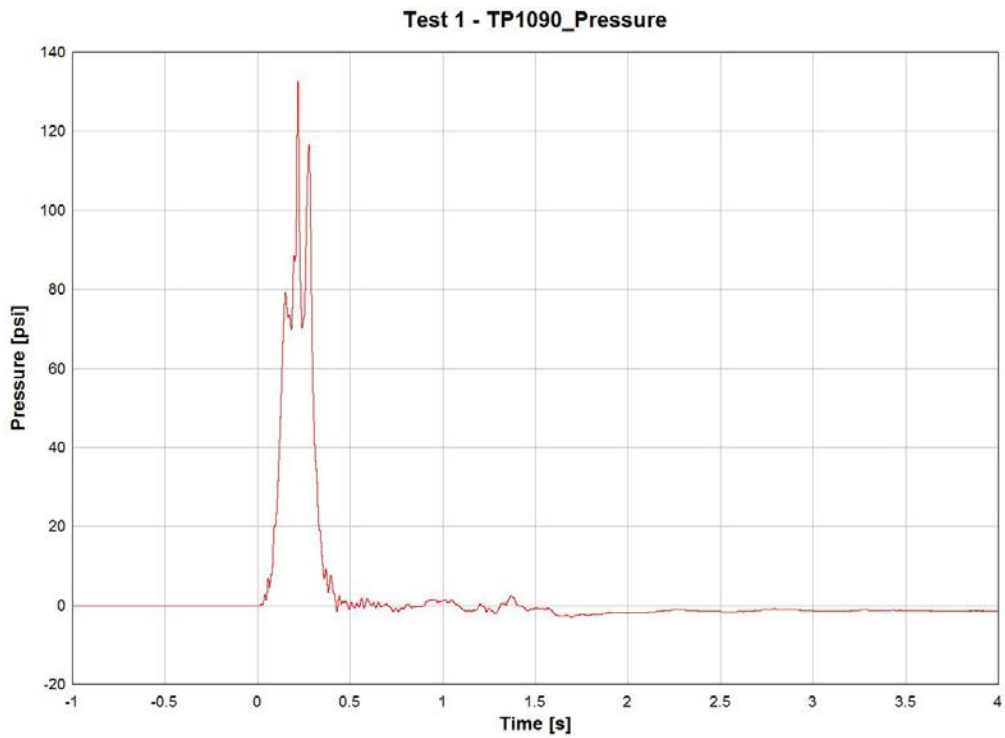

Figure C-18. TD_A_end String Gage Potentiometer Data

Figure C-19. TD_A_skid String Gage Potentiometer Data

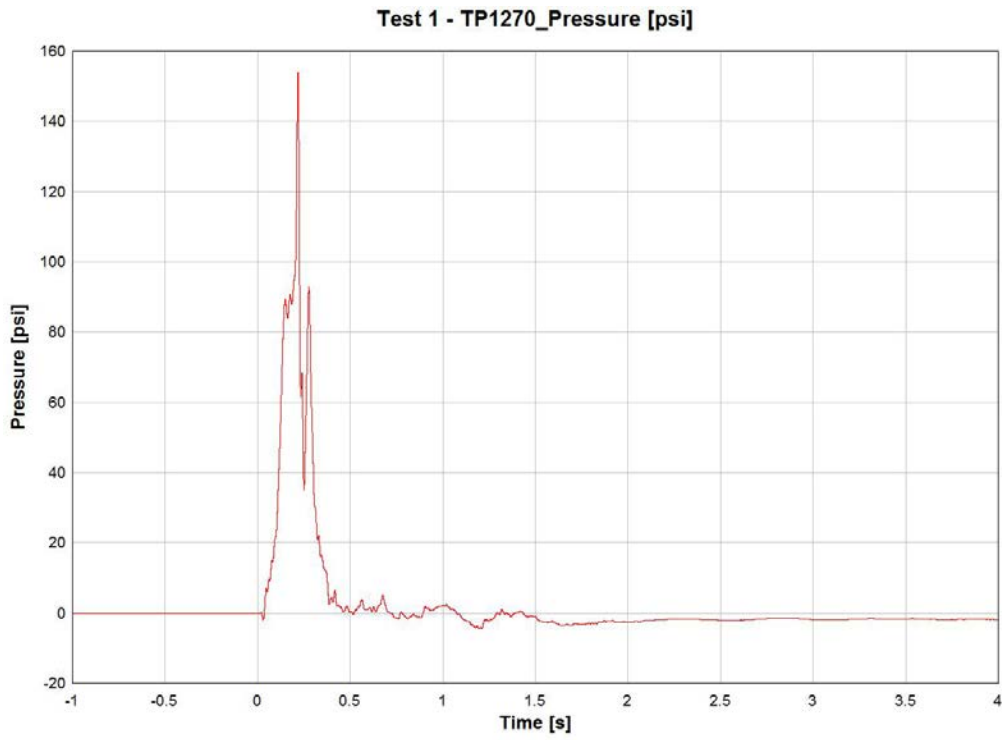**Figure C-20. TD_B_end String Gage Potentiometer Data**

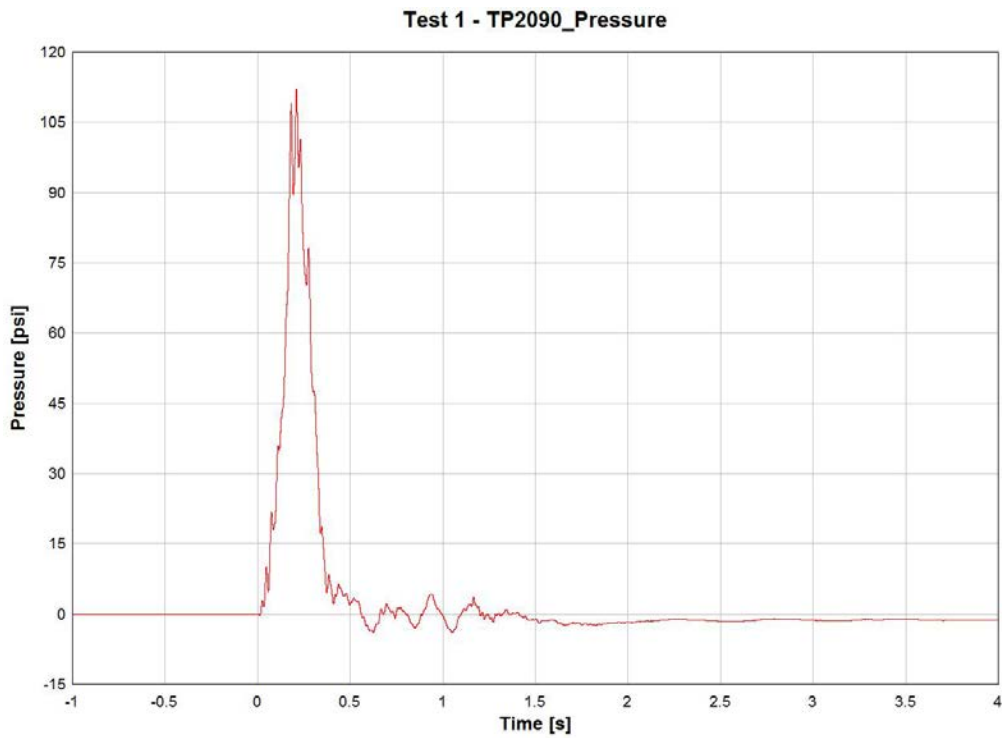**Figure C-21. TD_B_skid String Gage Potentiometer Data**

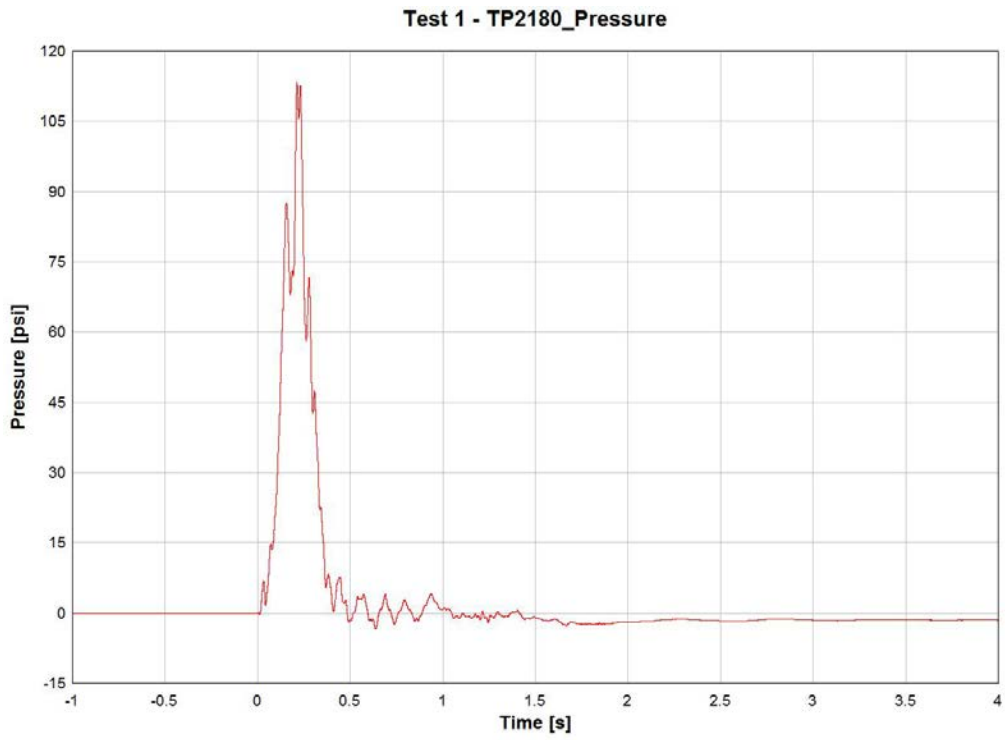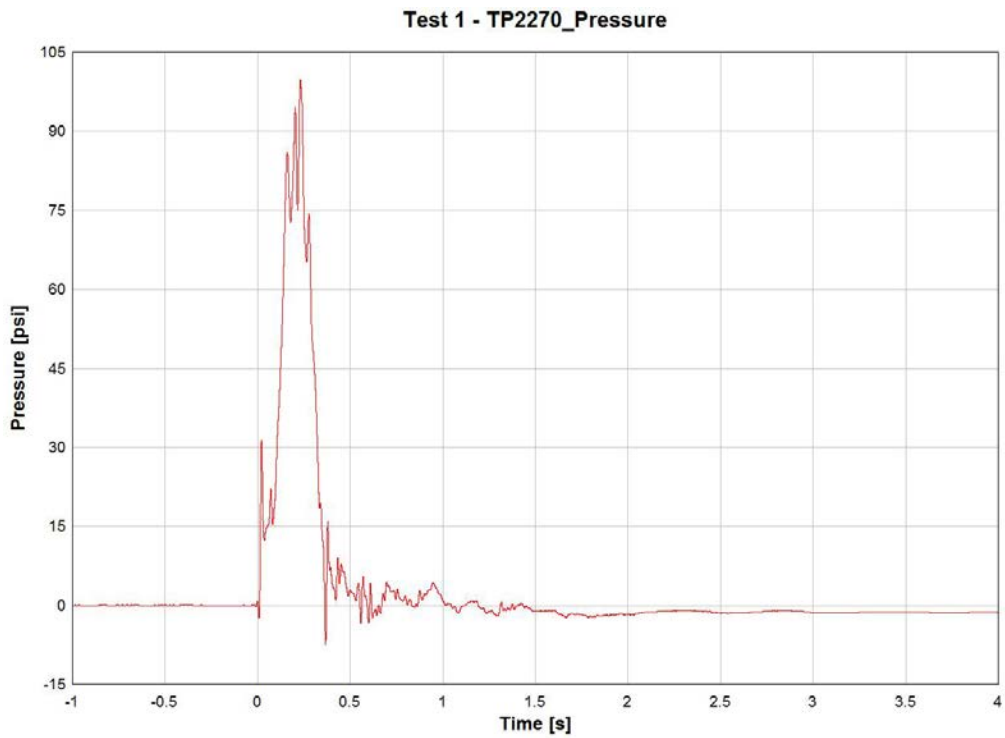**Figure C-22. TP1090 Pressure Transducer Data**

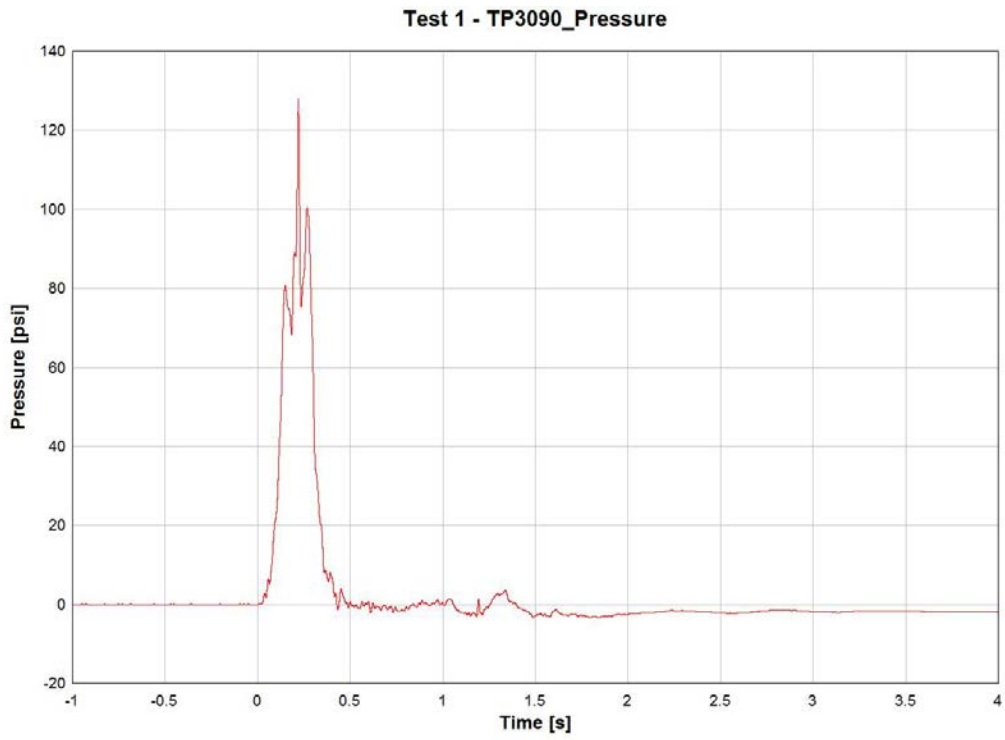**Figure C-23. TD1270 Pressure Transducer Data**

Figure C-24. TP2090 Pressure Transducer Data
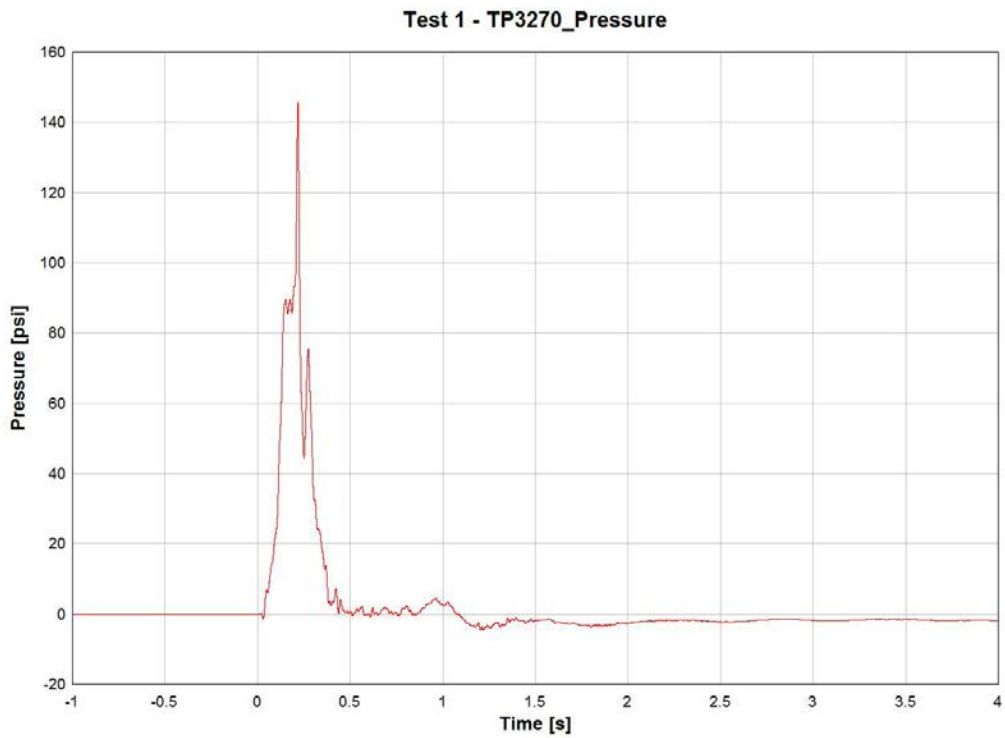
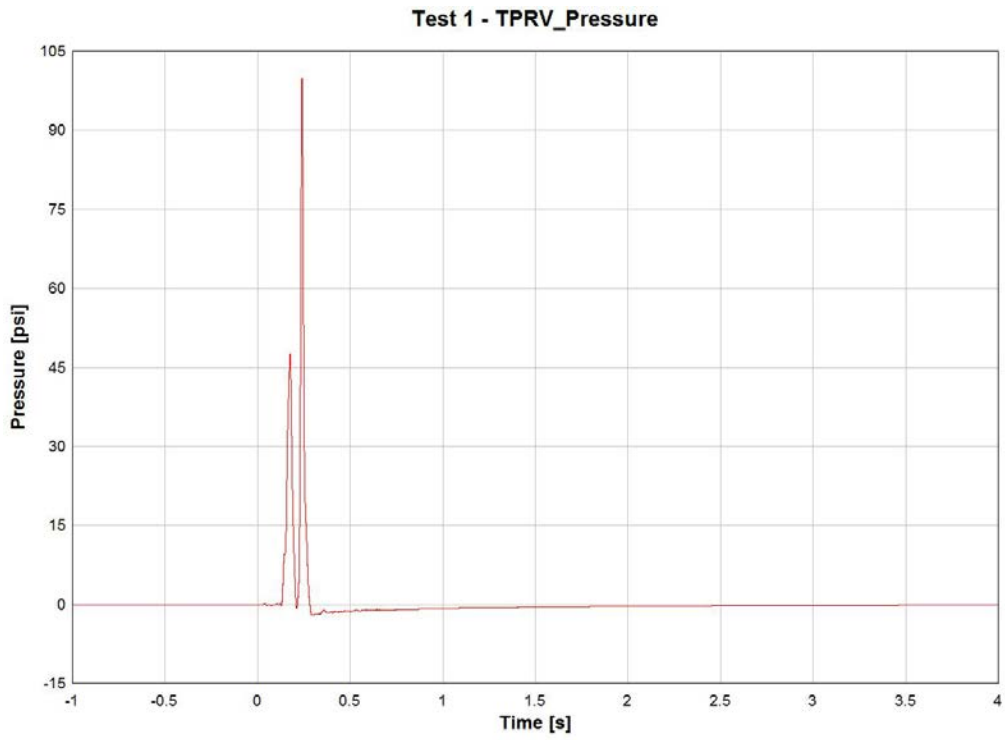**Figure C-25. TP2180 Pressure Transducer Data**

Figure C-26. TP2270 Pressure Transducer Data

**Figure C-27. TP3090 Pressure Transducer Data**

Figure C-28. TP3270 Pressure Transducer Data

Figure C-29. TPRV Pressure Transducer Data

Appendix D.   Material Test Results

Westmoreland Mechanical Testing & Research, Inc.

P.O.Box 388; 221 Westmoreland Drive
Youngstown, PA 15696-0388 U.S.A.
Telephone: 724-537-3131   Fax: 724-537-3151
Website: www.wmtr.com   E-Mail: admin@wmtr.com
WMT&R is a technical leader in the material testing industry.

TESTING CERT 621-01 & 621-02
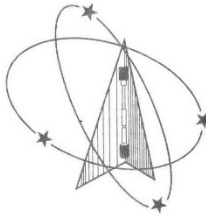
Section 1 of 1

WMT&R Report No. 4-54384
P.O. No. 28972
WMT&R Quote No. QN140452

CERTIFICATION

March 5, 2014
Transportation Technology Center Inc.
55500 DOT Road
P.O. Box 11130
Pueblo, CO 81001

Attention: Przemyslaw Rakoczy

Subject: All processes, performed upon the material as received, were conducted at WMT&R, Inc. in accordance with the WMT&R Quality Assurance Manual, Rev. 11, dated 12/03/2008.

The following tests were performed on this order: TENSILE

TENSILE RESULTS: ASTM E8-13a
SPEED OF TESTING: 0.005 in./in./min.

MATERIAL: Steel

DISPOSITION: Report

Sample	TestLog Number	Temp.	UTS ksi	0.2% YS ksi	Elong %	Modulus Msi	Ult. Load lbf	0.2% Y.LD. lbf	Orig. Width (in.)	Orig. Thick (in.)	4D Orig GL (in.)	4D Final GL (in.)	Orig. Area (sq. in.)	Machine Number	AU\R
1	U33757	Room	72.7	43.1	34	36.9	14373	8528	0.5034	0.3928	2.00	2.68	0.19773552	M10	R
2	U33758	Room	73.0	43.8	34	36.7	14746	8854	0.5025	0.4021	2.00	2.68	0.20205525	M10	R
3	U33759	Room	73.1	43.4	36	37.0	14795	8780	0.5039	0.4016	2.00	2.72	0.20236624	M10	R
4	U33760	Room	74.9	45.9	27	36.7	14965	9163	0.5034	0.3968	2.00	2.54	0.19974912	M10	R
5	U33761	Room	73.3	43.8	33	36.6	14886	8879	0.5046	0.4022	2.00	2.66	0.20295012	M10	R

AU\R: A=ACCEPTABLE, U=UNACCEPTABLE, R=REPORT

Matt Wojton
Tensile Supervisor

March 5, 2014

Testing Specialists for Aerospace, Automotive, and Material Testing Fields
Locations in Youngstown, PA U.S.A. ~ Tel. (724) 537-3131 and
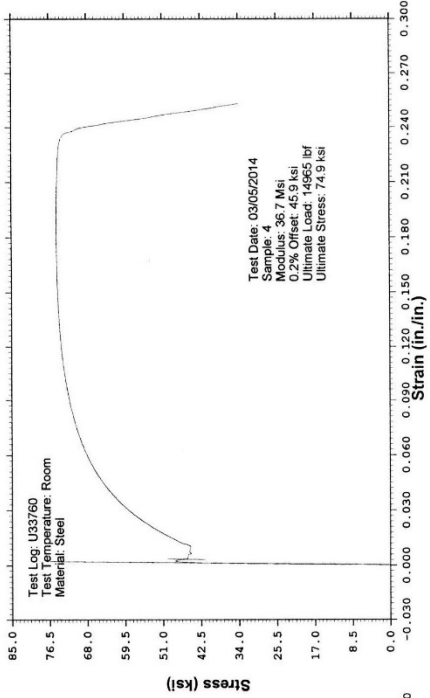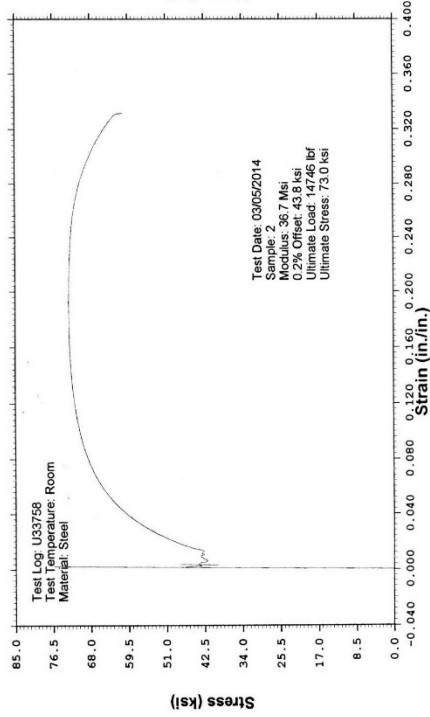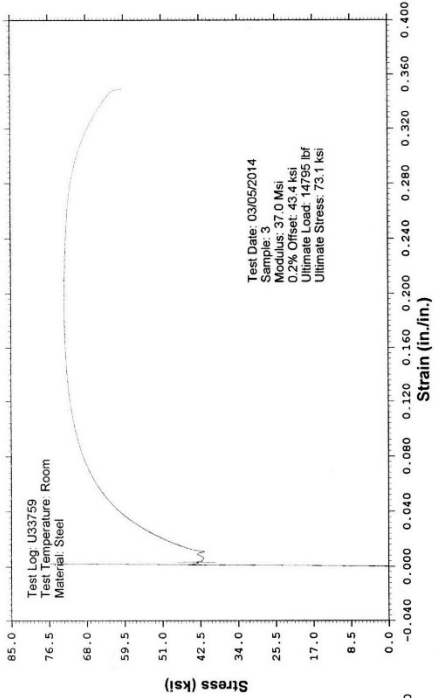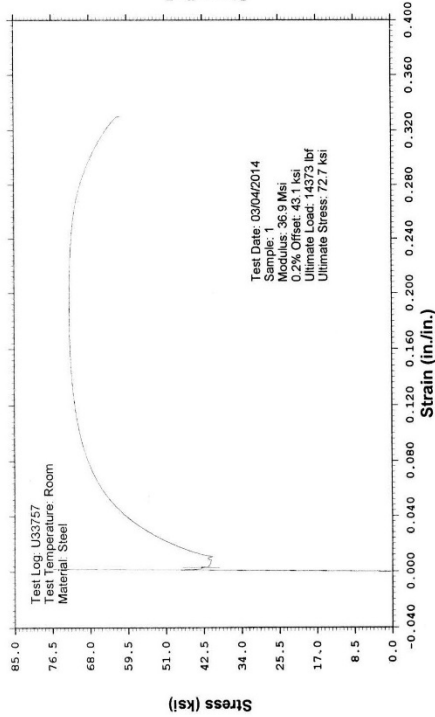Banbury, Oxon U.K. ~ Tel. +44 (0) 1295 261211

WESTMORELAND MECHANICAL TESTING & RESEARCH, Inc

Stress vs. Strain

Phone (724)537-3131

Customer: Transportation Technology Center Inc.
WMT&R Report: 4-54384

P.O. No.: 28972
WMT&R Quote No.: QN140452

Test Log: U33757
Test Temperature: Room
Material: Steel

Test Date: 03/04/2014
Sample: 1
Modulus: 36.9 Msi
0.2% Offset: 43.1 ksi
Ultimate Load: 14373 lbf
Ultimate Stress: 72.7 ksi

Test Log: U33759
Test Temperature: Room
Material: Steel

Test Date: 03/05/2014
Sample: 3
Modulus: 37.0 Msi
0.2% Offset: 43.4 ksi
Ultimate Load: 14795 lbf
Ultimate Stress: 73.1 ksi

Test Log: U33758
Test Temperature: Room
Material: Steel

Test Date: 03/05/2014
Sample: 2
Modulus: 36.7 Msi
0.2% Offset: 43.8 ksi
Ultimate Load: 14746 lbf
Ultimate Stress: 73.0 ksi

Test Log: U33760
Test Temperature: Room
Material: Steel

Test Date: 03/05/2014
Sample: 4
Modulus: 36.7 Msi
0.2% Offset: 45.9 ksi
Ultimate Load: 14965 lbf
Ultimate Stress: 74.9 ksi

Stress (ksi)

Strain (in./in.)

"NOTE: THE RECORDING OF FALSE, FICTITIOUS OR FRAUDULENT STATEMENTS OR ENTRIES ON THIS DOCUMENT
MAY BE PUNISHABLE AS A FELONY UNDER FEDERAL STATUTE."

82

Stress vs Strain

Customer: Transportation Technology Center Inc.
WMT&R Report: 4-54384

P.O. No.: 28972
WMT&R Quote No.: QN140452

Test Log: U33761
Test Temperature: Room
Material: Steel

Test Date: 03/04/2014
Sample: 5
Modulus: 36.6 Msi
0.2% Offset: 43.8 ksi
Ultimate Load: 14886 lbf
Ultimate Stress: 73.3 ksi

Stress (ksi) axis: 0.0, 8.5, 17.0, 25.5, 34.0, 42.5, 51.0, 59.5, 68.0, 76.5, 85.0

Strain (in./in.) axis: -0.035, 0.000, 0.035, 0.070, 0.105, 0.140, 0.175, 0.210, 0.245, 0.280, 0.315, 0.350

Abbreviations and Acronyms

ALE	Arbitrary Lagrangian-Eulerian
ARA	Applied Research Associates
ASTM	American Society for Testing and Materials
BW	Bao-Wierzbicki
CFC	Channel Frequency Class
CG	Center of Gravity
CTC	Canadian Transport Commission
DOT	Department of Transportation
EPFM	Elastic-Plastic Fracture Mechanics
FE	Finite Element
FEA	Finite Element Analysis
FRA	Federal Railroad Administration
FSI	Fluid-Structure Interaction
HAZ	Heat Affected Zone
LFM	Local Fracture Mechanics
LEFM	Linear Elastic Fracture Mechanics
NGRTC	Next Generation Railroad Tank Car
P-V	Pressure-Volume
TTCI	Transportation Technology Center, Inc.